

Fall 1999

The microchannel flow of a micropolar fluid

Guohua Liu
Louisiana Tech University

Follow this and additional works at: <https://digitalcommons.latech.edu/dissertations>



Part of the [Fluid Dynamics Commons](#), and the [Other Mechanical Engineering Commons](#)

Recommended Citation

Liu, Guohua, "" (1999). *Dissertation*. 176.
<https://digitalcommons.latech.edu/dissertations/176>

This Dissertation is brought to you for free and open access by the Graduate School at Louisiana Tech Digital Commons. It has been accepted for inclusion in Doctoral Dissertations by an authorized administrator of Louisiana Tech Digital Commons. For more information, please contact digitalcommons@latech.edu.

INFORMATION TO USERS

This manuscript has been reproduced from the microfilm master. UMI films the text directly from the original or copy submitted. Thus, some thesis and dissertation copies are in typewriter face, while others may be from any type of computer printer.

The quality of this reproduction is dependent upon the quality of the copy submitted. Broken or indistinct print, colored or poor quality illustrations and photographs, print bleedthrough, substandard margins, and improper alignment can adversely affect reproduction.

In the unlikely event that the author did not send UMI a complete manuscript and there are missing pages, these will be noted. Also, if unauthorized copyright material had to be removed, a note will indicate the deletion.

Oversize materials (e.g., maps, drawings, charts) are reproduced by sectioning the original, beginning at the upper left-hand corner and continuing from left to right in equal sections with small overlaps. Each original is also photographed in one exposure and is included in reduced form at the back of the book.

Photographs included in the original manuscript have been reproduced xerographically in this copy. Higher quality 6" x 9" black and white photographic prints are available for any photographs or illustrations appearing in this copy for an additional charge. Contact UMI directly to order.

UMI[®]

Bell & Howell Information and Learning
300 North Zeeb Road, Ann Arbor, MI 48106-1346 USA
800-521-0600

THE MICRO-CHANNEL FLOW OF A MICRO-POLAR FLUID

by

Guohua Liu, M.S.

**A Dissertation Presented in Partial Fulfillment
of the Requirements for the Degree
Doctor of Philosophy**

**COLLEGE OF ENGINEERING AND SCIENCE
LOUISIANA TECH UNIVERSITY**

November 1999

UMI Number: 9947114

**UMI Microform 9947114
Copyright 1999, by UMI Company. All rights reserved.**

**This microform edition is protected against unauthorized
copying under Title 17, United States Code.**

UMI
300 North Zeeb Road
Ann Arbor, MI 48103

LOUISIANA TECH UNIVERSITY

THE GRADUATE SCHOOL


October 26, 1999

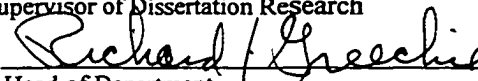
Date

We hereby recommend that the dissertation prepared under our supervision
by Guohua Liu

entitled The Micro-Channel Flow of A Micro-Polar Fluid

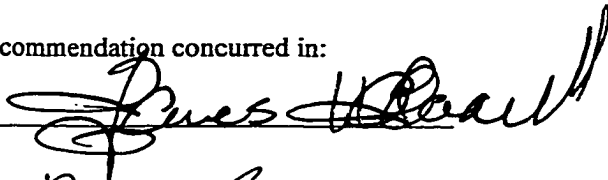
be accepted in partial fulfillment of the requirements for the Degree of
Doctor of Philosophy


Supervisor of Dissertation Research



Head of Department

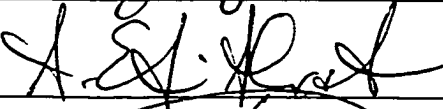
Applied Computational Analysis and Modeling
Department

Recommendation concurred in:









Advisory Committee

Approved:


Director of Graduate Studies

Approved:


Director of the Graduate School


Dean of the College

ABSTRACT

Micro-channel flows have been computed to investigate the influence of Navier-Stokes formulation for the slip-flow boundary condition, and a micro-polar fluid model, respectively.

The results of the slip boundary condition show that the current methodology is valid for slip-flow regime (i.e., for values of Knudsen number less than approximately 0.1). Drag reduction phenomena apparent in some micro-channels can be explained by slip-flow theory. These results are in agreement with some computations and experiments.

An *ad hoc* micro-polar fluid model is developed to investigate the influence of micro effects, such as micro-gyration, in micro-scale flows. The foundation of the *ad hoc* micro-polar fluid is based on Eringen's micro simple fluid, and is simplified for incompressible, two-dimensional, iso-thermal, and micro-isotropic case. Our model contains two material constants, μ and κ , one scale parameter, $m \times Kn$, and one boundary condition parameter n . The number of parameters is significantly reduced from general micro-polar fluid model and makes the theory practical.

The scale parameter $m \times Kn$ introduces the Knudsen number into the micro-polar fluid dynamics by statistical explanation. Therefore, the effect of rarefaction can be accounted into the model by modeling this parameter.

The parameter μ is classical bulk viscosity. The vortex viscosity κ is related to micro-gyration, and needs modeling at current time. It affects the flow field in two aspects, by modifying the apparent viscosity and by introducing the effect of micro-gyration. In the simplest case of fully-developed channel flow, the overall effect is equivalent to lessen the Reynolds number by $(1+k/2)$.

The current micro-polar fluid model explains the drag increase phenomenon in some micro-channel flows from both experimental and computational data. This result is exactly opposite to that predicted by slip-flow theory. The existence of micro-effect needs to be taken into account for the micro-scale flow.

A projection method is used as a numerical technique for both models to solve the difficulty of implicit pressure equation, with the help of staggered grids. An explicit Euler scheme is used for solving the steady flow.

APPROVAL FOR SCHOLARLY DISSEMINATION

The author grants to the Prescott Memorial Library of Louisiana Tech University the right to reproduce, by appropriate methods, upon request, any or all portions of this Dissertation. It is understood that "proper request" consists of the agreement, on the part of the requesting party, that said reproduction is for his personal use and that subsequent reproduction will not occur without written approval of the author of this Dissertation. Further, any portions of the Dissertation used in books, papers, and other works must be appropriately referenced to this Dissertation.

Finally, the author of this Dissertation reserves the right to publish freely, in the literature, at any time, any or all portions of this Dissertation.

Author *Phil Guebara*
Date *Nov. 3, 1999*

TABLE OF CONTENTS

ABSTRACT	iii
LIST OF TABLES	viii
LIST OF FIGURES	ix
LIST OF EQUATIONS	xii
NOMENCLATURE	xvii
ACKNOWLEDGMENTS	xxi
CHAPTER 1 INTRODUCTION	
1.1 General Overview	1
1.2 Classical Fluid Dynamics for Micro-Scale Flow	5
1.3 Development of Micro-Polar Fluid Model	9
1.4 Objectives	15
1.5 Organization of the Dissertation	15
CHAPTER 2 SLIP-FLOW MODEL	
2.1 Introduction	17
2.2 Governing Equations and Boundary Conditions	18
CHAPTER 3 MICRO-POLAR FLUID MODEL	
3.1 Introduction	22
3.2 General Micro-Polar Fluid Model	24
3.3 <i>Ad hoc</i> Two-Dimensional Micro-Polar Fluid Model.....	27
3.3.1 Basic Assumptions and Formulations	27
3.3.2 Relations among the Material Constants	29
3.3.3 Non-Dimensionalized Version	32
3.3.4 Boundary Conditions	34
3.3.5 Unidirectional Flow Solution.	35
CHAPTER 4 NUMERICAL METHOD	
4.1 Introduction	39
4.2 Pseudo-Time-Dependent Method	40
4.3 Projection Method	41
4.4 Discretization	45
4.5 Treatment of Boundary Conditions	48
CHAPTER 5 TWO-DIMENSIONAL MICRO-CHANNEL FLOW	
5.1 Description of Simulations	51
5.2 Simulation Results of Slip-Flow Model	52

5.3	Simulation Results of Micro-Polar Fluid Model	70
CHAPTER 6	CONCLUSION AND DISCUSSION	100
APPENDIX	THE COMPLETE GOVERNING EQUATIONS FOR THE MICRO-POLAR FLUID MODEL	105
REFERENCES	109

LIST OF TABLES

TABLE	DESCRIPTION	PAGE
5.1	The normalized friction factor C^* varies with Kn and σ	58
5.2	The normalized friction factor C^* varies with k	71
6.1	ΔP across orifice vs. k and r/d	102

LIST OF FIGURES

FIGURE	DESCRIPTION	PAGE
1.1	Sizes/Characteristics of micro-components comparison to other items	2
3.1	Variation of the velocity $u(y)$ with κ/μ for $n=1/2$ and $\gamma=1$	38
4.1	Geometrical distribution of grids near a boundary	44
4.2	The staggered grids	46
4.3	The staggered grids near a boundary	49
5.1	Physical domain for micro-channel flow	51
5.2	Effect of grid size	53
5.3	Variation of pressure with streamwise distance for $Kn=0$	54
5.4	Variation of pressure with streamwise distance for various Knudsen number (Slip-Flow Model, $\sigma=0.5$)	55
5.5	Variation of pressure with streamwise distance for various Knudsen number (Slip-Flow Model, $\sigma=1.0$)	56
5.6	Velocity profile for various Kn and σ (Slip-Flow Model)	59
5.7	Velocity field for $Kn=0.001$ and $\sigma=1.0$ (Slip-Flow Model)	60
5.8	Velocity field for $Kn=0.1$ and $\sigma=1.0$ (Slip-Flow Model)	61
5.9	Velocity field for uniform entrance flow (Slip-Flow Model)	62
5.10	v - component contour for uniform entrance flow (Slip-Flow Model)	63

5.11	Velocity field for impinging jet flow (Micro-Polar Fluid Model, $Re=100$, $k=0.1$)	64
5.12	v - component contour for impinging jet flow (Micro-Polar Fluid Model, $Re=100$, $k=0$)	65
5.13	v - component contour for impinging jet flow (Micro-Polar Fluid Model, $Re=100$, $k=0.1$)	66
5.14	v - component contour for impinging jet flow (Micro-Polar Fluid Model, $Re=100$, $k=1$)	67
5.15	v - component contour for impinging jet flow (Micro-Polar Fluid Model, $Re=100$, $k=5$)	68
5.16	Effect of the parameter $mxKn$	75
5.17	Effect of the parameter $mxKn$ (Amplified)	76
5.18	Variation of pressure with channel distance for various k values ($Re=100$)	77
5.19	Variation of pressure with channel distance for various k values (Amplified, $Re=100$)	78
5.20	Velocity profile for various k values ($Re=100$)	79
5.21	Micro-gyration contour ($Re=100$, $k=0.1$)	80
5.22	Velocity field for $Re=100$, $k=1$	81
5.23	Variation of pressure with channel distance for $k=0.1$	82
5.24	Variation of pressure with channel distance for $k=1$	83
5.25	Velocity field for flow through a straight channel with restriction 0.2, $k=0$	84
5.26	Velocity field for flow through a straight channel with restriction 0.2, $k=0.1$	85
5.27	Velocity field for flow through a straight channel with restriction 0.2, $k=1$	86

5.28	Velocity field for flow through a straight channel with restriction 0.2, $k=5$	87
5.29	Variation of pressure with the downstream distance for flows through a straight channel with restriction 0.2	88
5.30	Plots of v - component contour for flows through a straight channel with restriction 0.2	89
5.31	Velocity field for flow through a straight channel with restriction 0.6, $k=0$	90
5.32	Velocity field for flow through a straight channel with restriction 0.6, $k=0.1$	91
5.33	Velocity field for flow through a straight channel with restriction 0.6, $k=1$	92
5.34	Velocity field for flow through a straight channel with restriction 0.6, $k=5$	93
5.35	Variation of pressures with the downstream distance for flows through a straight channel with restriction 0.6	94
5.36	Velocity field for flow through a straight channel with restriction 0.44, $k=0$	95
5.37	Velocity field for flow through a straight channel with restriction 0.44, $k=0.1$	96
5.38	Velocity field for flow through a straight channel with restriction 0.44, $k=1$	97
5.39	Velocity field for flow through a straight channel with restriction 0.44, $k=5$	98
5.40	Variation of pressure with the downstream distance for flows through a straight channel with restriction 0.44	99

LIST OF EQUATIONS

EQUATION	DESCRIPTION	PAGE
2.1	Continuity equation for slip-flow model	18
2.2	Momentum equation (x direction) for slip-flow model	18
2.3	Momentum equation (y direction) for slip-flow model	18
2.4	Slip-velocity boundary condition at the wall	19
2.5	Boundary condition for v at the wall	20
2.6	Boundary condition for p at the wall	20
2.7	Inlet velocity distribution for u	20
2.8	Inlet velocity distribution for v	20
2.9	Inlet pressure condition	20
2.10	Outlet velocity condition for u	20
2.11	Outlet velocity condition for v	21
2.12	Outlet pressure condition	21
2.13	Non-slip velocity boundary condition at the wall	21
2.14	Boundary condition for p at the wall for non-slip flow	21
2.15	Non-dimensionalized continuity equation for slip-flow model	21
2.16	Non-dimensionalized momentum equation (x direction) for slip-flow model	21
2.17	Non-dimensionalized momentum equation (y direction) for slip-flow model	21
2.18	Definition of Reynolds number	21
3.1	Skew-symmetry of first stress moment tensor and gyration tensor	24

3.2	Continuity equation for micro-polar fluid model	25
3.3	Equation for conservation of micro-inertia for micro-polar fluid model	25
3.4	Momentum equation for micro-polar fluid model	25
3.5	Momentum moments equation for micro-polar fluid model	25
3.6	Definition of micro-gyration vector g	26
3.7	Definition of micro-inertia moment tensor j	26
3.8	Property of isotropic	26
3.9	Conservation of i	26
3.10	Conservation of j	26
3.11	Expression of i and j	26
3.12	Continuity equation for incompressible micro-polar fluid model	27
3.13	Continuity equation for micro-polar fluid model	28
3.14	Balance of momentum (x component) for micro-polar fluid model	28
3.15	Balance of momentum (y component) for micro-polar fluid model	28
3.16	Balance of angular momentum for micro-polar fluid model	28
3.17	Relations among μ , κ , j , and γ	29
3.18	Definition of <i>micro-inertia density</i>	29
3.19	Relation of j and d	30
3.20	Statistical mean of f	30
3.21	Variance of f	30
3.22	Coefficient for variation for the mean	30
3.23	Standard deviation s	31
3.24	Expression of n	31

3.25	Definition of m	32
3.26	Relation of m and Kn	32
3.27	Definition of non-dimensionalized variables	33
3.28	Non-dimensionalized continuity equation	33
3.29	Balance of non-dimensionalized momentum (x component)	33
3.30	Balance of non-dimensionalized momentum (y component)	33
3.31	Balance of non-dimensionalized angular momentum	33
3.32	Definition of Reynolds number	33
3.33	Definition of k	33
3.34	Boundary condition of g at the wall	34
3.35	Momentum equation for unidirectional flow	35
3.36	Angular momentum equation for unidirectional flow	35
3.37	Boundary condition at center line	35
3.38	Boundary condition at the wall	35
3.39	Solution of u for unidirectional flow	35
3.40	Solution of g for unidirectional flow	35
3.41	Intermediate parameter in the solution expression	36
4.1	General expression of continuity equation	40
4.2	General expression of momentum equation	40
4.3	General expression of angular momentum equation	40
4.4	Momentum equation for time-dependent problem	41
4.5	Angular momentum equation for time-dependent problem	41
4.6	First phase of split momentum equation	42

4.7	Second phase of split momentum equation	42
4.8	Applying continuity equation to the $n+1$ step	42
4.9	Poisson equation for pressure	42
4.10	Euler's forward scheme in time for g	42
4.11	Neumann condition for pressure at the boundary	43
4.12	Condition of compatibility for Neumann problem	43
4.13	Discretization of pressure equation	44
4.14	Discretization of Neumann condition	44
4.15	First-order scheme in time of the momentum equation	45
4.16	Discretization of $u \frac{\partial u}{\partial x}$	46
4.17	Discretization of $v \frac{\partial u}{\partial y}$	46
4.18	Interpolation of $v_{i+1/2,j-1/2}$	46
4.19	Discretization of $\frac{\partial^2 u}{\partial x^2}$	46
4.20	Discretization of $\frac{\partial^2 u}{\partial y^2}$	47
4.21	Discretization of $\frac{\partial g}{\partial y}$	47
4.22	Discretization of $u \frac{\partial v}{\partial x}$	47
4.23	Interpolation of $u_{i-1/2,j+1/2}$	47
4.24	Discretization of $v \frac{\partial v}{\partial y}$	47

4.25	Discretization of $\frac{\partial^2 v}{\partial x^2}$	47
4.26	Discretization of $\frac{\partial^2 v}{\partial y^2}$	47
4.27	Discretization of $\frac{\partial g}{\partial x}$	47
4.28	Discretization of $u \frac{\partial g}{\partial x}$	47
4.29	Interpolation of $u_{i,j+1/2}$	47
4.30	Discretization of $v \frac{\partial g}{\partial y}$	48
4.31	Interpolation of $u_{i+1/2,j}$	48
4.32	Discretization of $\frac{\partial^2 g}{\partial x^2}$	48
4.33	Discretization of $\frac{\partial^2 g}{\partial y^2}$	48
4.34	Discretization of $\frac{\partial v}{\partial x}$	48
4.35	Discretization of $\frac{\partial u}{\partial y}$	48
4.36	Definition of function $sgn(x)$	48
4.37	Treatment of virtual velocity	50
5.1	Fully developed condition for g and v	71
5.2	Simplified angular momentum equation	71
5.3	Expression of g	72
5.4	Equivalent x - component momentum equation	72

NOMENCLATURE

c	coefficient for variation for the mean
C^*	normalized friction factor
C_f	friction coefficient
d	characteristic length of microstructure diameter of sensitive volume element
D/Dt	material derivative operator
dM	mass in volume element
dV	theoretical volume element
dv	sensitive volume
dv'	atomic volume
f	Darcy friction coefficient physical property of a particle
\bar{f}	mean of f
g	gyration component normal to x - y plane
\mathbf{g}, g_k	gyration vector
H, h	channel height
i	micro-inertia moment constant
i_{km}	micro-inertia moment tensor
j	micro-inertia moment constant

j_{km}	micro-inertia moment tensor
k	κ/μ
Kn	Knudsen number
L	flow characteristic length
m	model parameter
N	the normal coordinate unit to the boundary
n	the normal coordinate at the wall
	number of molecules
	parameter related to micro-gyration vector and shear stress
p	pressure
Q	flowrate
s	standard deviation
t	time
t_{klm}	first stress moment tensor
Re	Reynolds number
U	characteristic velocity
u	velocity component in x direction
V	velocity vector
V	variance
v	velocity component in y direction
v_k	velocity vector
w	velocity component in z direction
	channel width

x	the Cartesian coordinate in streamwise direction
y	the Cartesian coordinate in normal direction
z	the Cartesian coordinate in spanwise direction
α	material constant
β	material constant
χ	atomic volume element spacing
Δt	time interval
ΔV	volume element
ΔV^*	limiting volume element
Δx	grid spacing in x direction
Δy	grid spacing in y direction
δ_{ij}	Kronecker delta
ε	small number
ε_{ijk}	third order alternating tensor
Γ	boundary
γ	material constant
κ	vortex viscosity
λ	mean free path of molecules
	material constant
μ	dynamic viscosity
ν	kinematic viscosity
ν_{ij}	gyration tensor

ρ	density
σ	tangential momentum accommodation coefficient
Ω	domain
ζ	parameter

Superscript

•	material derivative operator
*	non-dimensional variable
	provisional variable
n	iteration step

Subscript

∞	at outlet; at reference point
$,k$	differential operator in space direction k
i	index of grid in x direction
	tensor index
j	index of grid in y direction
	tensor index
k	tensor index
l	tensor index
m	tensor index
r	tensor index
s	tensor index

ACKNOWLEDGMENTS

I would like to express my gratitude and sincere appreciation to Dr. Richard Greechie for his encouragement and guidance through my graduate studies. I thank him especially for his kindness and financial support which provided me the opportunity to study at Louisiana Tech University.

I would also like to thank Dr. Hisham Hegab for his continuous guidance in this thesis. Many thanks for his office hours, patience, and effort in correcting the manuscript of this thesis. Sincere appreciation is also extended to Dr. Raja Nassar, Dr. Weizhong Dai, Dr. Albert Edwin Alexander, and Dr. James Maxwell for their support and service on my advisory committee.

I am grateful to Dr. Garry Pantelis of ANSTO, Australia, for helping me in developing the early version of the projection method code. I also thank Dr. Ali Beskok of Texas A&M University, Dr. Chih-Ming Ho of UCLA, and Dr. M. A. Leschziner of Institute of Science and Technology, University of Manchester for supplying valuable references used in this dissertation.

Finally, I dedicate this thesis to my family. Without their love and support from thousands of miles away, this dissertation could not have been completed.

CHAPTER 1

INTRODUCTION

1.1. General Overview

Micron-size mechanical devices are becoming more prevalent, both in commercial applications and in scientific inquiry. Research on micro-fluidic devices, fabricated with micro-mechanics technology, has its origin more than two decades ago. At IBM, integrated planar silicon ink-jet printer nozzles were developed (Bassous *et al.*, 1977). Within the last decade, a dramatic increase in research activities has taken place, mostly due to the rapidly expanding growth of applications in the areas of MEMS (Microelectromechanical Systems), bioengineering, chemical systems, and advanced energy systems. Micro-components currently in development include micro-channel heat exchangers, gas absorbers, liquid-liquid extractors, chemical reactors, micro-flow-sensors, and micro-actuators for pumps, valves and compressors (Gass *et al.*, 1993; Wegeng & Drost, 1994; Caruana, 1996). At present, micro-manufacturing technology provides mechanical parts of micron size, batch-fabricated in large quantities, and integratable with electronics (Ho & Tai, 1996). These features may even allow coupling of MEMS to macro-scale flow systems. More encouragingly, MIT developed a MEMS-based gas turbine generator whose 1 cm diameter by 3 mm thick SiC heat engine was designed to produce 10-20W of electric power while consuming 10 grams/hr of H₂. Their

second version was to produce up to 100W using hydrocarbon fuels (Epstein *et al.*, 1997).

Typical scales for micro-mechanical devices range from microns to millimeters, spanning the range of scales that also includes microelectronics, ultrasonics, visible and infrared radiation, and biological cells and tissues. Figure 1.1 shows the general comparison between these compact systems with their conventional counterparts (Wegeng *et al.*, 1996).

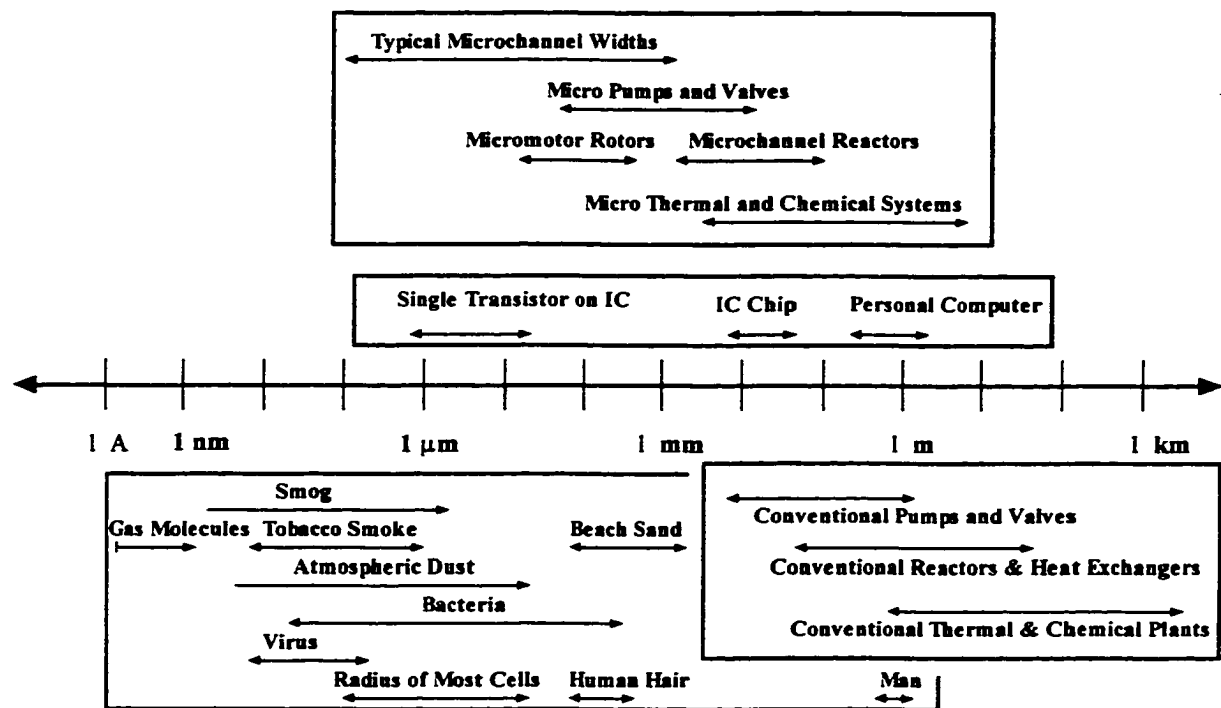


Figure 1.1 Sizes/Characteristics of micro-components comparison to other items

Micro-mechanics is a multidisciplinary research area. In this new area, with the application systems under development becoming more complex and much smaller, there are increasing new phenomena and hence increasing demands both for theoretical and

experimental work on fundamental physical and chemical mechanisms. Fluid mechanics is one of the many disciplines to be further explored (Gravesen *et al.*, 1993).

With these new features, a whole class of low Reynolds number flows needs to be revisited. The continuum assumption used in classical Navier-Stokes fluid dynamics may not be accurate enough when the flow scale becomes refined and comparable with the mean molecule free path. That phenomenon has also been demonstrated by much evidence. Several effects, normally neglected in conventional flow, may exist in micro-scale flow (Bailey *et al.*, 1995). For example, two and three dimensional transport effects are significant as micro-structure characteristic lengths are reduced to the same order of magnitude as the boundary layer thickness; therein the momentum and heat transfer in normal and span-wise directions increase significantly (Ma & Gerner, 1993). A slip-flow boundary condition may exist and has sound explanations in micro-channel flow but has no counterpart in macro-scale flow (Beskok & Karniadakis, 1992, 1993, 1994; Pong & Ho, 1994; Arkilic *et al.*, 1994; Chen *et al.*, 1998).

One of the most important flow dynamic characteristics is the pressure drop or alternative friction factor through the fluid-carrying components as it directly engages the energy efficiency of the system. Experimental studies have been performed in an effort to better understand this flow characteristic, but the currently available experimental data for micro tubes and channels are inconclusive.

Wu and Little (1983; 1984) used silicon and glass channels ranging in depth from 28 to 65 microns for nitrogen, argon, and helium flows. The data showed substantially higher friction factors than predicted by classical theory. The silicon channels showed up

to 60% deviation from the Moody chart, while the glass channels gave results that were over 3 times those of the Moody chart.

However, the later investigation of Choi *et al.* (1991) demonstrated the exact opposite. Their experiments were performed for nitrogen flow through micro-tubes having inside diameters ranging from 3 to 81 microns and relative roughness ranging from 0.00017 to 0.0116. The measured friction factors were below those predicted by the Moody chart. The friction coefficient C_f (i.e., the product of Darcy friction coefficient f times Reynolds number Re) was 53. This result is 20% lower than the theoretical value of 64 based on the Moody diagram.

Pfahler *et al.* (1991) conducted experiments for both liquids and gases in silicon channels ranging in depth from 0.5 to 50 micron. For both liquids and gases, they reported lower friction coefficients than those predicted by theory. The liquids studied were isopropanol and silicon oil. The isopropanol data showed the reduction in C_f as channel depth decreased and was independent of Re , whereas the silicon oil data showed that the reduction in C_f was independent of channel depth and increased with decreasing Re . The gases used in the study were helium and nitrogen. The results showed that the reduction in C_f , contrary to the liquid tests, decreased as channel depth decreased for both gases. In the smallest channel studied, both the nitrogen and helium data showed Re dependence for C_f , where C_f decreases for low Re .

Peng and Wang (1994) reported forced flow convection results for water and methanol through rectangular micro-channels having heights of 700 microns and width ranging from 200 to 800 microns. The laminar and transient heat transfer behaviors were strongly affected by fluid temperature, velocity, and channel size. Peng *et al.* (1994a,

1994b) performed a water flow through stainless steel channels ranging in hydraulic diameter from 0.133 to 0.367 mm, and their results showed that C_f decreased with an increase in Re .

Harley *et al.* (1995) conducted experimental and theoretical investigations of subsonic, compressible flow in micro-size long conduits. The Knudsen number was less than 0.38, and the data were within 8% of theoretical predictions of the friction constant based on isothermal, locally developed flow and incorporating a single coefficient wall-slip model. Their experimental uncertainty is 12%.

One possible explanation for these observed effects is that they are largely due to the limitation of continuum assumption used in classical fluid dynamics. The constitutive equation, based on the continuum assumption, may be no longer valid to describe the physical characteristic of fluid volume. Various models are thus needed to investigate micro-scale flow.

1.2. Classical Fluid Dynamics for Micro-Scale Flow

Slip-flow models are naturally considered to be a simple extension of conventional fluid dynamics to micro-scale flows. A slip-flow model may retain the Navier-Stokes equations as the governing equations in the flow field but replaces the non-slip wall boundary condition with slip condition. This model was originally used in rarefied gas dynamics.

The effect of flow scale on the continuum assumption is well measured by a dimensionless parameter, Kn , which is the ratio of the mean free path of the fluid molecules (λ) to the flow characteristic length scale (L). Mean free path λ varies with the

temperature and pressure in the gas state. The Kn number relates to the collision probability among the fluid molecules and hence affects the molecular statistical properties, based on which continuum is assumed in classical fluid mechanics. Rarefied gas dynamics show that the continuum assumptions are invalid when the mean free path of the gas is on the order of the characteristic dimension, or when the Kn number is of $O(1)$. This condition rarely happens for conventional fluid mechanics applications, but it may occur in micron flow depending on the fluid, flow condition, and channel size.

Rarefied dynamics theories focus on the flow of molecules near a solid surface (Grad, 1949; Cercignani, 1975; Kogan, 1972). Although it is not clear what the velocity distribution of the molecules near the solid boundary, three kinds of boundary conditions are assumed, i.e., specular, diffuse, and Maxwell's. For perfectly specular surfaces, molecules are reflected at the same angle as the incidence angle. For diffuse surfaces, the molecule can be reflected in any direction regardless of the incidence angle. Maxwell's boundary condition treats a portion of the reflection as specular and the other as diffuse. In reality, most engineering surfaces are diffuse so some momentum is always lost at the wall. For a continuum flow, where the mean free path is very short, there are many molecules in the region very close to the wall. Momentum exchange between the molecules is more likely to occur. This interaction results in a zero velocity or non-slip condition at the wall. On the other hand, free molecular flow exhibits the other extreme where interaction between molecules rarely occurs. There is little build-up of molecules near the wall, as in a continuum flow. This situation causes the flow to move along the surface due to a net velocity in the flow direction. Slip flow occurs between these extremes when there are slight rarefaction effects.

It is not completely clear when slip flow becomes important as fluid convection systems are reduced in size. A number of researchers have used analytical or computational models along with experiments in micro-channel flows. Ebert & Sparrow (1965) determined the velocity and pressure-drop characteristics of moderately rarefied gas flow in rectangular and annular ducts. It was found that the effect of slip flattened the velocity distribution relative to that for a continuum flow. Also, the axial pressure gradient was diminished under slip conditions. It was found that compressibility increased the pressure drop primarily through an increase in viscous shear rather than through an increase in momentum flux.

Arkilic *et al.* (1994) developed a two-dimensional model for rarefied gas flow through micro-channels by solving the Navier-Stokes equation using a velocity slip boundary condition, allowing for specification of a tangential momentum accommodation coefficient. It showed that the effect of rarefaction caused the pressure distribution to be nonlinear in the axial direction.

The reduced friction effects measured by Pfahler *et al.* (1991) and Choi *et al.* (1991) were verified by Beskok and Karniadakis (1994) through a computational model of slip-flow in micro-channels. The two-dimensional predictions closely matched the friction factors of Pfahler; however, the analysis provided no basis for Re dependence of friction coefficient in micro-channels. Reduced skin friction was also calculated using a three-dimensional model of a rectangular channel having a 3:1 aspect ratio for $Re=1.0$ with Knudsen number Kn as a parameter. In their papers (Beskok & Karniadakis, 1992, 1993, 1994, 1995, 1997; Beskok *et al.* 1996), Beskok and his co-investigators extended their work to include compressibility effects in addition to using higher order boundary

conditions. In his recent paper, Beskok (1996) showed that for a large pressure drop in airflow, the compressibility effect was dominant, and in more rarefied flows such as helium flow, the effect of rarefaction negated compressibility.

Kavehpour *et al.* (1997) used a two-dimensional flow and heat transfer model to study gas compressibility and rarefaction in micro-channels assuming a slip-flow regime. The numerical methodology is based on the control volume finite difference scheme. The computations were performed for a wide range of entrance Kn and Re numbers. It was found that the friction coefficient was substantially reduced for slip-flow compared with that of the continuum flows. The velocity and temperature distributions were flattened compared with a continuum flow, and the axial variation of pressure became nonlinear. It was shown that the effect of compressibility was important for high Re and that the effect of rarefaction was significant for lower Re.

Chen *et al.* (1998) adopted a slip boundary to study nitrogen and helium flow in micro-channels. The Knudsen numbers at the channel outlet ranged from 0.055 to 0.165. The differences between the numerical results and experimental data were within 1.15% for pressure drop and 3.13% for mass flow rate.

To relax the continuum assumption, a Direct Simulation Monte Carlo method (DSMC) was performed for flows related to MEMS by some researchers (Piekos & Breuer, 1996; Bird, 1994). The model makes no continuum assumption. Instead, they modeled the flow as it physically exists: a collection of discrete particles, each with a position, a velocity, an internal energy, a species identity, etc. These particles move and are allowed to interact with the domain boundaries in small time steps during the computation. Intermolecular collisions are all performed on a probabilistic basis at the

end of each time step to minimize computational work. Macroscopic quantities, such as flow speed and temperature, are then obtained by sampling the microscopic state of all particles in the region of interest. Unfortunately, in low-speed flow which is the case of most MEMS, the inlet and outlet flow conditions make DSMC difficult. DSMC's statistical nature makes the determination of its macroscopic state from an instantaneous sample inaccurate due to the unacceptable statistical scatter. Another drawback of DSMC is that it needs many more computational resources than classical computational fluid dynamics methodology.

1.3. Development of Micro-Polar Fluid Model

To remedy the drastic limitations of the concepts of the continuum field approach on the extent to which continuum descriptions of macroscopic behavior can mirror the fine structure of the medium, a micro-continuum fluid mechanics concept has been developed originally for such rheologically complex fluids as liquid crystals, polymeric suspensions, animal blood, etc. The outstanding reviews of the development and application of this model were made by Ariman *et al.* (1973, 1974). A systematic description of fluids with micro-structure was presented by Stokes (1984).

The earliest formulation of a general theory of fluid micro-continua was attributed to Eringen (1964) in which the mechanics of fluids with deformable micro-elements are considered. In his paper, a simple micro-fluid concept was presented. This article was the first complete work which originated the micro-fluid theory. Eringen's simple micro-fluid is "a fluent medium whose properties and behaviour are affected by the local motions of the material particles contained in each of its volume element." The simple micro-fluid

possesses local inertia. The laws of classical continuum mechanics are augmented with additional equations which account for conservation of micro-inertia moments and balance of first stress moments which arise due to consideration of microstructure in a medium. New kinematic variables, e.g., the gyration tensor and micro-inertia moment tensor, are introduced. Simple micro-fluids are isotropic, viscous fluids and need 22 viscosity and material coefficients to characterize the constitutive equation in the simplest linear case.

The theory was extended by Eringen (1972) to take into account thermal effects and was termed as the theory of thermo-micro-fluids. The exact nonlinear theory is presented and restricted by the axioms of constitution. The complete system of field equations and accompanying jump conditions result from the linear theory. It also discussed several internally constrained classes of these fluids, which include micro-polar fluids and inertia rateless fluids.

Eringen introduced various subclasses of simple micro-fluids, from which, as a special class, is micro-polar fluids. In micro-polar fluids, the local fluid elements are allowed to undergo only rigid rotations without stretch. In this way, the gyration tensor is to be considered skew-symmetric and to be reduced to one vector \mathbf{g} . Structured fluids consisting of dumb-bell molecules or short rigid cylindrical elements are properly represented by this model. The characteristic of our micro-scale flow may suggest itself to be in this category.

Eringen (1969) also extended micro-polar fluids to allow the micro-elements of the fluid to deform, and that was termed micro-polar fluids with stretch. He gave this kind of application to Newtonian fluids with polymeric additives, certain liquid crystals, and

blood plasma. He also developed a theory of anisotropic micro-polar fluids (1980). Anisotropic fluids occur in nature as either chemically stable substances or fluids that carry suspensions. The theory considers the fluid orientable at the outset rather than the interactive motions of its constituents. Eringen & Okada (1995) proposed a lubrication theory under the micro-structure framework. Non-local viscosity moduli were determined disregarding the inner structure of the fluid. The theoretical calculations for thin liquid films were in good agreement with several experimental observations.

Theories similar to Eringen's were presented by many researcher according to their own approaches. Allen *et al.* (1967) employed a continuum approach to develop the kinematics appropriate to media with deformable microstructure referred to as "simple deformable directed fluids." Kline & Allen (1970) developed a thermo-dynamical theory of fluid suspensions of deformable particles. They found that their theory qualitatively predicted the observed unsteady shear-flow behavior of dilute suspensions of randomly coiling macromolecules, such as solutions of polyisobutylene. This apparent successful prediction of experimental observations gives strong support in favor of the micro-continuum approach for describing the rheological behavior of fluid suspensions. Ciarletta (1995) established the linear theory of heat-conducting micro-polar fluids based on Eringen's framework.

Stokes recompiled different versions of micro-continua theories and presented a connected account of them in a common notation (1984). It made the theories clear in the physical concept. He suggested two main physical concepts --- couple stresses and internal spin --- that go into building theories of fluids with microstructure in addition to the conventional fluid mechanics. He also suggested a kinematic concept, micro-

structure. The couple stresses and micro-structures are conceptually different. The first concept deals with mechanical interaction, whereas the second one deals with the kinematic. Whereas in a general theory of fluids with micro-structure, couple stresses and internal spin may be present simultaneously, theories of fluids in which couple stresses are present, but micro-structure is absent, are also possible. Similarly, micro-structure may be considered in the absence of couple stresses. The effect of couple stresses in fluids was considered in his early paper (Stokes, 1966).

The successful application of the micro-continuum fluid theories covers a wide variety of flow problems. Ariman *et al.* (1974) gave a comprehensive review for early applications. These flow problems were categorized into six major divisions, namely, fluids with rigid non-spherical or deformable micro-elements, micro-polar fluids, polar and dipolar fluids, couple stress fluids, anisotropic fluids, and liquid crystals. In the micro-polar fluids division, applications include steady shearing flows like Couette flows, poiseuille flows; nonsteady flows like oscillatory flows, boundary-layer flows; stability analyses; suspension viscosity studies; turbulence studies; blood flow studies; and other flow studies.

Ariman & Cakmak (1967) applied couple stress and micro-polar theories to the problems of Couette and Poiseuille flows between two parallel plates and results were compared. Ariman *et al.* (1967) considered the micro-polar fluids flow between concentric cylinders for the case of Couette and Poiseuille flows. Kline & Allen (1970) investigated nonsteady flows of fluids with micro-structure. For parallel flows, a decomposition of velocity and micro-structure spin fields was given and used to reduce the governing equations to two uncoupled parabolic partial differential equations. These equations are

solved for the suddenly accelerated plane wall problem. For the boundary condition at the wall, they considered two limiting cases. In the first case, a rotational surface friction was neglected and slip condition applied; in the second case, a fluid-solid interaction was set so strong that no rotation permitted and non-slip condition applied. They also considered the effects of fluid micro-structures in two limiting cases. The first case was interpreted physically as dilute suspensions flow, where the characteristic micro-structure length becomes increasingly small with respect to the characteristic flow field length. This characteristic leads to the classical solution or small Knudsen like continuum flow solution. The second case is just the opposite, where the micro-structure characteristic length dominates the corresponding flow field length. In this case, the boundary-layer thickness is increased due to the effect of the ratio of vortex viscosity to classical viscosity. In other words, vortex viscosity influences the flow behavior as much as the classical shear viscosity. We will extensively investigate this behavior in a later chapter.

Experimental determination of material micro-polar fluid constants was made by Kolpashchikov *et al.* (1983). Their results of viscometric measurements allowed the determination of two characteristic parameters, i.e., viscosity coefficients, of a micro-polar fluid.

However, most recent works are still restricted to theoretical investigation. Olmstead & Majumdar (1983) used micro-polar fluid model to examine steady, incompressible Oseen flows in two dimensions. The solution of the fundamental problem was obtained in explicit form under a certain restriction on the physical parameters of the problem. Ahmad (1976) obtained a self-similar solution of incompressible micro-polar boundary layer low concentration suspension flow over a semi-infinite flat plate. In his

method, the partial differential equations of motion are reduced to two couple differential equations. Rees & Bassom (1996) considered the Blasius boundary layer flow of a micro-polar fluid over a flat plate. They assumed the micro-inertia density to be constant, and non-zero micro-rotation vector on a solid surface. An asymptotic analysis was performed. Can *et al.* (1989) studied the convective motion in a micro-polar fluid. It was shown that the principle of exchange of stabilities holds for the convective motion in a micro-polar fluid, and the convective motion is less stable for micro-polar than for Newtonian viscous fluid. Easwaran & Majumdar (1990) constructed some causal fundamental solutions for the slow two-dimensional flow of a micro-polar fluid. An explicit solution required the factorization of a fourth order partial operator into two quadratic operators, which was achieved under a certain condition on the parameters of the problem. Das & Sanyal (1990) discussed unsteady flow of a micro-polar fluid with a periodic pressure gradient through a rectangular channel. Hung *et al.* (1996) used a perturbation method to investigate analytically the nonlinear stability behavior of a thin micro-polar liquid film flowing down a vertical plate. They analyzed the effect of the vortex viscosity with the classical bulk viscosity.

Of more importance to this work is the paper by Papautsky *et al.* (1998). The authors employed micro-polar fluid theory to investigate numerically micro-channel fluid flow behavior, and experimentally verified the model. The significance of Papautsky's work is that it is the first time the micro-polar model is applied to the area of micro-scale flow. The feature of micro-scale flow poses the micro-polar fluid a new challenge. The flow they considered was two dimensional, steady, and incompressible. However, they did not indicate clearly other assumptions such as unidirectional flow or small Reynolds

number flow. They used momentum and angular momentum equations that do not contain the convection terms and that may be deduced only by small Reynolds assumption or unidirectional flow assumption, and this factor makes their theory severely bounded. They also specified the pressure drop in their computations so as to avoid the difficulty of solving the pressure equation in the case of incompressible flow. At the same time, their model was not applicable to a general case of non-pressure-driven flow.

1.4. Objectives

With the forementioned drive to explore the micro-scale flow and the current research progress in micro-polar fluid flow, it is inspiring to develop an *ad hoc* micro-polar fluid model to better suit the micro-channel flow. Our interest is in extending the micro-polar fluid model to a steady, incompressible, two dimensional flow in a micro-channel. The flow behavior will be our concern and will be compared to the classical Navier-Stokes solution. A numerical scheme from conventional computational fluid dynamics for incompressible flow, will be used in this investigation.

1.5. Organization of the Dissertation

This dissertation is organized as follows: In chapter 2, we present the governing equations and slip boundary conditions for a slip-flow model based on classical fluid dynamics. In chapter 3, we present the details of the micro-polar fluid model, the simplifying assumptions for modeling, an exact solution obtained for unidirectional flow, and nondimensionlization. In chapter 4, we discuss the numerical method including numerical schemes and various computation details. In chapter 5, we describe the specific

simulation problem and computational results. In chapter 6, we give a conclusion and discussion.

CHAPTER 2

SLIP-FLOW MODEL

2.1. Introduction

Typically, a flow is considered to be in one of four regimes according to its Knudsen number. Different authors defined these regimes using slightly different Knudsen number ranges. For gas flow, Beskok & Karniadakis (1992) proposed the following classification:

$Kn \leq 0.001$	Continuum Flow
$0.001 < Kn \leq 0.1$	Slip Flow
$0.1 < Kn \leq 10$	Transition Flow
$Kn > 10$	Free Molecular Flow

We follow this classification as have other researchers (Bailey *et al.*, 1995; Kavehpour *et al.*, 1997; Chen *et al.*, 1998).

For continuum flow, the Navier-Stokes equations govern the flow. In the slip-flow regime, deviations from the state of continuum are relatively small, and the flow is still governed by the Navier-Stokes equations. The rarefaction effect is modeled through the partial slip at the wall using Maxwell's velocity slip and von Smoluchowski's temperature jump boundary condition. The validity of this kind of model was assessed by various authors (Beskok, 1996; Chen *et al.*, 1998). For flows in the high transition or free

molecular regimes, the Navier-Stokes equations break down and have to be substituted either by the Boltzmann equation, which is valid at the microscopic level, or by continuum approximations.

The aspect ratio, defined as channel width to channel height, of a micro-channel often is large. If we neglect flow change in the direction of width, usually achieved when the aspect ratio is greater than 7, then the flow can be reasonably assumed to be two-dimensional in the streamwise direction. It can be shown that for flows with a large aspect ratio the three dimensional flow rate is calculated to the leading order by $Q_{3D} = Q_{2D}(1 - h^2/w^2)$, where h and w are channel height and width, respectively (Chen *et al.*, 1998).

2.2. Governing Equations and Boundary Conditions

The steady, two dimensional, isothermal, incompressible flow is governed by the Navier-Stokes' equations, i.e.:

Continuity:

$$\frac{\partial u}{\partial x} + \frac{\partial v}{\partial y} = 0 \quad (2.1)$$

Momentum (x direction):

$$u \frac{\partial u}{\partial x} + v \frac{\partial u}{\partial y} = -\frac{1}{\rho} \frac{\partial p}{\partial x} + \nu \left(\frac{\partial^2 u}{\partial x^2} + \frac{\partial^2 u}{\partial y^2} \right) \quad (2.2)$$

Momentum (y direction):

$$u \frac{\partial v}{\partial x} + v \frac{\partial v}{\partial y} = -\frac{1}{\rho} \frac{\partial p}{\partial y} + \nu \left(\frac{\partial^2 v}{\partial x^2} + \frac{\partial^2 v}{\partial y^2} \right) \quad (2.3)$$

where, x, y are the Cartesian coordinates in streamwise and normal direction; u, v are the velocity components corresponding to x, y ; p , the pressure; ρ , the fluid density; ν , the fluid kinematic viscosity.

In the slip-flow regime, the Navier-Stokes equations (2.1, 2.2, 2.3) are solved subject to the first order velocity slip boundary conditions at the wall given by:

$$\frac{u_{wall}}{U} = \frac{2-\sigma}{\sigma} Kn \left(\frac{\partial u / U}{\partial y / L} \right)_{wall} \quad (2.4)$$

where, U is the characteristic velocity; Kn , local Knudsen number; L , the characteristic length, the channel height in this case; σ , the tangential momentum accommodation coefficient.

The normal gradient of the tangential velocity shows the effect of vorticity on the velocity itself at the wall. The nature of the momentum exchange between impinging fluid molecules and the surface is reflected by the accommodation coefficient. For example, $\sigma = 0$ corresponds to specular reflection and $\sigma = 1$ corresponds to diffuse reflection. In the first case, the tangential velocity of the molecules reflected from the walls is unchanged, and the normal velocity of the molecules is reversed due to the normal momentum transfer to the wall. In the second case, the molecules are reflected from the walls with zero average tangential velocity. The diffuse reflection in particular is an important phenomenon for tangential momentum exchange and thus friction of the fluid with the walls. Equation (2.4) assumes slip even for the diffuse reflection case. The non-slip condition on the walls is obtained only when $Kn = 0$. The accommodation coefficient depends on the fluid and the surface roughness, temperature, local pressure, and possibly the velocity and the mean direction of the local flow.

Several authors assumed $\sigma = 1$ (Chen *et al.*, 1998; Kavehpour *et al.*, 1997) as experiments with gases over various solids and fluid surfaces show that σ is approximately equal to 1.0. It is possible to obtain higher-order corrections to the velocity slip boundary conditions by retaining higher-order terms in the Taylor series expansion of the tangential velocity near the wall (Beskok, 1996).

In this research, σ is varied between 0 and 1.

The other boundary conditions at the walls are

$$v = 0 \quad (2.5)$$

$$\frac{\partial p}{\partial n} = 0 \quad (2.6)$$

where, n is the normal coordinate at the wall.

The flow at the inlet is assumed to be of a parabolic velocity profile as well as a uniform profile. The parabolic velocity profile is not physically necessary but may accelerate the convergence of the solution as compared with a uniform flow. The flow at the outlet is assumed fully developed. Thus, the mathematical representations are

Inlet:

$$u(0, y) = U(1 - y^2) \quad (2.7)$$

$$v(0, y) = 0 \quad (2.8)$$

$$p(0,0) = 0 \quad (\text{as reference point}); \quad (2.9)$$

Outlet:

$$\frac{\partial u(x_{\infty}, y)}{\partial x} = 0 \quad (2.10)$$

$$\frac{\partial v(x_\infty, y)}{\partial x} = 0 \quad (2.11)$$

$$\frac{\partial p(x_\infty, y)}{\partial x} = 0 \quad (2.12)$$

To better understand the effect of slip condition, we need to simulate a non-slip condition as a benchmark. The non-slip wall boundary conditions are

$$u = v = 0 \quad (2.13)$$

$$\frac{\partial p}{\partial n} = 0 \quad (2.14)$$

The other boundary conditions are the same as for the slip-flow.

Introducing flow characteristic length L , characteristic velocity U , we non-dimensionalize the above governing equations by setting

$$x^* = x/L, \quad y^* = y/L, \quad u^* = u/U, \quad v^* = v/U, \quad p^* = (p - p_\infty)/(\rho U^2)$$

where, the * indicates non-dimensional variables. Hence, the final non-dimensional equations are as follows (omitting *):

$$\frac{\partial u}{\partial x} + \frac{\partial v}{\partial y} = 0 \quad (2.15)$$

$$u \frac{\partial u}{\partial x} + v \frac{\partial u}{\partial y} = -\frac{\partial p}{\partial x} + \frac{1}{\text{Re}} \left(\frac{\partial^2 u}{\partial x^2} + \frac{\partial^2 u}{\partial y^2} \right) \quad (2.16)$$

$$u \frac{\partial v}{\partial x} + v \frac{\partial v}{\partial y} = -\frac{\partial p}{\partial y} + \frac{1}{\text{Re}} \left(\frac{\partial^2 v}{\partial x^2} + \frac{\partial^2 v}{\partial y^2} \right) \quad (2.17)$$

where Re is the Reynolds number defined by

$$\text{Re} = \frac{\rho UL}{\mu} = \frac{UL}{\nu} \quad (2.18)$$

The boundary conditions are nondimensionalized in a similar way.

CHAPTER 3

MICRO-POLAR FLUID MODEL

3.1. Introduction

In continuum theories the mass is assumed to be a continuous measure, so that a continuous mass density ρ exists in a volume element dV that is infinitesimally small. However, this continuum concept of density breaks down when the volume compares with the cube of the mean free path, say ΔV^* . Thus mathematical idealization is meaningful only when dV models ΔV such that $\Delta V > \Delta V^*$. This continuum hypothesis is well illustrated by Batchelor (1967) under the conditions of everyday experience. In reality, the volume element dV cannot be infinitesimally small, but it should at least be insensitive to current available measuring instrument. Batchelor used term “sensitive” volume to describe this volume element, and we will follow this terminology in this thesis. The theory of micro-continuum fluids attempts to account for the microstructure that exists for $\Delta V < \Delta V^*$ by using a continuum description. The limiting volume ΔV^* could also be interpreted as a volume, containing microstructures such as suspended particles or even turbulent structures, for which the effects of microstructure cannot be accounted for by a continuum distribution.

In order to account for the microstructure that exists in the case of $\Delta V < \Delta V^*$, the deformations of the material within ΔV have to be considered. The macro mass element dM is assumed to contain continuous mass distributions such that the total macro mass

dM is the sum of all the masses in dV . Thus a continuous mass distribution is assumed to exist at each point of the macro element dV , such that the sum of the local masses over dV gives the total mass dM , and implies that the continuum theory is valid at each point of a macro element dV . Statistical averages then have to be taken to obtain the micro deformation theory of continuous media.

Eringen (1964) introduced an important tensor called the gyration tensor v_{ij} to determine the motion of a micro element relative to the center of mass of a macro element. This gyration tensor determines the motion at the micro element level. A micro-inertia moment i_{km} was correspondingly defined for the deformed body.

The kinematics of deformation measures for micro elements are established with the help of five theorems related to:

1. Micro-inertia moments, which satisfy specific partial differential equations that are the complements to the continuity equations of the hydrodynamics for micro-fluids and are named as the equations of conservation of micro-inertia moments
 2. The material derivative of micro-displacement differentials
 3. The material derivative of the square of arc length in the deformed body
 4. A necessary and sufficient condition for micro-rigid motion, which is that both deformation rate tensor and the second order micro-deformation rate tensor are zero
 5. A property of the micro-deformation rate tensors, which are objective tensors
- New principles are added to the basic principles of classical fluid dynamics,

which deal with:

1. Conservation of micro-inertia moments;
2. Balance of first stress moments.

A fluent medium called a simple micro fluid is defined by Eringen (1964) based on the property of its constitutive equations. It is a viscous fluid and in the simplest case of constitutively linear theory, this fluid contains 22 viscosity coefficients. The nonlinear Stokesian fluid turns out to be a special class of simple micro fluids.

The simple micro fluid is very general and allows for a wide variety of microstructures through the gyration tensor. It is almost untractable. A simpler subclass of micro fluids, in which a microstructure is still present, which is obtained by restricting the form of the gyration tensor, and which is more tractable, is the class of micro-polar fluids.

A fluid is micro-polar if, for all motions,

$$t_{klm} = -t_{kml}, \quad v_{kl} = -v_{lk} \quad (3.1)$$

where t_{klm} is the first stress moment tensor and v_{kl} the gyration tensor. Such fluids exhibit only micro-rotational effects and can support surface and body couples.

3.2. General Micro-Polar Fluid Model

In the general case of a micro fluid, the gyration tensor has nine independent components. For micro-polar fluids, the assumption of the skew-symmetry of v_{kl} reduces the number of independent components to three, so that, in addition to their usual convection due to the motion of the fluid element, points contained in a small element of

fluid can rotate about the centroid of the volume element in the average sense described by the gyration tensor $v_{kl} = -v_{lk}$. From theorem 3 of Eringen's paper (1964), micro-stretch of particles is not possible for this case so the directors are rigid.

The governing equations of the micro-polar fluid for isothermal, no body force, and couples flow are following in tensor forms, and their complete expansion form in Cartesian coordinates is in the appendix.

Continuity:

$$\frac{\partial \rho}{\partial t} + (\rho v_k)_{,k} = 0 \quad (3.2)$$

Conservation of micro-inertia:

$$\frac{\partial j_{kl}}{\partial t} + j_{kl,m} v_m + (\varepsilon_{krs} j_{rl} + \varepsilon_{lrs} j_{sk}) g_s = 0 \quad (3.3)$$

Balance of momentum:

$$-p_{,k} + (\lambda + \mu) v_{l,k} + (\mu + \kappa) v_{k,ll} + \kappa \varepsilon_{klm} g_{m,l} - \rho \dot{v}_k = 0 \quad (3.4)$$

Balance of momentum moments:

$$(\alpha + \beta) g_{l,k} + \gamma g_{k,ll} + \kappa \varepsilon_{klm} v_{m,l} - 2\kappa g_k - \rho \dot{j}_{kl} g_l = 0 \quad (3.5)$$

where t is time; ρ is mass density; v_k velocity vector; p pressure; g_k micro-rotation vector; j_{kl} micro-inertia moment tensor; α , β , γ , κ , λ and μ are the material constants; the notation $,k$ denotes the differential operator in space; $\dot{\quad}$ the operator of the material derivative; ε_{klm} is the third order alternating pseudo tensor. The micro-rotation vector g , and micro-inertia moment tensor j are defined based on the relations with the gyration tensor and the micro-inertia tensor, respectively.

$$v_{kl} = -\varepsilon_{klm} g_m \quad (3.6)$$

$$j_{kl} = i_{rr} \delta_{kl} - i_{kl} \quad (3.7)$$

The equations for conservation of energy and entropy inequality are omitted under the framework of isothermal fluid assumption.

The problem is now formulated in terms of a system of 17 partial differential equations. The above field equations are subjected to initial conditions and boundary conditions.

A useful concept termed micro-isotropic is introduced to simplify the model further. A micro fluid is said to be micro-isotropic if the micro-inertia moment is isotropic, i.e. if

$$i_{km} = i \delta_{km} \quad \text{or} \quad j_{kl} = j \delta_{kl} \quad (3.8)$$

where i, j are scalars and δ_{km} the Kronecker delta. Then, from equation (3.1) and Eringen's theorem 1 (1964), we have

$$\frac{D}{Dt}(i_{km}) = 0, \quad \text{or} \quad \frac{D}{Dt}(i) = 0 \quad (3.9)$$

and

$$\frac{D}{Dt}(j_{km}) = 0, \quad \text{or} \quad \frac{D}{Dt}(j) = 0 \quad (3.10)$$

Thus, on material lines,

$$i = \frac{1}{2} j = \text{const} \quad (3.11)$$

For micro-isotropic micro-polar fluids, the equation of conservation of micro-inertia is satisfied identically.

After applying micro-isotropic constraints, the equation number is reduced to 8 from 17 with 7 material coefficients.

3.3. Ad hoc Two-Dimensional Micro-Polar Fluid Model

The equations (3.2), (3.4), (3.5) with the corresponding initial and boundary conditions are still too complex to be practical. One main reason is that there are still 7 material constants ($j, \alpha, \beta, \gamma, \kappa, \lambda,$ and μ) that appear in the equations, and some of them are not so easily determined for a real fluid. We try to simplify further the micro-polar fluid onto our *ad hoc* two-dimensional micro-polar fluid model.

3.3.1. Basic Assumptions and Formulations

In addition to the isothermal, no body force, and micro-isotropic assumptions, additional constraints are assumed for this micro-polar fluid model.

Flow is steady. Thus all the terms with partial derivative with respect to time vanish.

Fluids are assumed incompressible. In this case $\rho = const$ and therefore the continuity equation reduces to

$$v_{k,k} = 0. \quad (3.12)$$

The term $(\lambda + \mu)v_{i,i}$ in the momentum equations represents the effect of compressibility of fluid, and thus vanishes. The λ , second-order viscosity coefficient, will not appear in the equations. This assumption agrees with the result of the incompressible case of Navier-Stokes equations.

Flows are two-dimensional. We consider the flows (u, v) in the x - y plane, and then only the component normal to the x - y plane ($k=3$) of the micro-rotation vector g_k appears in the momentum equation, and the other components will not be taken into account.

The term $(\alpha + \beta)g_{i,k}$ in the equation of momentum moments vanishes as $k=3$ from the two-dimension assumption. Therefore, the spin gradient viscosity coefficient, α , β will not appear in the equations.

Thus the unknowns of the *ad hoc* theory are now 4 in number, namely,

$$u, v, g_3, p.$$

satisfying 4 reduced equations with 4 material coefficients, which are (omitting the subscript 3 of g):

Continuity:

$$\frac{\partial u}{\partial x} + \frac{\partial v}{\partial y} = 0 \quad (3.13)$$

Balance of momentum (x- component):

$$u \frac{\partial u}{\partial x} + v \frac{\partial u}{\partial y} = -\frac{1}{\rho} \frac{\partial p}{\partial x} + \frac{1}{\rho} (\mu + \kappa) \left(\frac{\partial^2 u}{\partial x^2} + \frac{\partial^2 u}{\partial y^2} \right) + \frac{\kappa}{\rho} \frac{\partial g}{\partial y} \quad (3.14)$$

Balance of momentum (y- component):

$$u \frac{\partial v}{\partial x} + v \frac{\partial v}{\partial y} = -\frac{1}{\rho} \frac{\partial p}{\partial y} + \frac{1}{\rho} (\mu + \kappa) \left(\frac{\partial^2 v}{\partial x^2} + \frac{\partial^2 v}{\partial y^2} \right) - \frac{\kappa}{\rho} \frac{\partial g}{\partial x} \quad (3.15)$$

Balance of angular momentum:

$$u \frac{\partial g}{\partial x} + v \frac{\partial g}{\partial y} = -\frac{2\kappa}{\rho j} g + \frac{\gamma}{\rho j} \left(\frac{\partial^2 g}{\partial x^2} + \frac{\partial^2 g}{\partial y^2} \right) + \frac{\kappa}{\rho j} \left(\frac{\partial v}{\partial x} - \frac{\partial u}{\partial y} \right) \quad (3.16)$$

where x, y are the coordinates in streamwise and normal directions, respectively. u, v are the corresponding velocities in x, y directions, p the pressure, g the component of the gyration vector normal to the $x-y$ plane, and j the micro-inertia density. Further, ρ is the fluid density, μ the classical bulk viscosity, κ the micro-rotation parameter (also known as the coefficient of gyro-viscosity and as the vortex viscosity), and γ is the spin-gradient viscosity.

The momentum equations simplify to the Navier-Stokes equations when $\kappa=0$.

3.3.2. Relations among the Material Constants

The above viscosity parameters are not independent. A further analysis can give useful relations among them.

It is clear that g is the total spin of the microstructure of fluid media in the flow field. It is possible that in some cases the microstructure effects become negligible and the flow behaves like a regular viscous flow. Therefore, if we demand that g be a possible solution, then it is only possible if

$$\gamma = (\mu + \kappa / 2)j \quad (3.17)$$

which gives some relationship between the coefficients of viscosity and micro-inertia. All material constants j, μ, κ, γ are non-negative.

The derivation of this relationship has been given by Olmstead and Majumdar (1983) for the Oseen flow problem, and also by Ahmadi (1976).

The micro-inertia density j is defined as

$$\rho j dv = \frac{2}{3} \int_{dv} \rho' \chi \chi dv' \quad (3.18)$$

where dv and dv' are the sensitive volume and micro atomic volume elements, respectively, and χ is the distance measured from the mass center of the sensitive volume element. ρ' is the mass density at any point inside it. Two densities are identical since the flow is in single-phase in our consideration. Assume the sensitive volume element is spherical and its diameter is d , evaluating the integral yields

$$j = d^2 / 10. \quad (3.19)$$

It is then that the micro-inertia is proportional to the square of the length scale of the sensitive volume element. The length scale of that sensitive volume element or microstructure element is defined as the smallest volume for which average quantity, such as velocity, density, gyration, has statistical meaning.

Let f be a property of a particle; then the average or statistical mean of f in the micro sensitive volume element is

$$\bar{f} = \frac{\sum_{i=1}^n f_i}{n} \quad (3.20)$$

where f_i represents the property f of individual molecules, and n represents the total number of molecules in the microstructure element.

The variance of the f has relation with the variance of the mean of f :

$$\frac{V(f)}{n} = V(\bar{f}). \quad (3.21)$$

Further, assume c to be the coefficient for variation for the mean, we have

$$\sqrt{\frac{V(f)}{n}} = c \cdot \bar{f}. \quad (3.22)$$

Introducing another parameter, standard deviation s , as

$$s = \sqrt{V(f)}, \quad (3.23)$$

we have

$$n = \left(\frac{s}{\bar{f}c}\right)^2. \quad (3.24)$$

We assume $c = 0.005$, $s/\bar{f} = 0.2$, then $n = 1600$. This assumption means that the micro-element must have at least 1600 molecules in the “sensitive volume” to make the variation in the mean not greater than 0.5%.

If Loschmidt’s number applies, then the sensitive volume characteristic length d can be determined from n .

However, the difficulty still exists in determining the microstructure characteristic length. For most suspension flows, determination of this length scale was proposed by Eringen (1980). The magnitude order is about 10^{-3} to 10^{-5} cm for flow characteristic length $L \geq 1$ cm and flow characteristic velocity $U \geq 1$ cm/sec. Kolpashchikov *et al.* (1983) deduced formulae for micro-polar fluid material constants as well as a boundary condition parameter from experimental data. What was needed were measurements of the volumetric flow rate and the pressure gradient in channel flow with different channel dimensions. The explicit microstructure characteristic length still remains unanswered. Kline and Allen (1970) discussed the effects of fluid microstructure on the unsteady flow. They investigated especially the limiting cases, i.e., maximum effects of microstructure and dilute suspensions. However, what the appropriate length scale is in-between was unanswered. For micro-scale flows, even these kinds of relations are untouched. Clearly,

two limiting constraints for micro-scale flow exist. The minimum effect of microstructure is shown when its length scale decreases until it approaches the order of magnitude of the free path length while its length approaches the flow length.

We introduce the relation of free path length to the microstructure characteristic length with the help of another parameter m as follows,

$$d = m\lambda \quad (3.25)$$

where, λ is the molecule free path length. Since the microstructure characteristic length is less than the flow characteristic length, $d < L$, where L is the flow characteristic length; substituting Knudsen number $Kn = \lambda/L$, we have

$$Kn \leq \frac{1}{m} \quad (3.26)$$

The upper bound of the reciprocal of parameter m may be determined statistically from d .

Therefore, two different length scales appear in the model, the flow characteristic length and the microstructure characteristic length. In micro-scale flow, such as micro-channel flow, the characteristic length scale of the flow usually may be chosen as the height (or width) of the channel since it accommodates well the length scales including gradients of density, velocity, pressure, and temperature within the flow. The microstructure characteristic length may vary with the modeling parameter m and will be examined under the simulation tests.

3.3.3. Non-Dimensionalized Version

We now can non-dimensionalize equations (3.13 – 3.16) by setting

$$x^* = x/L, \quad y^* = y/L, \quad u^* = u/U, \quad v^* = v/U \quad (3.27)$$

$$g^* = gL/U, \quad p^* = (p - p_\infty)/(\rho U^2)$$

where, the * indicates non-dimensional variables, L is the flow characteristic length, U the velocity, p_∞ is some representative value of the modified pressure in the field. Hence, the final non-dimensional equations are as follows (omitting *):

Continuity:

$$\frac{\partial u}{\partial x} + \frac{\partial v}{\partial y} = 0 \quad (3.28)$$

Balance of momentum (x-component)

$$u \frac{\partial u}{\partial x} + v \frac{\partial u}{\partial y} = -\frac{\partial p}{\partial x} + \frac{1+k}{\text{Re}} \left(\frac{\partial^2 u}{\partial x^2} + \frac{\partial^2 u}{\partial y^2} \right) + \frac{k}{\text{Re}} \frac{\partial g}{\partial y} \quad (3.29)$$

Balance of momentum (y-component)

$$u \frac{\partial v}{\partial x} + v \frac{\partial v}{\partial y} = -\frac{\partial p}{\partial y} + \frac{1+k}{\text{Re}} \left(\frac{\partial^2 v}{\partial x^2} + \frac{\partial^2 v}{\partial y^2} \right) - \frac{k}{\text{Re}} \frac{\partial g}{\partial x} \quad (3.30)$$

Balance of angular momentum:

$$u \frac{\partial g}{\partial x} + v \frac{\partial g}{\partial y} = -\frac{20k}{\text{Re}(m\text{Kn})^2} g + \frac{1+k/2}{\text{Re}} \left(\frac{\partial^2 g}{\partial x^2} + \frac{\partial^2 g}{\partial y^2} \right) + \frac{10k}{\text{Re}(m\text{Kn})^2} \left(\frac{\partial v}{\partial x} - \frac{\partial u}{\partial y} \right) \quad (3.31)$$

where Re is the Reynolds number defined by

$$\text{Re} = \frac{\rho UL}{\mu}, \quad (3.32)$$

and k is the ratio of vortex viscosity to translational viscosity, i.e.

$$k = \frac{\kappa}{\mu} \quad (3.33)$$

3.3.4. Boundary Conditions

Equations (3.28 – 3.31) are subjected to boundary conditions. The solution domain has three kinds of boundaries present, namely inlet, outlet, and walls.

Along the inlet boundary, all conventional fluid and flow properties must be known and prescribed like that of a Navier-Stokes solution. The specification of the micro-rotation variable is not so direct since we lack physical information. Hence, we assume it is determined from other flow properties by satisfying the equation of angular momentum. For a long channel flow, the fully developed condition may apply.

Across the outlet, the flow direction must be uniformly out of the domain. In channel flow, the boundary is usually positioned in such a way that the flow there can be assumed to be reasonably fully developed. In this case, zero streamwise gradients of all properties may be implemented with little danger of any adverse effects far upstream of that boundary.

At the walls, the velocity, including both the u , v components, is zero. The micro-rotation variable is assigned a relation with the surface shear stress, as

$$g = -n \frac{\partial u}{\partial y} \quad (3.34)$$

where, n is a parameter related to micro-rotation vector and the shear stress. The value $n=0$ corresponds to the case where the particle density is sufficiently great that micro-elements close to the wall are unable to rotate. The value $n=0.5$ is indicative of weak concentrations, and when $n=1$ flows are believed to represent turbulent boundary layers (Rees & Bassom, 1996). n lies between these two extremes.

The gradient of pressure normal to the wall surface is assumed to be zero.

3.3.5. Unidirectional Flow Solution

It is important to know whether the model has a physical solution or not. We choose a steady locally fully developed micro-channel flow as a test. After applying the locally fully developed flow assumption, the term $\partial u/\partial x$, $\partial v/\partial x$, $\partial g/\partial x$ vanish, and $\partial p/\partial x$ becomes constant. The partial differential operator $\partial/\partial y$ is identical to the differential operator d/dy . Substituting $\partial u/\partial x$ into the continuity equation, it follows at once that $v=0$. Thus flow is unidirectional. The governing equations, given by (3.29 – 3.31), reduces to

$$-\frac{d p}{d x}+(\mu+\kappa)\frac{d^2 u}{d y^2}+\kappa\frac{d g}{d y}=0 \quad (3.35)$$

$$-2\kappa g+\gamma\frac{d^2 g}{d y^2}-\kappa\frac{d u}{d y}=0 \quad (3.36)$$

The corresponding boundary conditions are

At center line:

$$y=0 : du/dy=0, \quad g=0; \quad (3.37)$$

At upper wall:

$$y=1 : u=0, \quad g=-n du/dy. \quad (3.38)$$

The solution of this problem is

$$u = -\frac{1}{2\mu+\kappa}\frac{\partial p}{\partial x}\left[-\frac{\kappa(2n+1)}{\zeta(e^\zeta-e^{-\zeta})(n\kappa-\kappa-\mu)}(e^{\zeta y}+e^{-\zeta y})+y^2+\frac{\kappa(2n+1)(e^\zeta+e^{-\zeta})}{\zeta(e^\zeta-e^{-\zeta})(n\kappa-\kappa-\mu)}-1\right] \quad (3.39)$$

and

$$g = \frac{1}{2\mu+\kappa}\frac{\partial p}{\partial x}\left[-\frac{(2n+1)\mu+\kappa}{\zeta(e^\zeta-e^{-\zeta})(n\kappa-\kappa-\mu)}(e^{\zeta y}-e^{-\zeta y})-y\right] \quad (3.40)$$

where,

$$\zeta = \sqrt{\frac{\kappa(2\mu + \kappa)}{\gamma(\mu + \kappa)}} \quad (3.41)$$

The solution of a plane Poiseuille flow may be obtained by putting $\kappa=0$ in equation (3.39), in which case, equations (3.35) and (3.36) are decoupled and the solution of g is solved by equation (3.36) and thus solution (3.40) does not apply. It follows that the velocity will not be affected by the micro-rotation and *vice versa*. The value of κ is a measure of the effect of the microstructure on the macroscopic velocity and stress fields.

If $\gamma=0$, the solution of g is immediately obtained from equation (3.36), and it is identical to the local vorticity. Thus, the couple stress will be zero irrespective of variation of velocity and micro-rotation g fields.

Even though all the effects are present simultaneously, the motion may be assumed to be affected by three parts. First, viscous action, measured by μ ; second, the effect of couple stresses, measured by γ ; and third, the direct coupling of the microstructure to the velocity field, measured by κ . These three constants can have any nonnegative value and then the ratio of any two of them, which can measure the relative strength of their property effects, can have any nonnegative value.

The boundary condition coefficient n can also affect the solutions (3.35) and (3.36). But since the variation of n is confined between 0 and 1, the effect will not change the characteristic of the solution, and is not significant. An arbitrary chosen value of n should reflect the property of the solution.

The variation of the velocity profile with κ/u for $n=1/2$ and $\gamma=1$ is shown in Figure 3.1.

The maximum velocity u occurs at $y=0$ and it varies with κ/u . It is not necessary to have a maximum for $\kappa=0$.

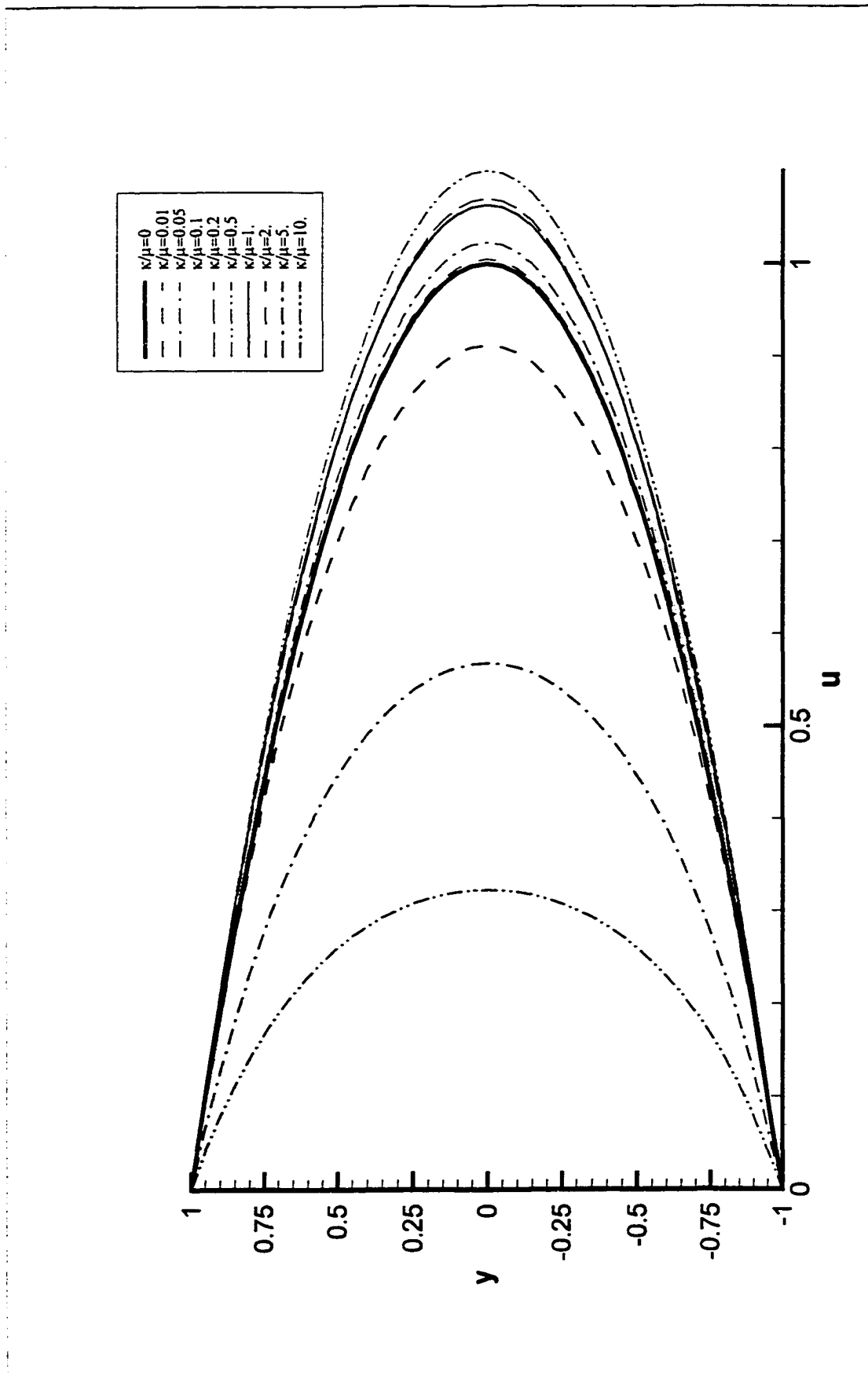


Figure 3.1. Variation of the velocity $u(y)$ with κ/μ for $n=1/2$ and $\gamma=1$

CHAPTER 4

NUMERICAL METHOD

4.1. Introduction

The governing equations of micro-polar fluid possess similar properties to the Navier-Stokes equations, where the equations of the balance of momentum can be divided according to convection, diffusion, and source terms. Therefore, classical CFD methods are applicable to this kind of system.

Among the various numerical methods for computing incompressible flows, the primitive variable approach offers the fewest complication in extending two-dimensional calculations to three-dimensions. It also has the advantage of obtaining directly the solution of commonly known physical variables, velocity and pressure. A difficulty with this approach is in solving the pressure field due to the absence of an equation explicitly governing the pressure. Rather, the pressure is implied by the continuity equation, which imposes a compatibility condition on the velocity field. Patankar (1980) introduced a revised version of an algorithm for handling the velocity-pressure linkage, namely, the "Semi Implicit Method for Pressure Linked Equations", which is widely used in turbulent flow and heat transfer computations.

Another treatment of solving the pressure field is by the projection method, proposed independently by Chorin in 1968 and by Temam in 1969. The explicit version of such a method was presented by Fortin *et al.* in 1971, and detailed by Peyret and

Taylor (1990). We employ this method in this work.

4.2. Pseudo-Time-Dependent Method

We rewrite the governing equations for both the Navier-Stokes system in chapter 2 and the micro-polar fluid model in chapter 3 as follows:

$$\nabla \cdot \mathbf{V} = 0 \quad (4.1)$$

$$\nabla p + \mathbf{F}(\mathbf{V}, \mathbf{g}) = 0 \quad (4.2)$$

$$\mathbf{G}(\mathbf{V}, \mathbf{g}) = 0 \quad (4.3)$$

where, $\mathbf{F}(\mathbf{V}, \mathbf{g})$ is all terms except pressure for balance of momentum equation and \mathbf{g} is null in the case of the Navier-Stokes system; $\mathbf{G}(\mathbf{V}, \mathbf{g})$ expresses all terms for balance of angular momentum and appears only for the micro-polar fluid model. Thus, the governing equations for these two models are unified and our discussion will be made in general.

The main difficulties associated with the solution of equations (4.1-4.3) are the following:

First, the presence of the constraint $\nabla \cdot \mathbf{V} = 0$, which must be satisfied at any time, does not allow the use of a simple explicit method that avoids solution of an algebraic system of equations.

Second, there is a lack of boundary condition for the pressure.

We notice the fact that the solution of a steady equation can be obtained by solving its associate unsteady equation as the limit when the steady state $\partial/\partial t$ is reached. The method is then called the pseudo-time-dependent method because the time t involved

has no physical meaning.

Equations (4.2) and (4.3) then become:

$$\frac{\partial \mathbf{V}}{\partial t} + \nabla p + \mathbf{F}(\mathbf{V}, g) = 0 \quad (4.4)$$

$$\frac{\partial g}{\partial t} + \mathbf{G}(\mathbf{V}, g) = 0 \quad (4.5)$$

Equations (4.1), (4.4), and (4.5) become the governing equations of the pseudo-time-dependent problem.

The object of the pseudo-time-dependent method is to obtain a steady state solution, characterized by

$$\frac{1}{\Delta t} |u^{n+1} - u^n| < \varepsilon_u, \quad \frac{1}{\Delta t} |v^{n+1} - v^n| < \varepsilon_v, \quad \frac{1}{\Delta t} |p^{n+1} - p^n| < \varepsilon_p, \quad \frac{1}{\Delta t} |g^{n+1} - g^n| < \varepsilon_g$$

where ε_u , ε_v , ε_p , and ε_g are small numbers. The possibility of obtaining convergence is based upon two facts: (1) the solution of a perturbed time-dependent fluid dynamic system is toward the solution of the steady problem concerning the limit when $t \rightarrow \infty$; and (2) the consistency and stability of the scheme employed in the projection method. The consistency follows from the construction of the finite-difference scheme.

4.3. Projection Method

The most common method used to solve the unsteady equations deals with a Poisson equation for the pressure and with the momentum equations for the computation of velocity. A method called the projection method, in some cases where explicit schemes are used, is the prototype of such an implementation.

The projection method is a fractional step method in time. It can be explicit with

first-order accuracy in time.

Introducing a provisional value \mathbf{V}^* , we split the equation (4.4) as

$$\frac{\mathbf{V}^* - \mathbf{V}^n}{\Delta t} + \mathbf{F}(\mathbf{V}^n, \mathbf{g}^n) = 0 \quad (4.6)$$

$$\frac{\mathbf{V}^{n+1} - \mathbf{V}^*}{\Delta t} + \nabla p^{n+1} = 0 \quad (4.7)$$

Equation (4.6) is the momentum equation without a pressure gradient. Note that only the discretization in time is considered here. Equation (4.7) establishes the relation between the correction of velocity and the pressure gradient. Equation (4.1) is expressed as

$$\nabla \cdot \mathbf{V}^{n+1} = 0 \quad (4.8)$$

to help enforce the equations.

By taking the divergence of equation (4.7) and by making use of (4.8) which states that \mathbf{V}^{n+1} must be a divergence-free vector, we get the Poisson equation for pressure p , i.e.:

$$\nabla^2 p^{n+1} = \frac{1}{\Delta t} \nabla \cdot \mathbf{V}^* \quad (4.9)$$

After that, equation (4.5) is also explicitly discretized in time by the Euler's scheme as

$$\frac{\mathbf{g}^{n+1} - \mathbf{g}^n}{\Delta t} + \mathbf{G}(\mathbf{V}^n, \mathbf{g}^n) = 0 \quad (4.10)$$

The boundary condition for p is obtained by projecting the vector equation (4.7) on the outward normal unit \mathbf{N} to the boundary Γ . Thus, we obtain the Neumann condition

$$\left(\frac{\partial p}{\partial N}\right)_{\Gamma}^{n+1} = -\frac{1}{\Delta t} (\mathbf{V}_{\Gamma}^{n+1} - \mathbf{V}_{\Gamma}^*) \cdot \mathbf{N} \quad (4.11)$$

where \mathbf{V}_{Γ}^* is the value of \mathbf{V}^* on Γ , and \mathbf{V}^* is not yet defined. The condition of compatibility for the Neumann problem is

$$\frac{1}{\Delta t} \int_{\Omega} \nabla \cdot \mathbf{V}^* ds = -\frac{1}{\Delta t} \int_{\Gamma} (\mathbf{V}^{n+1} - \mathbf{V}^*) \cdot \mathbf{N} dl \quad (4.12)$$

where Ω is the domain bounded by Γ . It expresses the factor that the velocity on the boundary Γ has a zero total flux. It is important that the discretization with respect to space conserves the above compatibility condition.

The algorithm is then derived as follows,

1. Initialize the variables at time t or step n ;
2. Solve equation (4.6) to obtain \mathbf{V}^* ;
3. Solve equation (4.9) to obtain p^{n+1} ;
4. Solve equation (4.7) to obtain \mathbf{V}^{n+1} ;
5. Solve equation (4.10) to obtain g^{n+1} ;
6. Go to step 2 until the convergent condition is met.

For the case of the Navier-Stokes equations, step 5 should be skipped. That step 5 can be performed simultaneously with step 2 to step 4 depends on the adopted scheme.

The projection method has a feature that the numerical solution is independent of the value \mathbf{V}_{Γ}^* ; in another word, we do not need the boundary condition for \mathbf{V}^* . This assertion is clear because (1) \mathbf{V}^* at inner points is independent of \mathbf{V}_{Γ}^* since it is calculated by an explicit scheme; (2) the value $\mathbf{V}_{\Gamma}^* \cdot \mathbf{N}$ appears in the Neumann problem

simultaneously in the right-hand side of the Poisson equation (4.9), and in the Neumann condition (4.11) and it cancels identically.

To prove this assertion, it is sufficient to analyze the discretization of (4.9) for points near the boundary Γ , since V_Γ^* appears in the problem only for these points.

Applying the staggered grids storage, the discretization of (4.9) is

$$\begin{aligned} & \frac{1}{\Delta x^2} (p_{i-1,1}^{n+1} - 2p_{i,1}^{n+1} + p_{i+1,1}^{n+1}) + \frac{1}{\Delta y^2} (p_{i,0}^{n+1} - 2p_{i,1}^{n+1} + p_{i,2}^{n+1}) \\ &= \frac{1}{\Delta t} \left[\frac{1}{\Delta x} (u_{i+\frac{1}{2},1}^\bullet - u_{i-\frac{1}{2},1}^\bullet) + \frac{1}{\Delta y} (v_{i,\frac{1}{2}}^\bullet - v_{i,\frac{1}{2}}^\bullet) \right] \end{aligned} \quad (4.13)$$

and the Neumann condition (4.11) is

$$\frac{1}{\Delta y} (p_{i,1}^{n+1} - p_{i,0}^{n+1}) = -\frac{1}{\Delta t} (v_{i,0}^{n+1} - v_{i,0}^\bullet) \quad (4.14)$$

Figure 4.1 shows the geometrical distribution of grids.

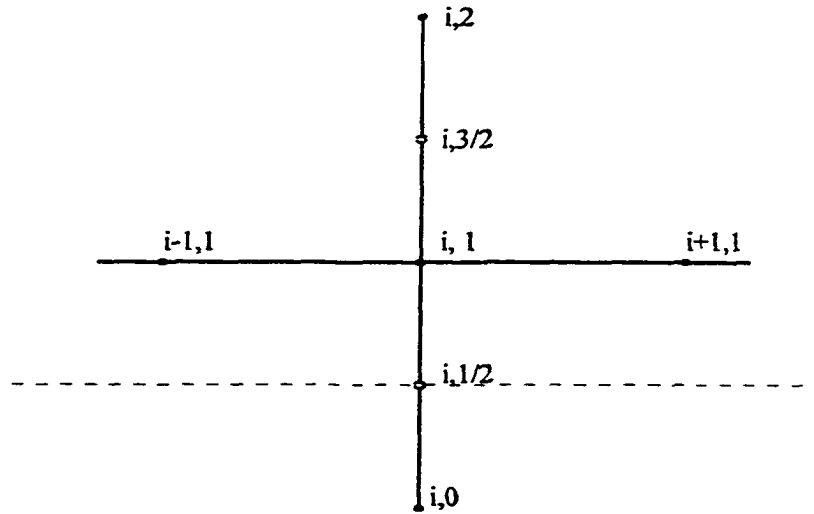


Figure 4.1 Geometrical distribution of grids near a boundary.

The quantity $v_{i,1/2}^*$ is the value of v_{Γ}^* at boundary point $(i, 1/2)$. Now, it is easy to see that, when the value of $p_{i,1}^{n+1} - p_{i,0}^{n+1}$ given by (4.14) is substituted into (4.13), the unknown quantity $v_{i,1/2}^*$ cancels from both sides of equation (4.13). From this, one concludes that the solution is independent of the value $v_{i,1/2}^*$ or v_{Γ}^* . In particular, we can choose $v_{i,0}^{n+1} = v_{i,0}^*$ and get a zero normal difference for the pressure on Γ . However, it must be clear that this zero-derivative condition is purely numerical and does not imply that the real pressure gradient is zero.

It is worth note that the time split scheme is equivalent to solving the momentum equation as one equation. If \mathbf{V}^* is eliminated from (4.6) and (4.7) we obtain the scheme

$$\frac{\mathbf{V}^{n+1} - \mathbf{V}^n}{\Delta t} + \mathbf{F}(\mathbf{V}^n, \mathbf{g}^n) + \nabla p^{n+1} = 0 \quad (4.15)$$

which is a first-order approximation in time of the momentum equation. Therefore, the stability of the projection method is the stability of the difference equation associated with (4.15). The stability conditions depend partly on the discretization approximation of the convective term in \mathbf{F} .

4.4. Discretization

Since time has no physical meaning here, a very simple explicit first-order scheme in time as discussed above is considered. The spatial discretization makes use of the staggered grids, which is extended from conventional CFD applications, such as TEAM (Huang & Leschziner, 1984), MAC (Marker-And-Cell). The different physical variables are stored in different location on the grids, and are shown in Figure 4.2.

The approximation of the convective terms employs first-order upwind scheme; the approximation of the diffusive and the other terms uses second-order centered scheme.

$$u \frac{\partial u}{\partial x} \Big|_{i,j} = \frac{1}{\Delta x} u_{i,j} \left((u_{i,j} - u_{i-1,j}) * \text{sgn}(u_{i,j}) + (u_{i+1,j} - u_{i,j}) * \text{sgn}(-u_{i,j}) \right) \quad (4.16)$$

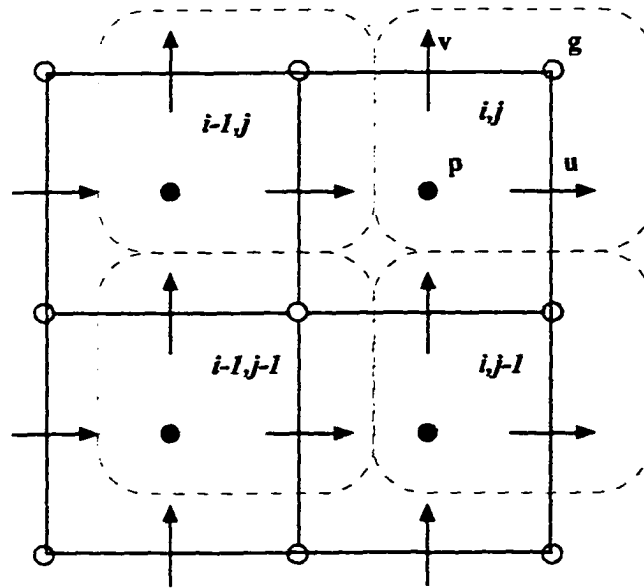


Figure 4.2 The staggered grids

$$v \frac{\partial u}{\partial y} \Big|_{i,j} = \frac{1}{\Delta y} v_{i+1/2,j-1/2} \left((u_{i,j} - u_{i,j-1}) * \text{sgn}(v_{i+1/2,j-1/2}) + (u_{i,j+1} - u_{i,j}) * \text{sgn}(-v_{i+1/2,j-1/2}) \right) \quad (4.17)$$

where

$$v_{i+1/2,j-1/2} = \frac{1}{4} (v_{i,j} + v_{i+1,j} + v_{i,j-1} + v_{i+1,j-1}) \quad (4.18)$$

$$\frac{\partial^2 u}{\partial x^2} \Big|_{i,j} = \frac{1}{(\Delta x)^2} (u_{i-1,j} - 2u_{i,j} + u_{i+1,j}) \quad (4.19)$$

$$\left. \frac{\partial^2 u}{\partial y^2} \right|_{i,j} = \frac{1}{(\Delta y)^2} (u_{i,j-1} - 2u_{i,j} + u_{i,j+1}) \quad (4.20)$$

$$\left. \frac{\partial g}{\partial y} \right|_{i,j} = \frac{1}{\Delta y} (g_{i,j} - g_{i,j-1}) \quad (4.21)$$

$$\left. u \frac{\partial v}{\partial x} \right|_{i,j} = \frac{1}{\Delta x} u_{i-1/2,j+1/2} \left((v_{i,j} - v_{i-1,j}) * \text{sgn}(u_{i-1/2,j+1/2}) + (v_{i+1,j} - v_{i,j}) * \text{sgn}(-u_{i-1/2,j+1/2}) \right) \quad (4.22)$$

where

$$u_{i-1/2,j+1/2} = \frac{1}{4} (u_{i,j} + u_{i-1,j} + u_{i,j+1} + u_{i-1,j+1}) \quad (4.23)$$

$$\left. v \frac{\partial v}{\partial y} \right|_{i,j} = \frac{1}{\Delta y} v_{i,j} \left((v_{i,j} - v_{i,j-1}) * \text{sgn}(v_{i,j}) + (v_{i,j+1} - v_{i,j}) * \text{sgn}(-v_{i,j}) \right) \quad (4.24)$$

$$\left. \frac{\partial^2 v}{\partial x^2} \right|_{i,j} = \frac{1}{(\Delta x)^2} (v_{i-1,j} - 2v_{i,j} + v_{i+1,j}) \quad (4.25)$$

$$\left. \frac{\partial^2 v}{\partial y^2} \right|_{i,j} = \frac{1}{(\Delta y)^2} (v_{i,j-1} - 2v_{i,j} + v_{i,j+1}) \quad (4.26)$$

$$\left. \frac{\partial g}{\partial x} \right|_{i,j} = \frac{1}{\Delta x} (g_{i,j} - g_{i-1,j}) \quad (4.27)$$

$$\left. u \frac{\partial g}{\partial x} \right|_{i,j} = \frac{1}{\Delta x} u_{i,j+1/2} \left((g_{i,j} - g_{i-1,j}) * \text{sgn}(u_{i,j+1/2}) + (g_{i+1,j} - g_{i,j}) * \text{sgn}(-u_{i,j+1/2}) \right) \quad (4.28)$$

where

$$u_{i,j+1/2} = \frac{1}{2} (u_{i,j} + u_{i,j+1}) \quad (4.29)$$

$$v \frac{\partial g}{\partial y} \Big|_{i,j} = \frac{1}{\Delta y} v_{i+1/2,j} \left((g_{i,j} - g_{i,j-1}) * \text{sgn}(v_{i+1/2,j}) + (g_{i,j+1} - g_{i,j}) * \text{sgn}(-v_{i+1/2,j}) \right) \quad (4.30)$$

where

$$v_{i+1/2,j} = \frac{1}{2} (v_{i,j} + v_{i+1,j}) \quad (4.31)$$

$$\frac{\partial^2 g}{\partial x^2} \Big|_{i,j} = \frac{1}{(\Delta x)^2} (g_{i-1,j} - 2g_{i,j} + g_{i+1,j}) \quad (4.32)$$

$$\frac{\partial^2 g}{\partial y^2} \Big|_{i,j} = \frac{1}{(\Delta y)^2} (g_{i,j-1} - 2g_{i,j} + g_{i,j+1}) \quad (4.33)$$

$$\frac{\partial v}{\partial x} \Big|_{i,j} = \frac{1}{\Delta x} (v_{i+1,j} - v_{i,j}) \quad (4.34)$$

$$\frac{\partial u}{\partial y} \Big|_{i,j} = \frac{1}{\Delta y} (u_{i,j+1} - u_{i,j}) \quad (4.35)$$

The function $\text{sgn}(x)$ is defined as

$$\text{sgn}(x) = \begin{cases} 0 & \text{if } x \leq 0 \\ 1 & \text{if } x > 0 \end{cases} \quad (4.36)$$

4.5. Treatment of Boundary Conditions

We need to make a special treatment of boundary conditions for staggered grids. Since the variables are not stored at the same points, virtual points are needed for some variables in implementation. Figure 4.3 shows the distribution of boundary Γ and grids of the lower-left corner.

The boundary Γ coincides with the storage location of u and g for $i=0$, and does

so also with the storage location of v and g for $j=0$. Therefore, the pressure p is not defined on the boundary and this fact is essential: solving the pressure field via the Poisson equation can be applied to the first points adjacent to the boundary without modification. But we may fix a reference point for p at any location for numerical reason. The algorithm allows the computation of the pressure without requiring the explicit prescription of boundary conditions for it. The variable g is defined at boundaries and thus no special numerical treatment of boundary conditions is needed for it.

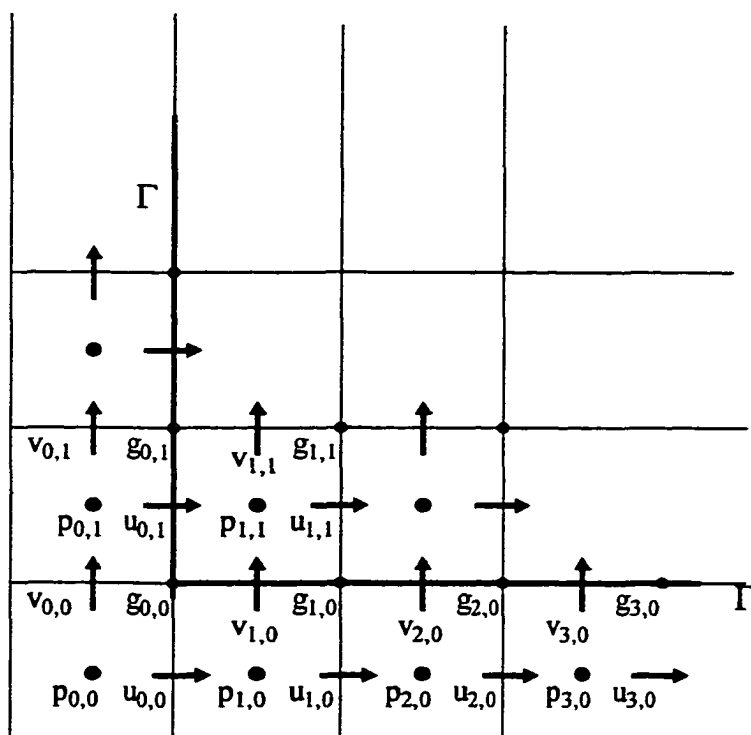


Figure 4.3 The staggered grids near a boundary

The staggered grids bring disadvantages in velocity boundary treatment. As seen in Figure 4.3, difficulties occur when computing $u_{i,1}$ and $v_{i,j}$. A way so-called reflection

technique is used here by introducing virtual values $u_{i,0}$ and $v_{0,j}$.

Along $j=l$, we write the velocity component $u_{1/2}$ on as the mean value of the two velocities u_0 and u_1 , so that

$$u_0 = 2u_{1/2} - u_1 \quad (4.37)$$

i.e., u_0 is defined by a linear extrapolation.

Same treatments apply to the other boundaries.

CHAPTER 5

TWO-DIMENSIONAL MICRO-CHANNEL FLOW

5.1. Description of Simulations

To illustrate the use of the present methods, we apply them to the developing flow in a two dimensional micro-channel, as shown in Figure 5.1. This flow situation is found in micro-components, and in many experiments. It was also analyzed by many authors, and we have their solutions for comparison.

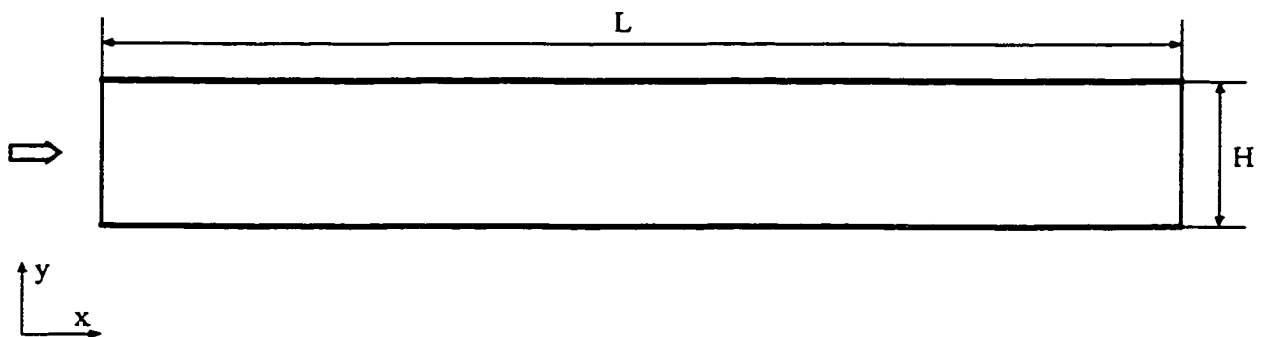


Figure 5.1 Physical domain for micro-channel flow

Flow parameters cover Reynolds number that ranges from 10 to 2000. The channel length is 20 times its height, and the flow is assumed fully developed at the exit. Typical results show that this value of ratio of channel length to channel height is large enough to obtain a fully-developed flow. Examples in Peyret & Taylor (1990) also gave a similar conclusion for the Navier-Stokes solution in the case of non-slip flow.

No apparent Knudsen number needs to be specified since the characteristic length is given, but its effect will be in the model parameters.

Numerical computations have been performed for both slip-flow and micro-polar fluid models. The computations were performed on a SUN/Sparc workstation with four 450MHz processors at Louisiana Tech University. C++ was used in programming, and TECPLOT in data post-processing. A uniform rectangular grid of 502×27 nodes was used for all runs except those made to examine the effect of the grid size. The solution is regarded as steady state when the pseudo-time reaches 10 with time interval 0.0001, where $\varepsilon < 10^{-5}$ is satisfied. Typically, 20 hours of CPU time is needed for each run. The CPU time is one of the main reasons for us to choose the current grid number.

5.2. Simulation Results of Slip-Flow Model

Figure 5.2 presents the prediction of pressure variation for various grid sizes. As can be expected, the successive refinement of the grid takes us asymptotically towards the correct solution. We can conclude that a 25 grid in the y direction gives us a sufficiently accurate solution for this problem.

Figure 5.3 shows the variation of the pressure with the distance along the channel for various Reynolds numbers. Non-slip boundary conditions are prescribed by setting $Kn=0$ in boundary condition treatments. The linear pressure variation means a constant pressure drop. The result is in agreement with the analytical prediction.

Figure 5.4 shows the variation of the pressure with the distance along the channel for various Knudsen numbers. The Reynolds number is 100. The momentum

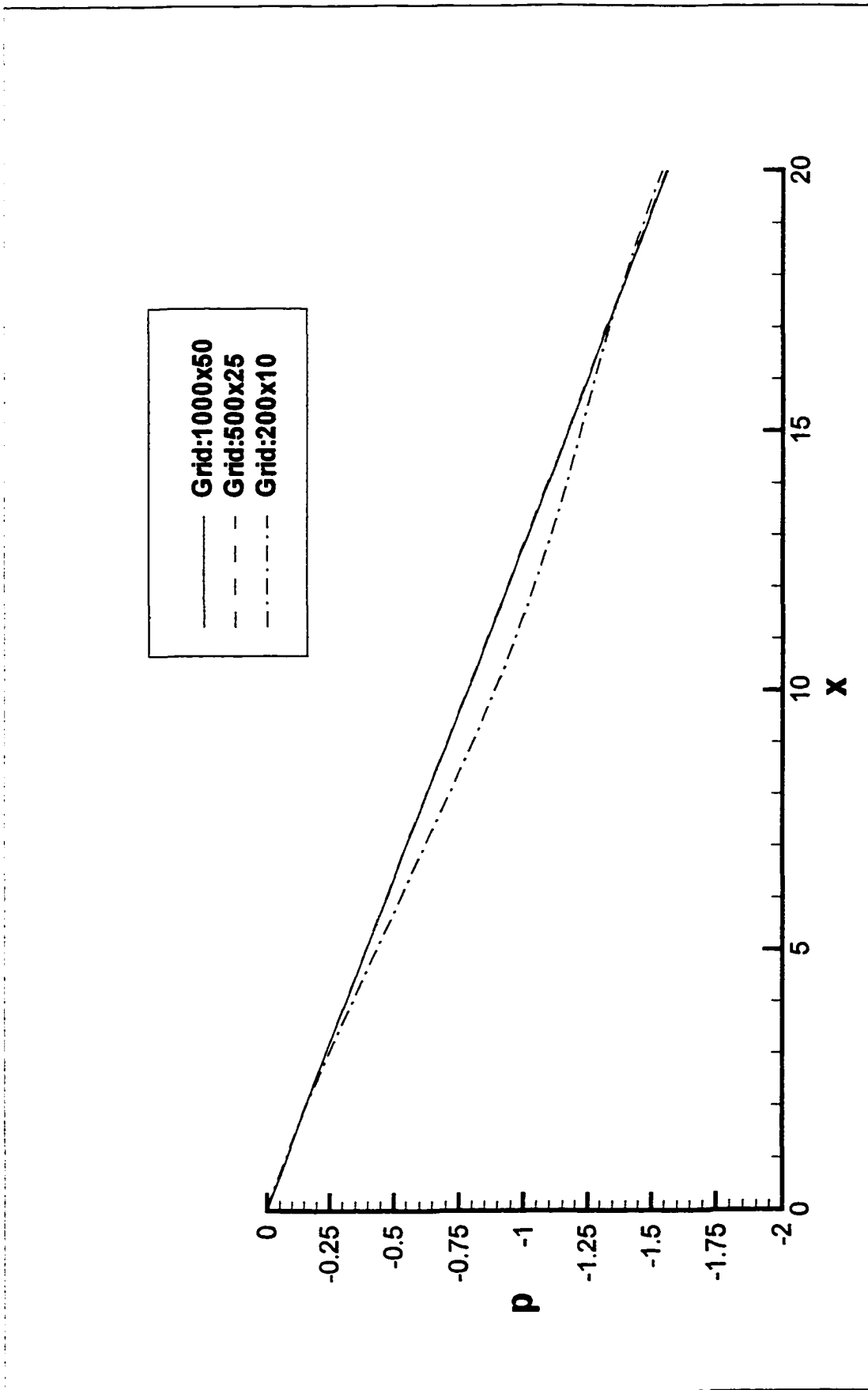


Figure 5.2. Effect of grid size

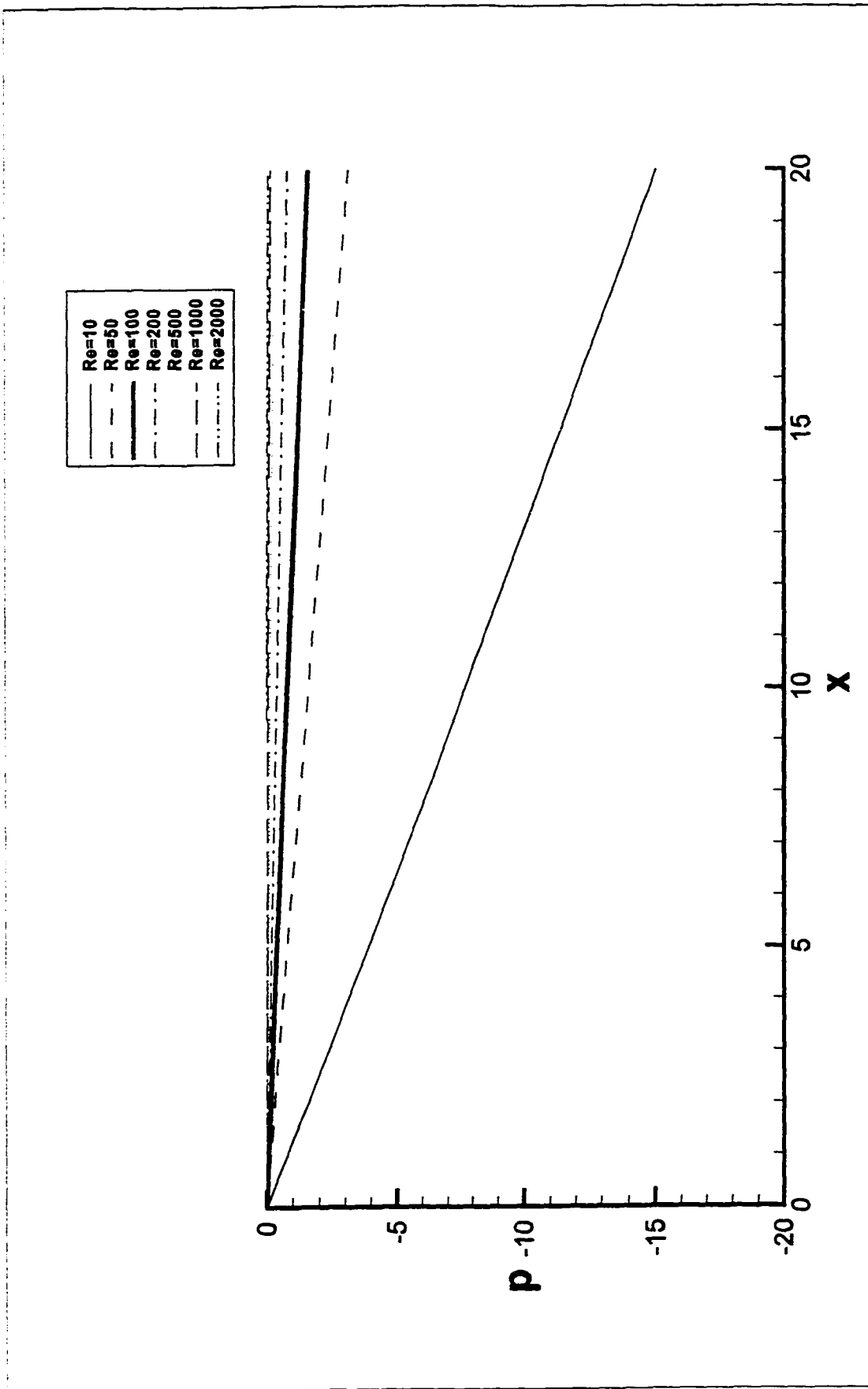


Figure 5.3. Variation of pressure with streamwise distance for $Kr=0$

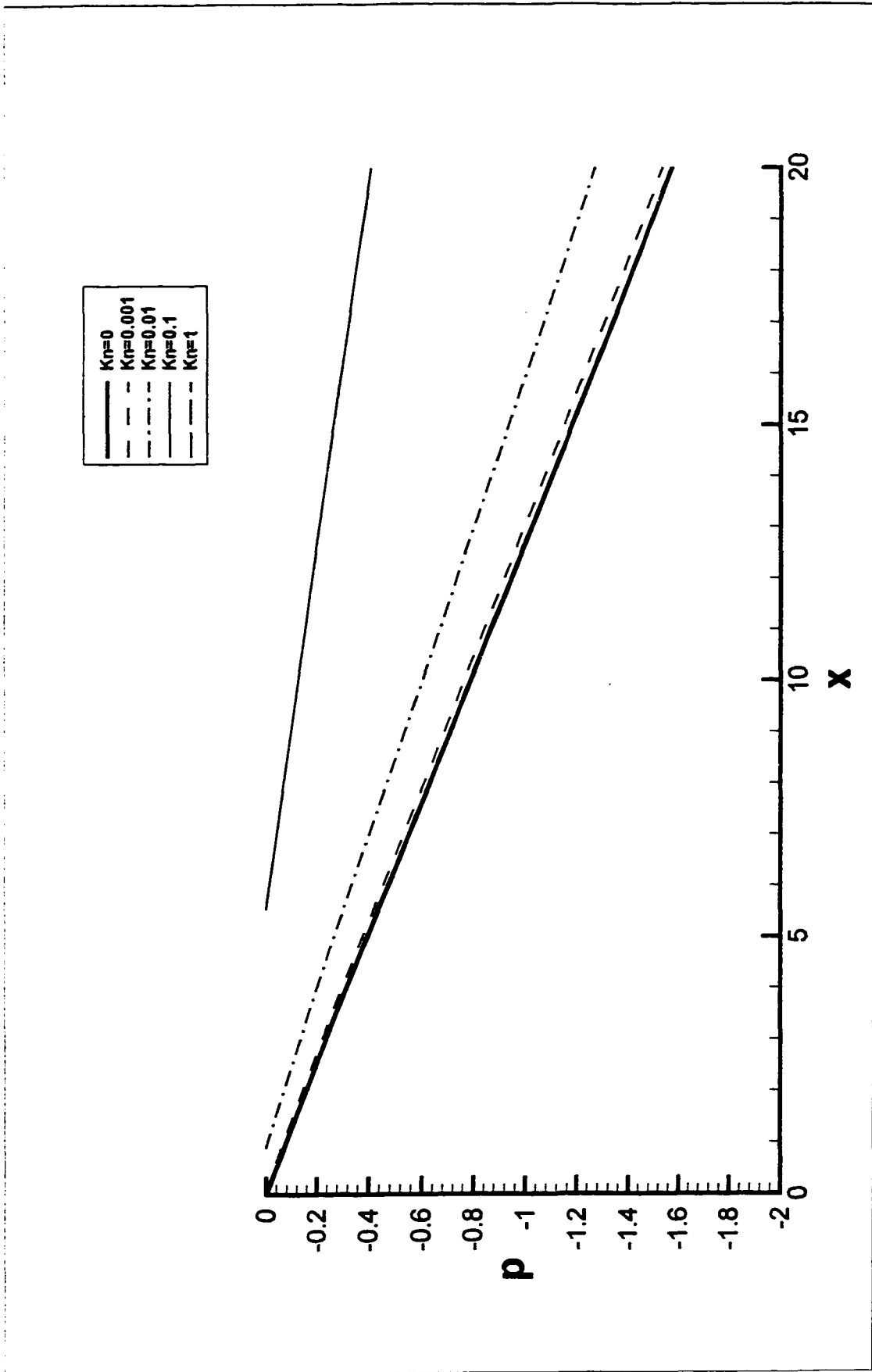


Figure 5.4. Variation of pressure with streamwise distance for various Knudsen number (Slip-Flow Model, $\sigma=0.5$)

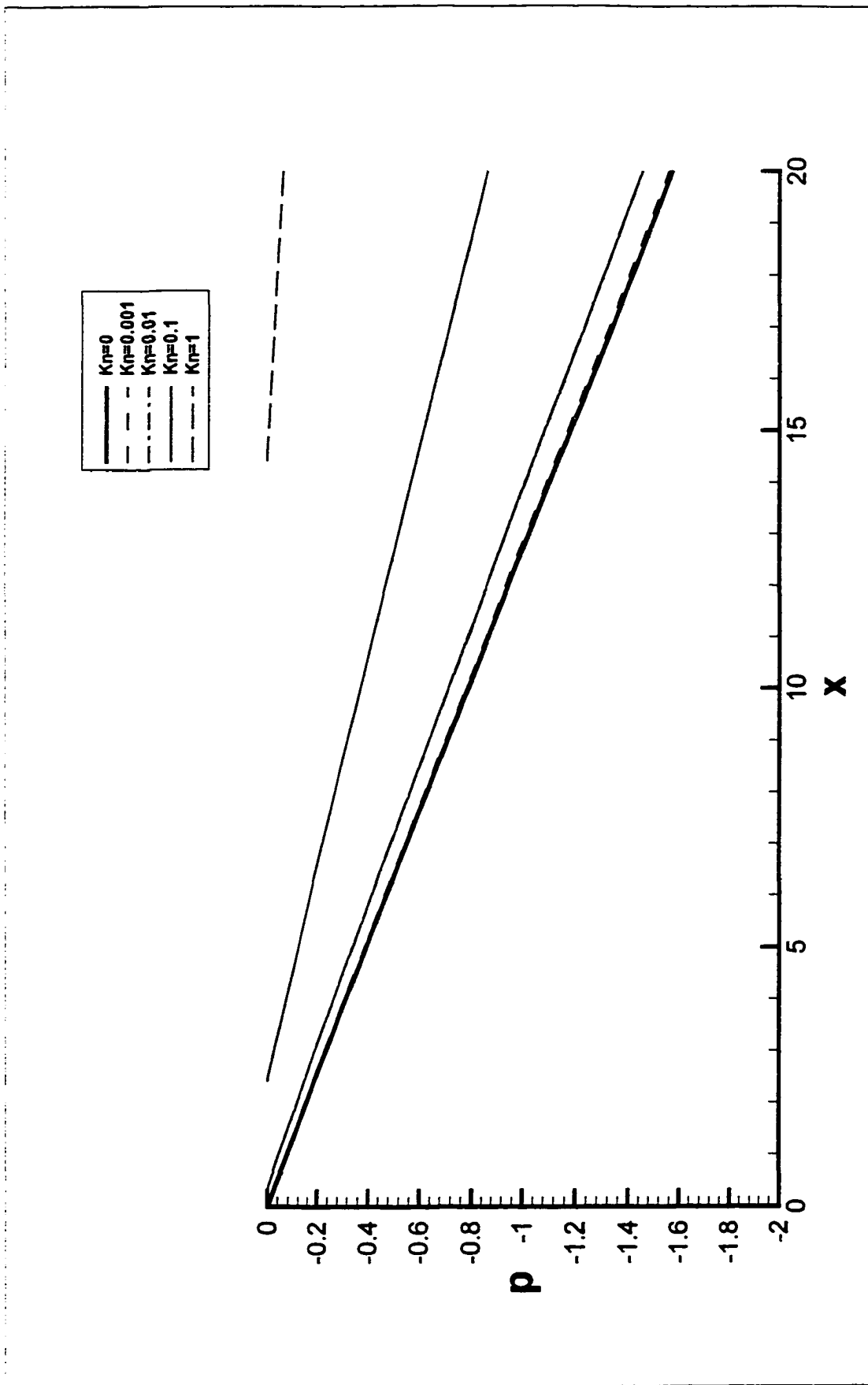


Figure 5.5. Variation of pressure with streamwise distance for various Knudsen number (Slip-Flow Model, $\sigma=1.0$)

accommodation factor $\sigma=0.5$ is used for slip condition. The pressure drop is apparently affected by the variation of Kn. When Kn=0.001, the difference from non-slip condition is small. As Kn increases, the deviation becomes large. Numerically an adjusting zone appears near the entrance boundary since the incompatibility of the prescribed velocity field at entrance. The pressure may be adverse in that zone but drops after that. The pressure drop becomes gentle compared with the small Kn case, and is steady after the adjustment. The adjustment distance for Kn=0.01 is less than one channel in height, but changes to about 5 times of the channel height for Kn=0.1. We may suggest that the model is applicable for Kn=0.01 and marginally acceptable for Kn=0.1. For much larger Kn, the pressure is always higher than that of the entrance in our computational region and is not shown in Figure 5.4. Similar results are shown for $\sigma=1$ in Figure 5.5. Compared with $\sigma=0.5$, the effect of slip boundary condition is less significant and much larger Kn can be explored at this time.

The normalized friction factor C^* , defined as $C^* = \frac{f Re}{f Re_{theory}}$, is tabulated in

Table 5.1. The C^* value is less than 1, which is tendentially in agreement with most authors, such as Beskok and Karniadakis (1994), Kavehpour et al. (1997). They used gas as the work medium and thus the Re number and compressibility are not comparable. Pfahler (1992) performed liquid transport experiment in micron size channel, and his C^* is around 0.85 for the 24.5 μm deep channel in which Re is about 100. But since it is still unclear about the Kn number in liquid flow, no Kn number can be given from his experiments, and we can conclude only that the agreement holds. Other comparable test includes water flow in a tube performed by Yu *et al.* (1994) in which C^* was 0.78.

The effect of the slip-boundary condition in the velocity field is also shown. Figure 5.6 shows the velocity profile in an arbitrary section. In the case of small Kn number $Kn=0.001$, the velocity profile differs little from that of non-slip boundary condition. When Kn increases to 0.01, the difference of the velocity profile becomes obvious. In that case, the maximum velocity obtained at the centerline is smaller than that from the non-slip boundary condition. At the same Kn, big σ usually corresponds to small deviations in that profile since it implies bigger friction drag at the walls. When Kn is 0.1, the velocity profile changes significantly, the maximum velocity is much smaller, and the slip velocity at the walls are significant. The velocity profile explains the corresponding pressure changes shown in Figure 5.4 and 5.5.

Table 5.1 The normalized friction factor C^* varies with Kn and σ

σ	Kn			
	0.001	0.01	0.1	1
0.5	0.97	0.86	0.35	N/A
1.0	0.99	0.96	0.67	0.14
		0.96 (Beskok)	0.77(Beskok)	
		0.96 (Kavehpour)	0.75(Kavehpour)	

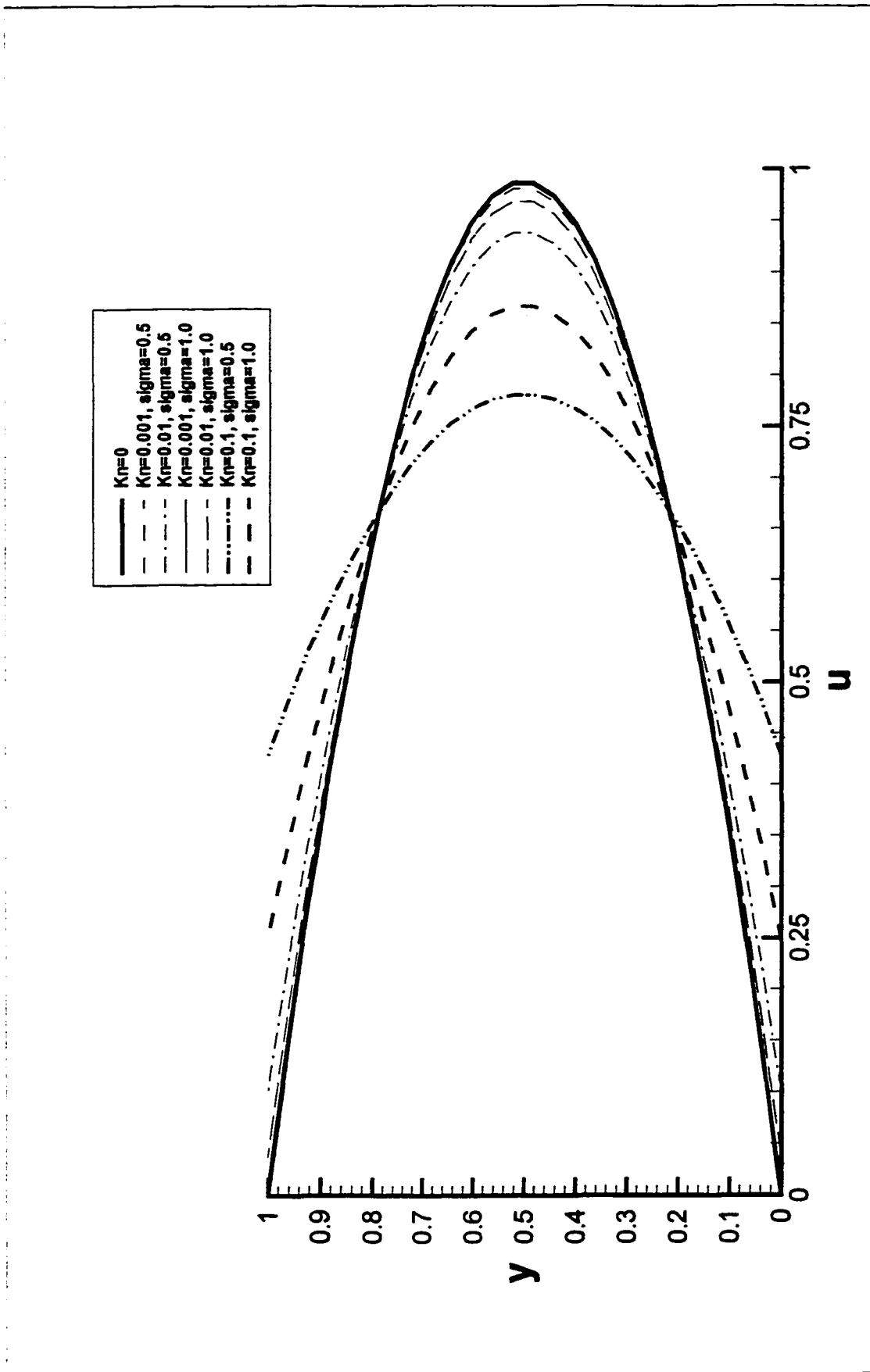


Figure 5.6. Velocity profile for various Kn and σ (Slip-Flow Model)

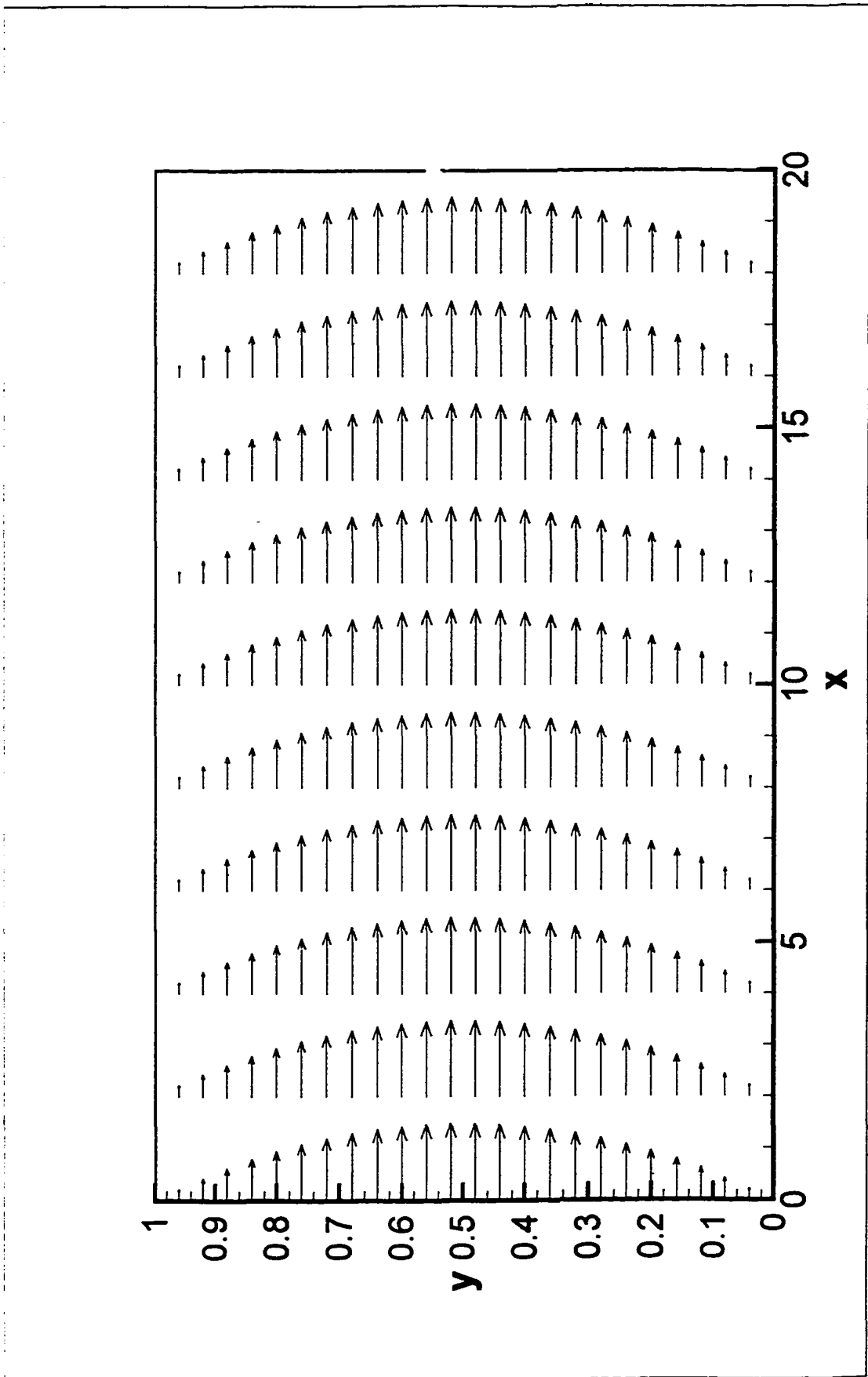


Figure 5.7. Velocity field for $Kn=0.001$ and $\sigma=1.0$ (Slip-Flow Model)

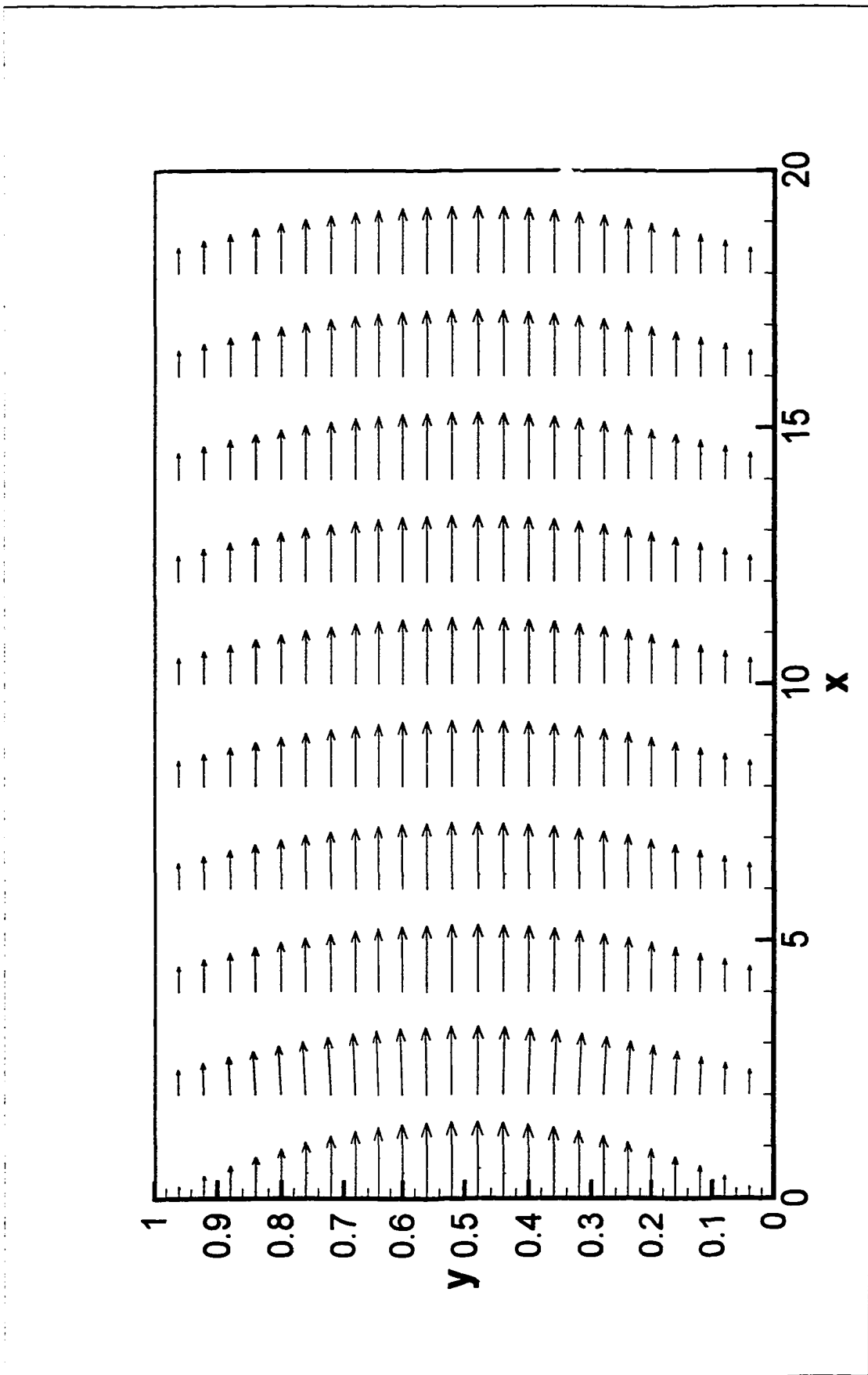


Figure 5.8. Velocity field for $Kn = 0.1$ and $\sigma = 1.0$ (Slip-Flow Model)

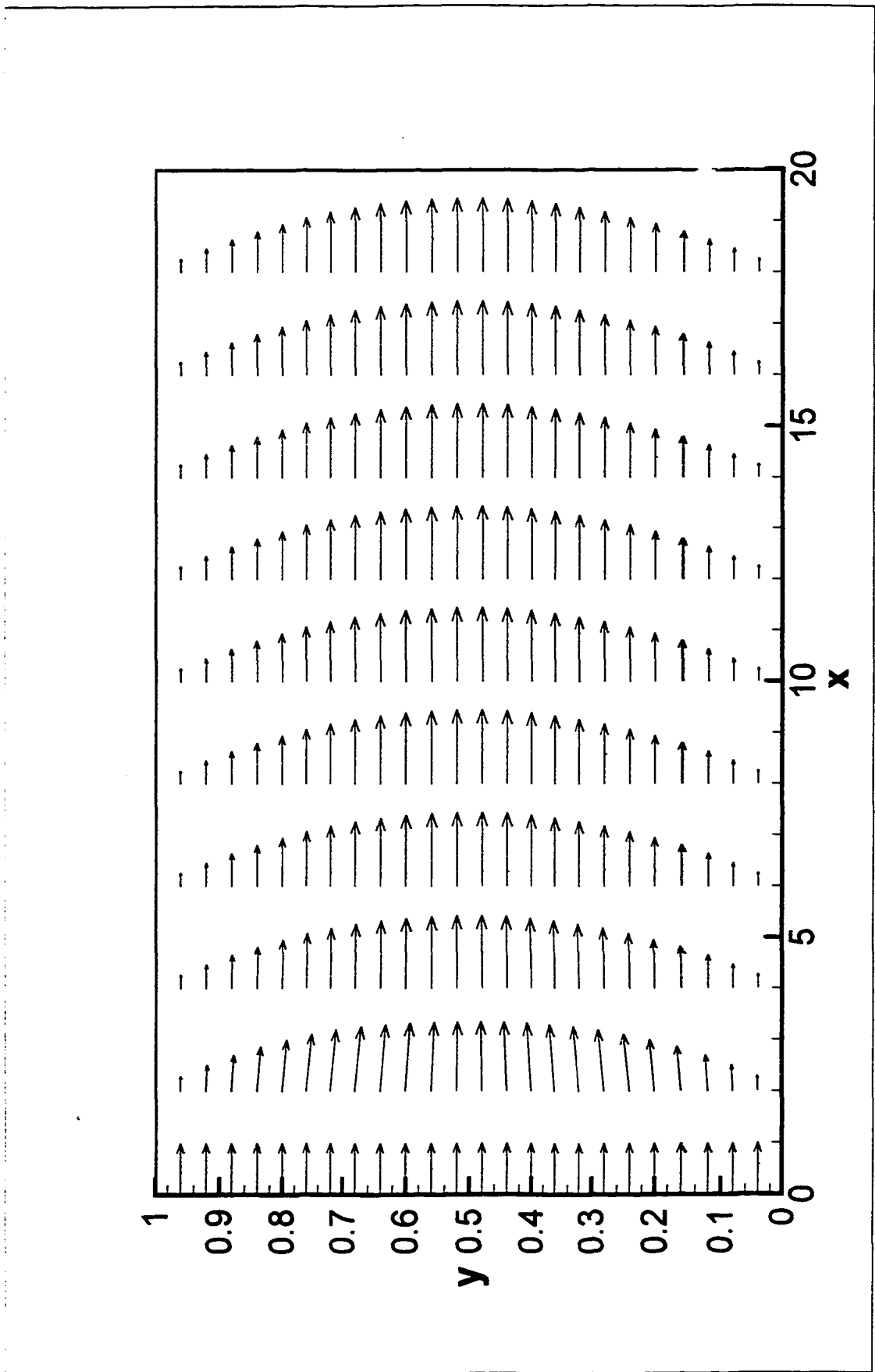


Figure 5.9 Velocity field for uniform entrance flow (Slip-Flow Model)

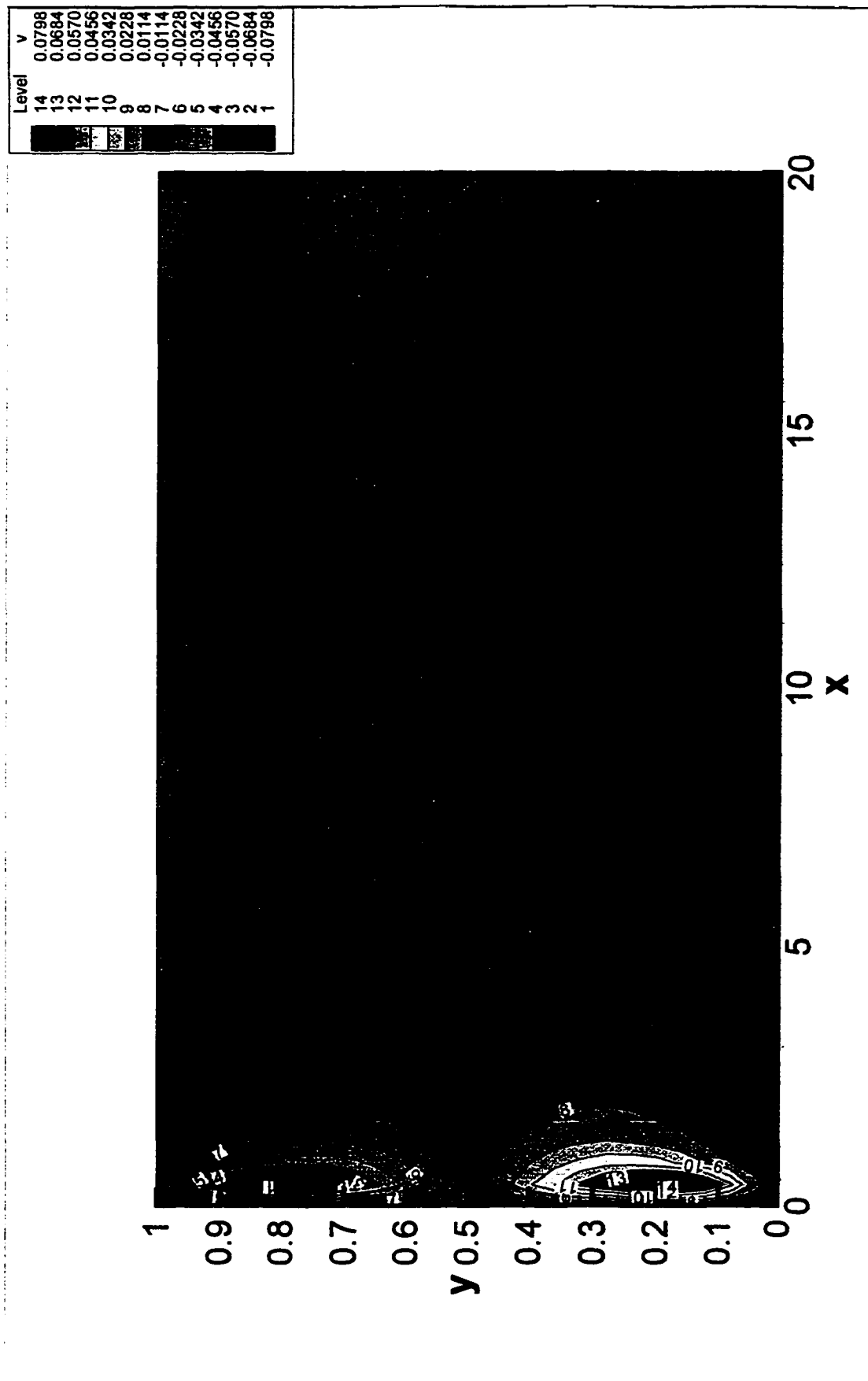


Figure 5.10 v- component contour for uniform entrance flow (Slip-Flow Model)

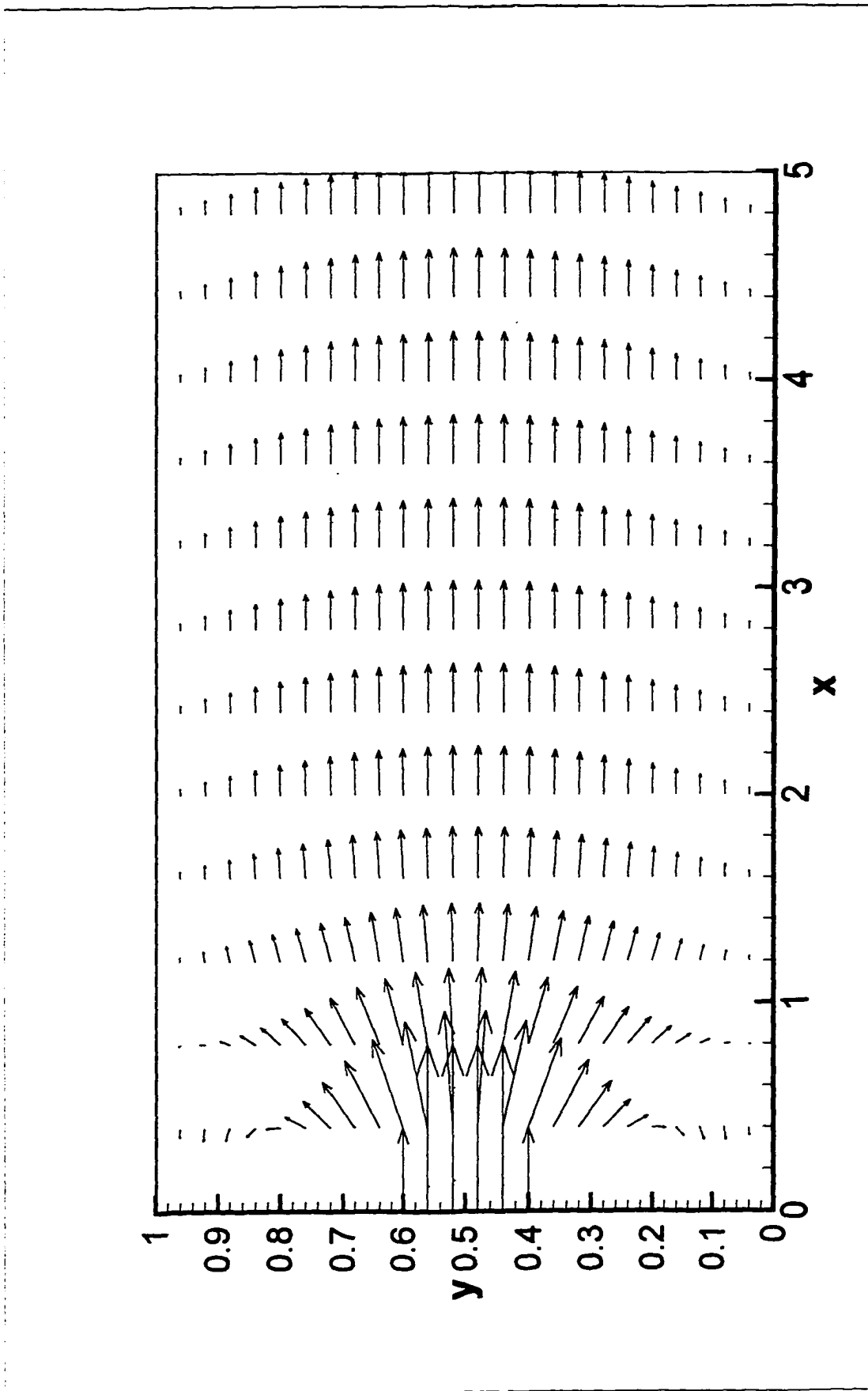


Figure 5.11. Velocity field for impinging jet flow (Micro-Polar Fluid Model, $Re=100$, $k=0.1$)

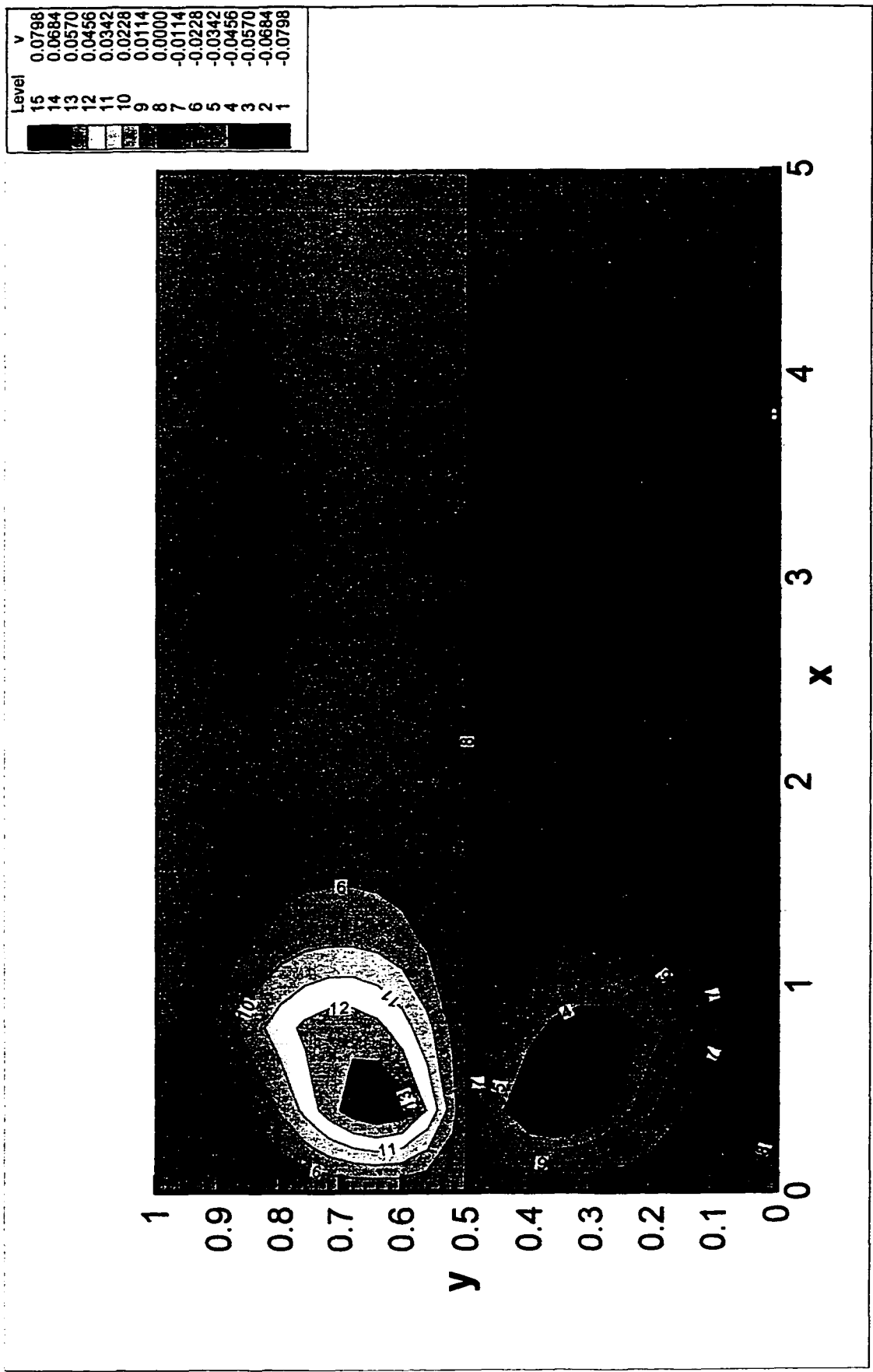


Figure 5.12. v -component contour for impinging jet flow (Micro-Polar Fluid Model, $Re=100$, $k=0$)

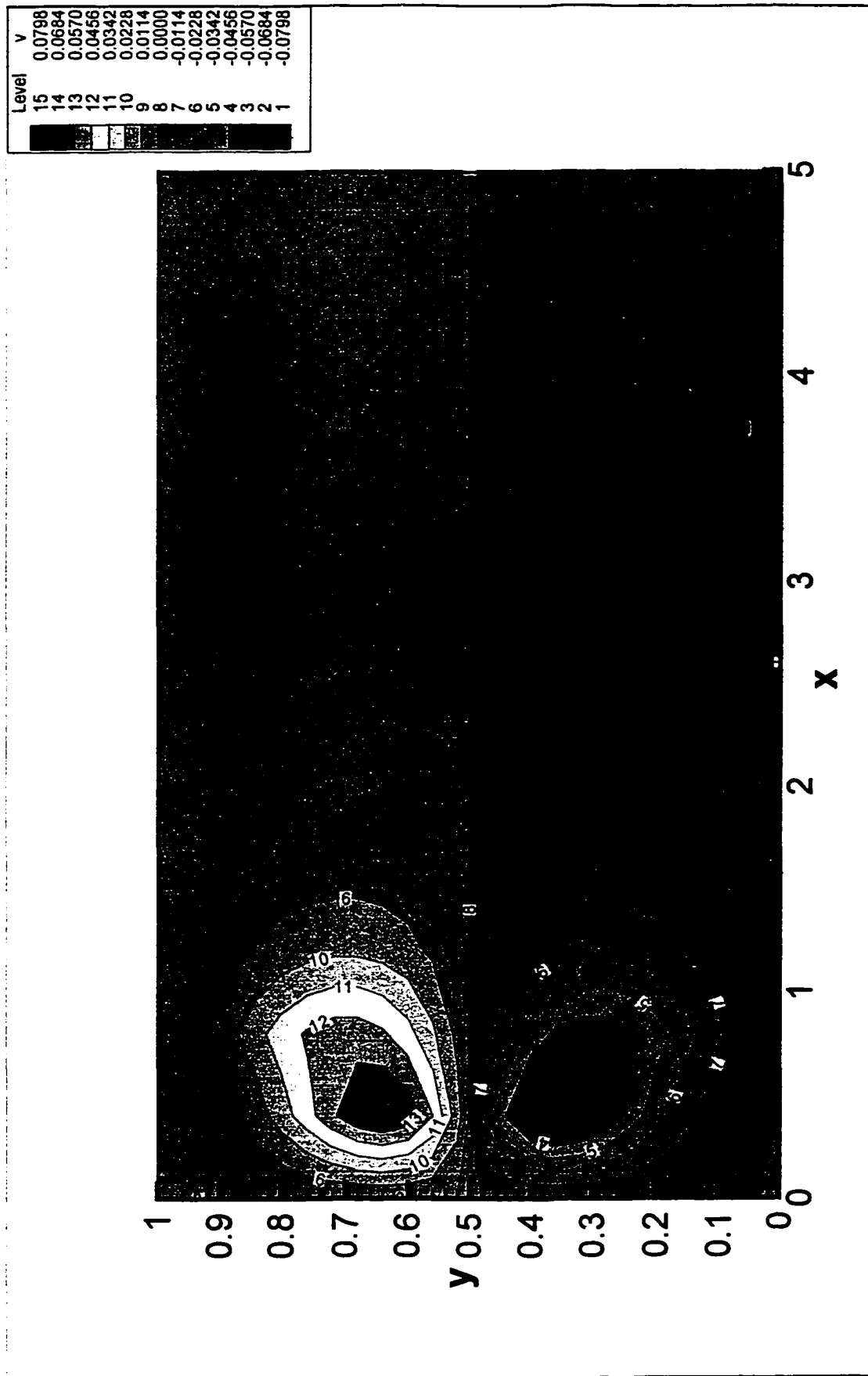


Figure 5.13. v -component contour for impinging jet flow (Micro-Polar Fluid Model, $Re=100$, $k=0.1$)

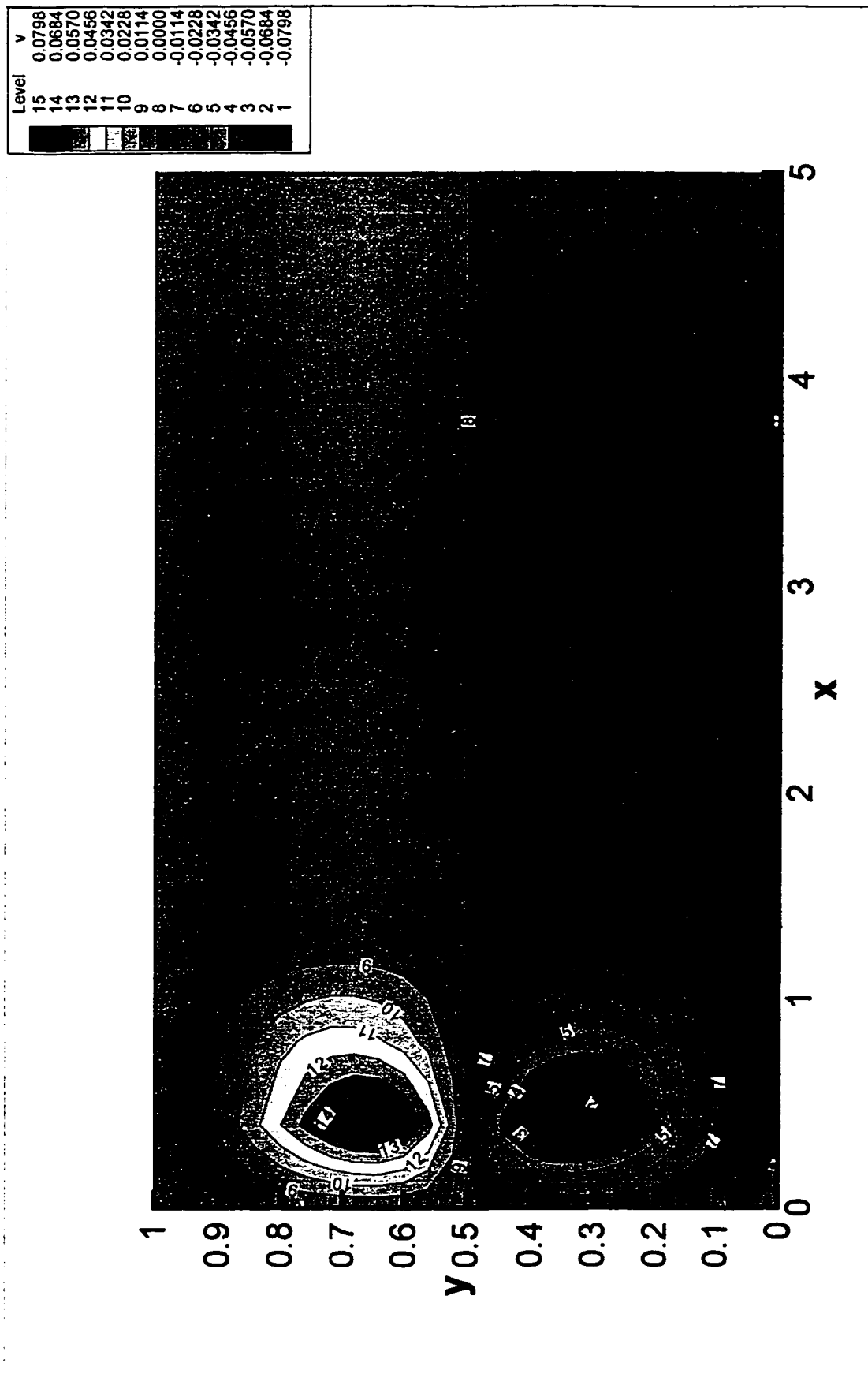


Figure 5.14. v -component contour for impinging jet flow (Micro-Polar Fluid Model, $Re=100$, $k=1$)

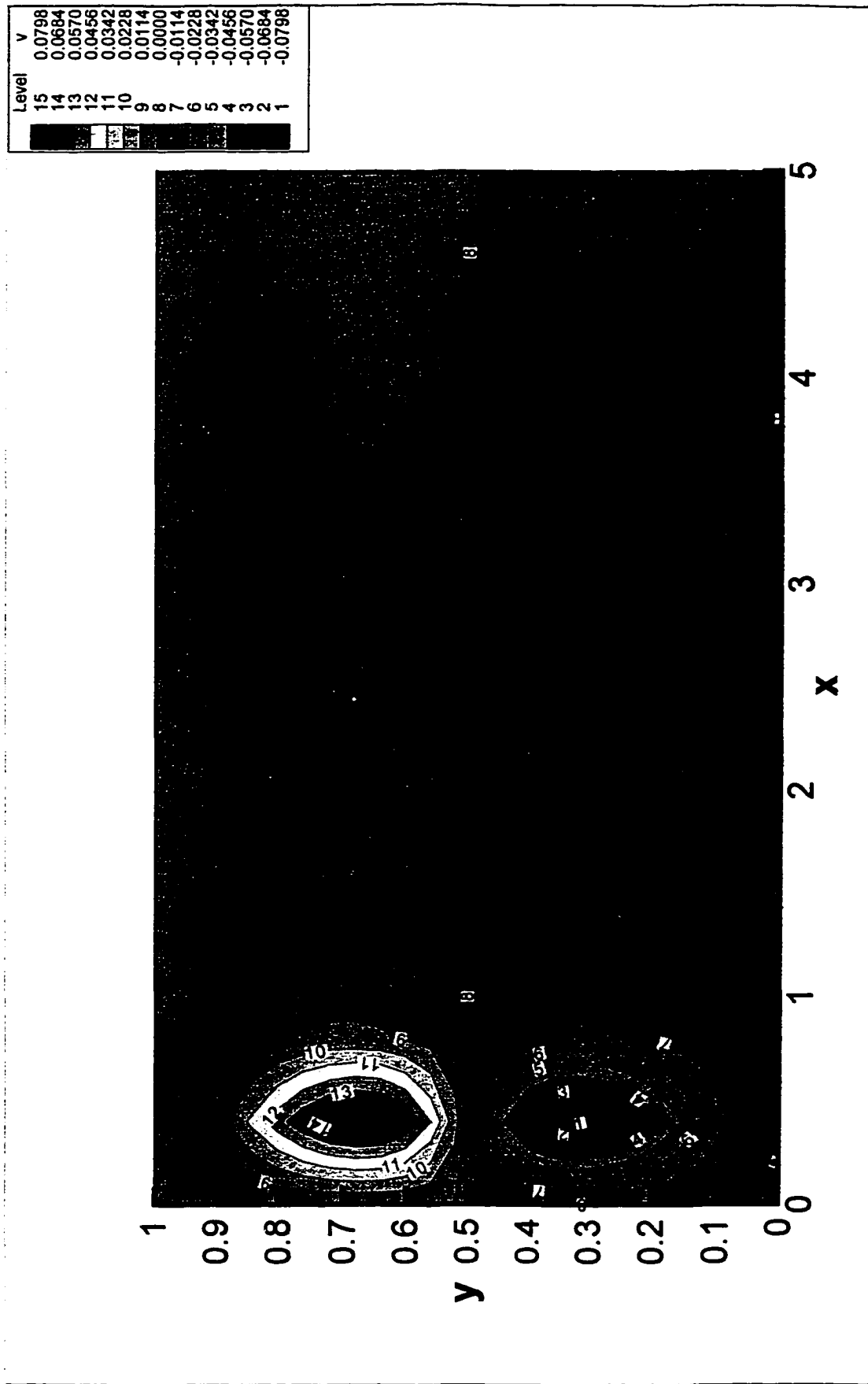


Figure 5.15. v -component contour for impinging jet flow (Micro-Polar Fluid Model, $Re=100$, $k=5$)

The vector plots of the velocity field are shown in Figure 5.7 and 5.8. Figure 5.7 is for the case of $Kn=0.001$, and Figure 5.8 for $Kn=0.1$. In both cases, $\sigma=1$. The velocity variation along the channel for different Kn is clear. The decreasing of the maximum velocity at centerline is compensated for by the increase in the velocity at the walls. The figures of velocity also show evidence that the flow is fully-developed.

To verify that the prescribed channel length is long enough for fully-developed exit assumption in this computational domain, we calculated cases where a uniform velocity profile or impinging jet profile is set in the entry of the channel. Figure 5.9 shows the velocity field of uniform entry profile. Near the entrance, the velocity near the wall is retarded due to the friction, and flow is pushed off the wall, which increases the velocity in the middle core. It forms a parabolic profile at a short distance downstream. The changing distance is less than 4 compared to channel height 1 in this calculation. The v - component velocity better illustrates the entrance adjustment. When flow is pushed, velocity component v becomes visible and reaches maximum halfway from the wall to the core. The v is back to quiescence after the flow becomes unidirectional again. Figure 5.10 shows the v contour for this case.

An impinging jet flow through a straight channel is computed via the micro-polar fluid model for the same purpose. The flow can also reach a fully developed state in less than 5 channel height distance downstream. Figure 5.11 shows the velocity field for $Re=100$ and $k=0.1$. The effect of different k on the flow is also investigated. The v -component contours are shown for various k through Figure 5.12, 5.13, 5.14 and 5.15. A

general result is that with the increase of the micro-gyration k , the vortex length is shortened and thus the flow is more quickly adjusted to a fully-developed state.

5.3. Simulation Results of Micro-Polar Fluid Model

The computations are performed for the micro-polar fluid model using the same strategy as the slip-flow model. The $Re=100$ is extensively used as a flow parameter. The modeling parameter $m \times Kn$ is adopted as 0.1 except those made to examine the effect of this parameter. Another modeling parameter n which appeared in the boundary condition is set to 0.5.

Figure 5.16 shows the pressure variation for various modeling parameter $m \times Kn$. $m \times Kn = 0.1, 0.01$ and 0.005 are used in these scenarios. Other parameter includes $Re=100$, and $k=1$. The plot shows that this parameter has little effect on the computation for the chosen $m \times Kn$. Each of them is acceptable in this computation. A higher-resolution plot shows little difference between that of 0.1 and the other two cases, and the latter two cases have much closer results. This result is shown in Figure 5.17.

Figure 5.18 shows the variation of pressure for various nondimensional viscosity k . k ranges from 0 to 10. $k=0$ presents the Navier-Stokes solution. The vortex viscosity or micro gyration viscosity increases as k increases, and when $k=10$, the micro effect due to the vortex viscosity dominates the flow. The pressure drop changes predictably with that feature of k . When k is within 0.1, the deviation from the Navier-Stokes prediction is small. When k is large, a large pressure drop is apparent, and the pressure drop changes significantly when finally vortex viscosity dominates the flow.

Figure 5.19 shows the magnified plot near $k=0$.

The normalized friction factor C^* is calculated for all cases and is tabulated in Table 5.2.

Table 5.2 The normalized friction factor C^* varies with k

k	0.01	0.05	0.1	0.25	0.5	1	2	5	10
C^*	1.01	1.03	1.05	1.12	1.25	1.5	2	3.5	6

The effect of vortex viscosity does not only affect the apparent Reynolds number, which is presented in diffusion term in the momentum equation, but also comes from the micro-rotation term in the same equation. The apparent Reynolds number may be expressed as $Re/(1+k)$, and the big vortex viscosity seems to decrease the Re , and thus enhances the friction. The micro-rotation term, on the other hand, lessens the effect of vortex viscosity, and reduces the friction.

For the almost fully-developed channel flow, with our assumed material parameter relationship (Chapter 3), we substitute the angular momentum equation by

$$\frac{\partial g}{\partial x} = 0, \quad v = 0 \quad (5.1)$$

to obtain

$$0 = -\frac{20k}{Re(mKn)^2}g + \frac{1+k/2}{Re} \left(\frac{\partial^2 g}{\partial x^2} + \frac{\partial^2 g}{\partial y^2} \right) + \frac{10k}{Re(mKn)^2} \left(\frac{\partial v}{\partial x} - \frac{\partial u}{\partial y} \right) \quad (5.2)$$

Since $m \times Kn < 1$, the middle term in the above equation may be neglected as compared to the other terms, and thus we obtain

$$g = \frac{1}{2} \left(\frac{\partial v}{\partial x} - \frac{\partial u}{\partial y} \right) \quad (5.3)$$

Substituting g in the x-component momentum equation, we obtain

$$u \frac{\partial u}{\partial x} + v \frac{\partial u}{\partial y} = -\frac{\partial p}{\partial x} + \frac{1+k/2}{\text{Re}} \left(\frac{\partial^2 u}{\partial x^2} + \frac{\partial^2 u}{\partial y^2} \right) \quad (5.4)$$

This equation means that the whole effect of micro-gyration is equivalent to decreasing the Re by $(1+k/2)$, and thus increasing the friction factor by this same factor. Table 5.2 shows this relation.

Experiments performed by Papautsky *et al.* (1998) showed that the normalized friction coefficient was approximately 1.45. This result may be achieved by setting $k=0.9$. Since the authors did not give the flow parameters, specific comparisons seem difficult to make. The micro-polar fluid model is also capable of predicting results which are in agreement with the experimental data from Pfahler (1992) for a channel depth of $41.5 \mu\text{m}$ for isopropanol and $38.7 \mu\text{m}$ for silicon oil. The large normalized friction coefficients (greater than 1) were obtained by them but cannot be explained by the slip-flow theory.

The corresponding velocity profile is shown in Figure 5.20. The velocity profile varies a little with k . When k increases, the maximum velocity obtained at the center line becomes smaller.

The micro-rotation g field is also shown in Figure 5.21. g is x independent and varies in the y direction for a straight channel flow.

The vector plot of the velocity field is shown in Figure 5.22.

The variation of pressure for the different Re when $k=0.1$ and $k=1$ are also shown in Figure 5.23 and 5.24, respectively.

Flow through a straight channel with sudden restriction is of great interest in experimental research. We computed three cases with three restriction ratios (passage height in restriction over channel height) 0.2, 0.44, and 0.6, respectively, using the micro-polar fluid model. Other flow parameters include $Re=100$, and $k=0.1$, $k=1$, $k=5$ as well as $k=0$.

Figures 5.25 to 5.30 show the result for restriction ratio 0.2. Velocity fields are plotted in Figure 5.25, 5.26, 5.27, and 5.28 for the entire computation domain with respect to $k=0$, $k=0.1$, $k=1$, and $k=5$, respectively. In each case, the flow is almost unidirectional before the restriction protrusion and has a sudden contraction in the beginning of the restriction block. Sudden accelerated flow passes the orifice, and diverges after restriction. In the rear of the restriction, a pair of vortices is formed to pad the flow into a suddenly enlarged space.

Big pressure losses in this restriction are clearly shown in Figure 5.29, which plots the variation of the pressure at the centerline with the downstream distance. The pressure loss in the restriction area is much larger than the usual friction loss along the wall and becomes the major pressure loss if the channel is not very long. Similar to the result of the channel without restriction, pressure loss is always large for large k . In this respect, we may conclude that large micro-gyration increases the flow drag.

Figure 5.30 shows the contours of v - component velocity according to varied micro-gyration k . A pair of increasing zone of v - component velocity is clearly shown in the front corner of the restriction block, and so is the circulation zone in the rear of the

block. The back vortex varies its length with the micro-gyration strength. The vortex length becomes short as the micro-gyration parameter k increases. Also, the maximum value of v - component velocity decreases with an increase in k . The maximum value of the v - component is generally larger from the Navier-Stokes solution than from this micro-polar fluid model.

Figure 5.31, 5.32, 5.33, 5.34, and 5.35 show the result for restriction ratio 0.6. Similar to the last case, velocity fields are plotted in Figure 5.31 to to 5.34 for case $k=0$, $k=0.1$, $k=1$, and $k=5$. In Figure 5.35, pressures at the centerlines along the downstream distance are shown for this restriction ratio. Compared to restriction ratio 0.2, the restriction effect is weaker, but the back vortices are still visible as well as the sudden pressure drop in the restriction region. The pressure loss is substantially reduced from the last case.

In-between the above two restrictions, cases for restriction ratio 0.44 are also computed and the results are shown in Figures 5.36 to 5.40. The results fall, as expected, between the last two cases.

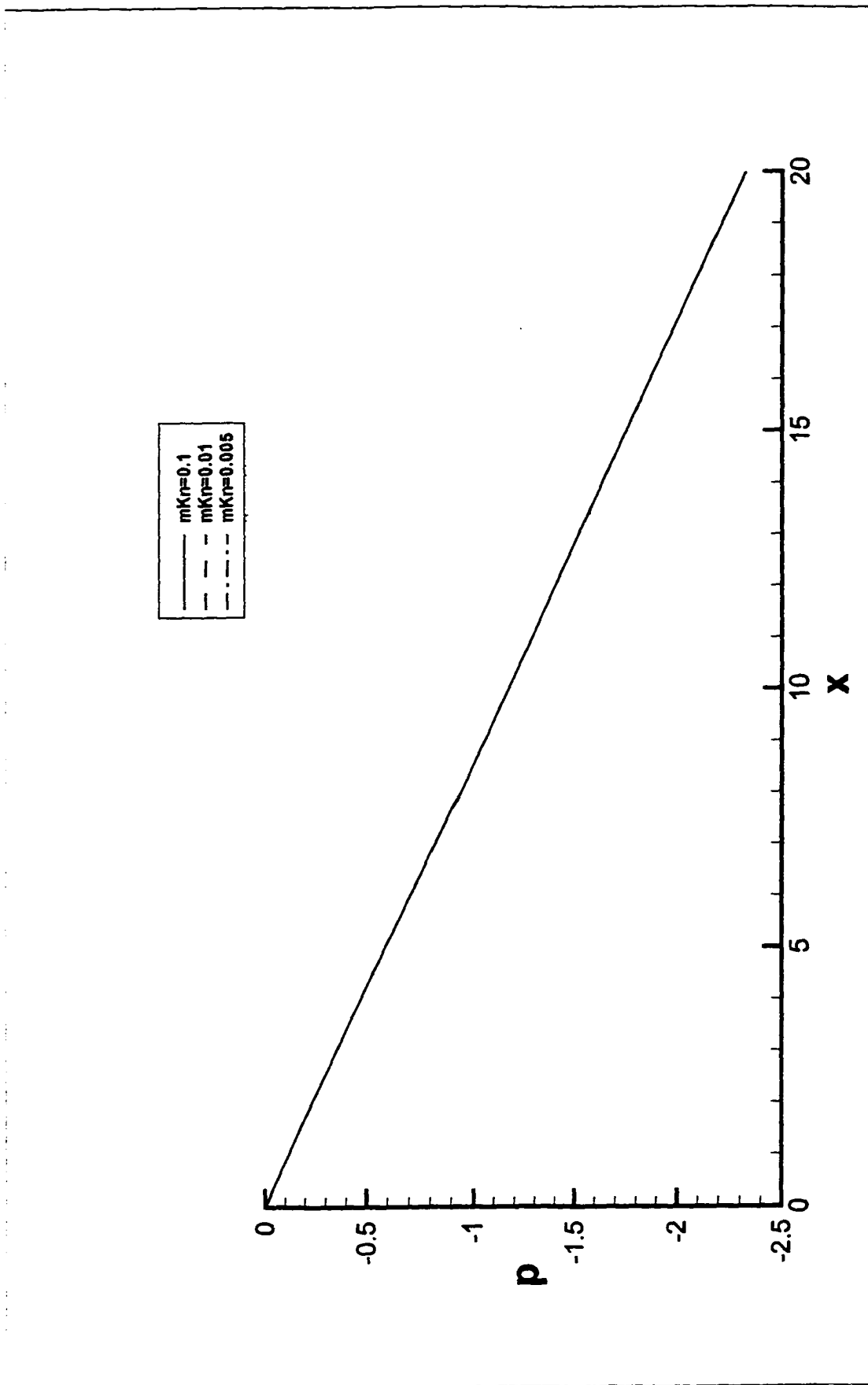


Figure 5.16. Effect of the parameter $m \times Kn$

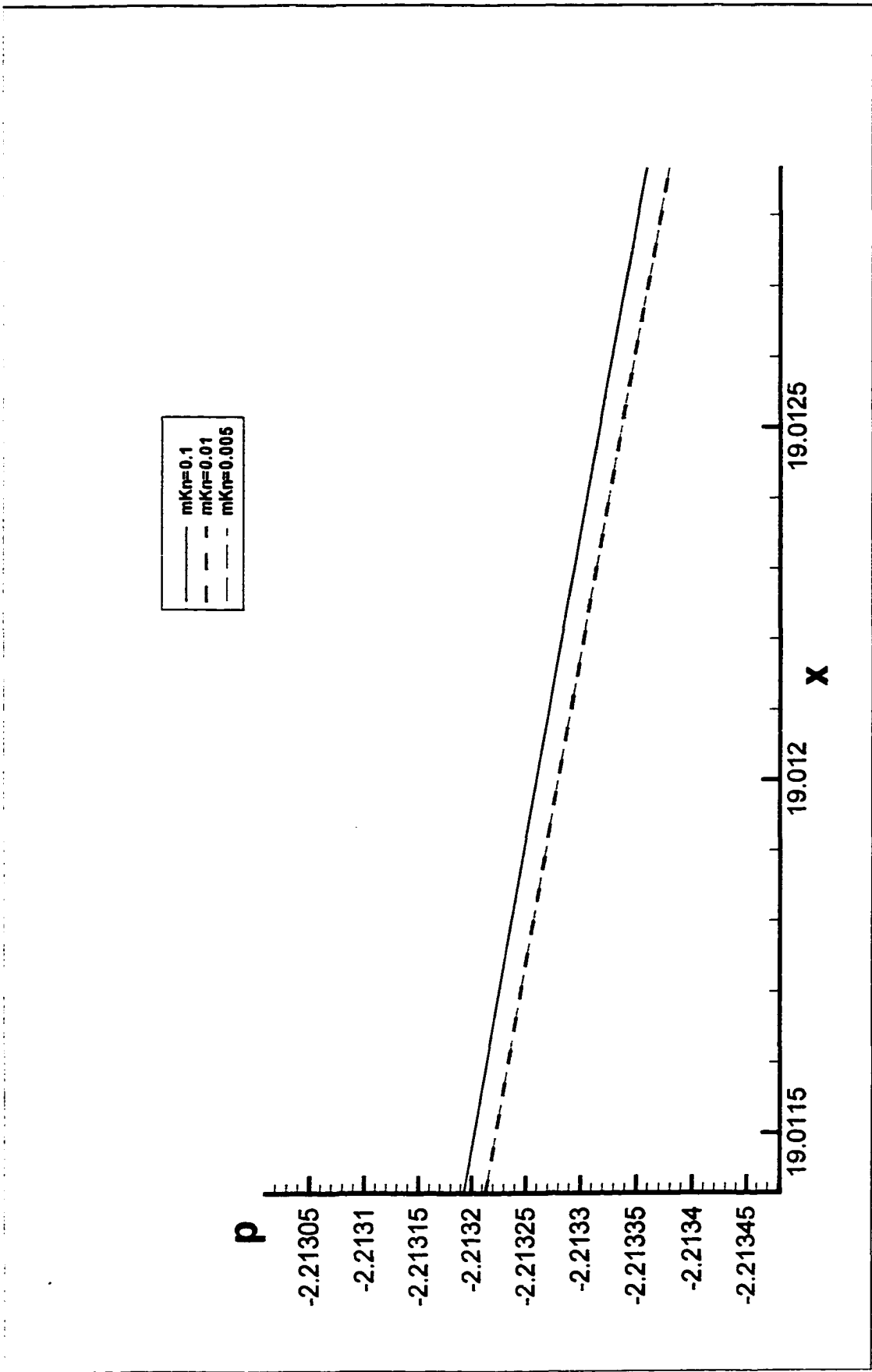


Figure 5.17. Effect of the parameter $m \times Kn$ (Amplified)

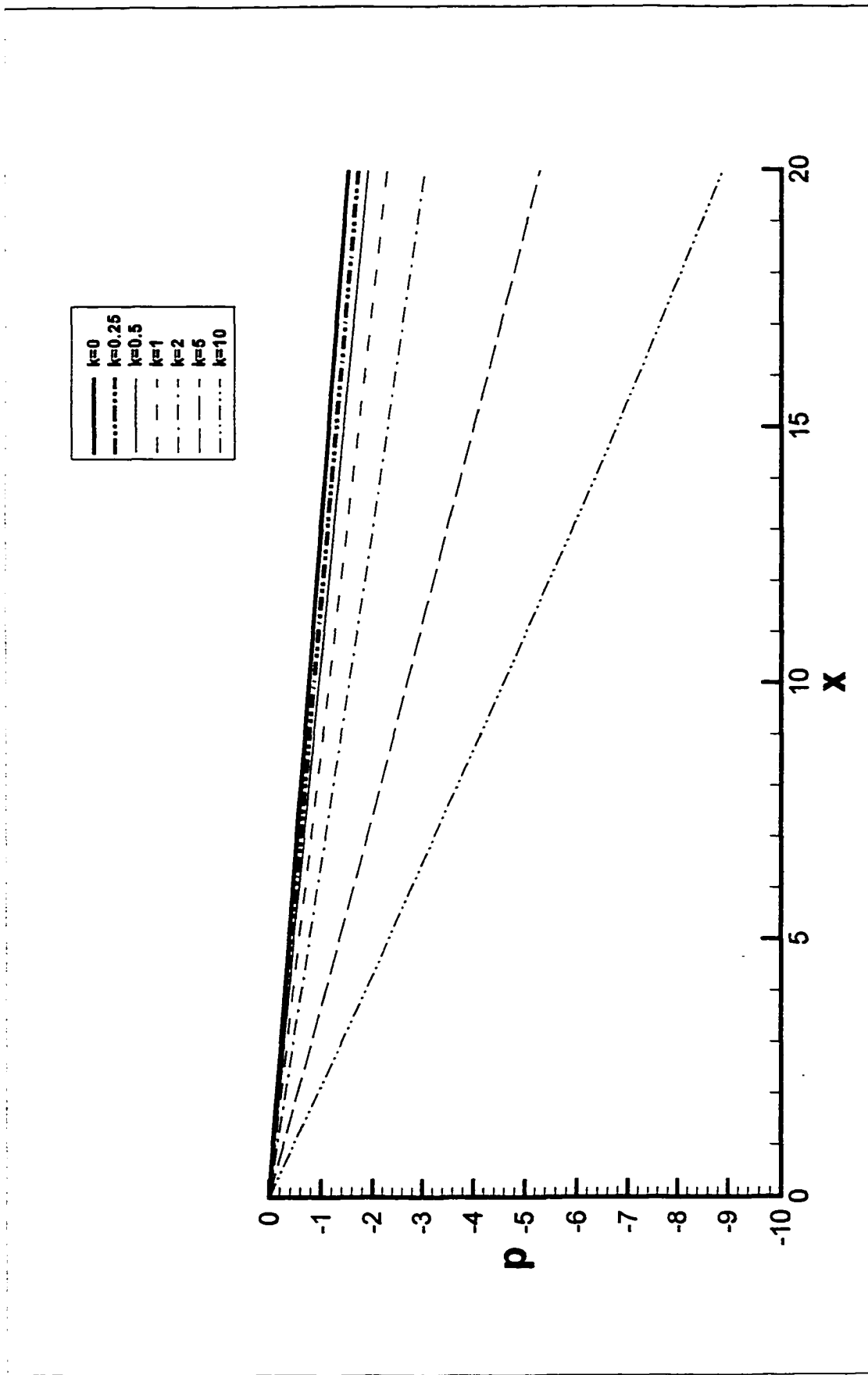


Figure 5.18. Variation of pressure with channel distance for various k values ($Re=100$)

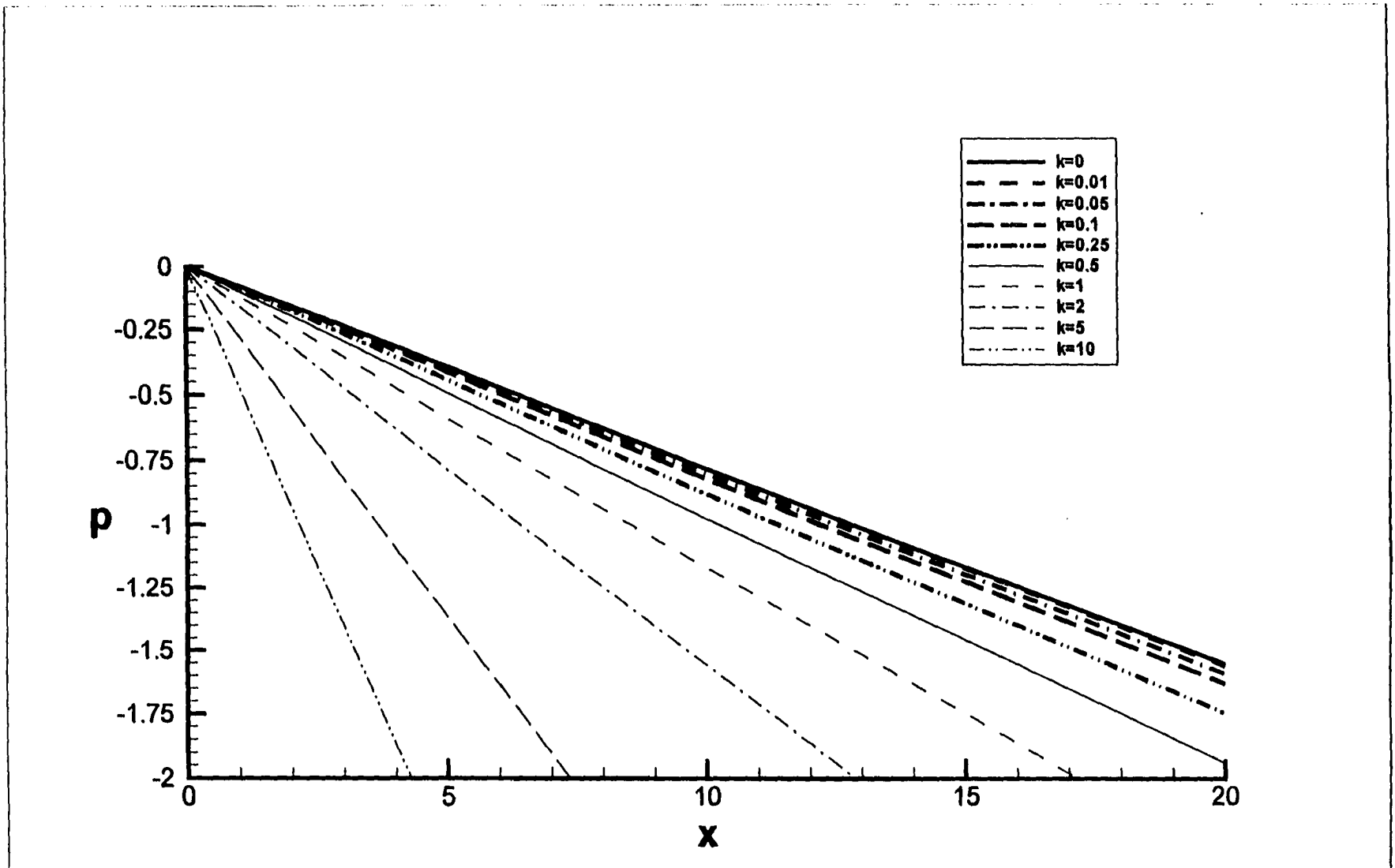


Figure 5.19. Variation of pressure with channel distance for various k values (Amplified, $Re=100$)

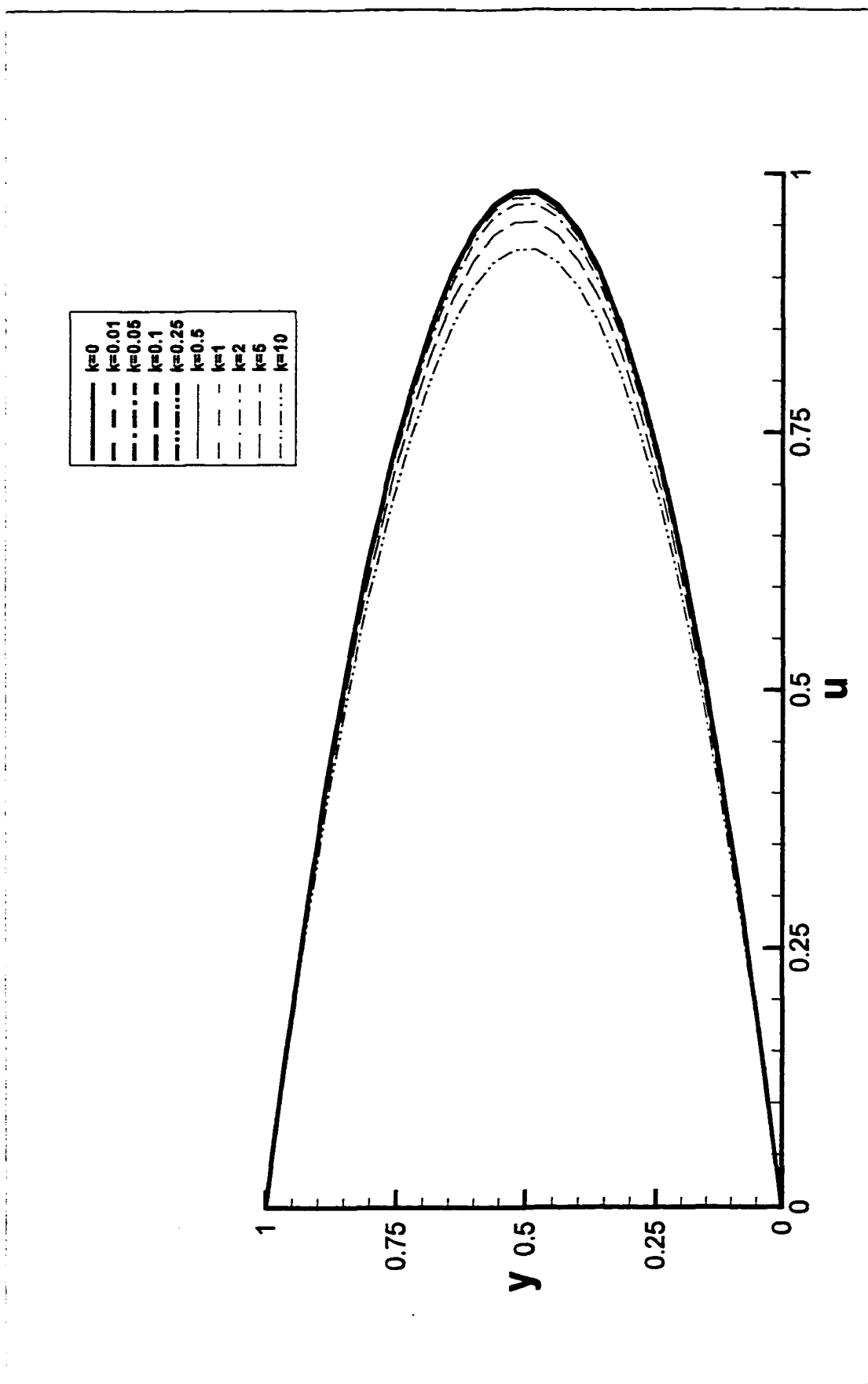


Figure 5.20. Velocity profile for various k values. ($Re=100$)

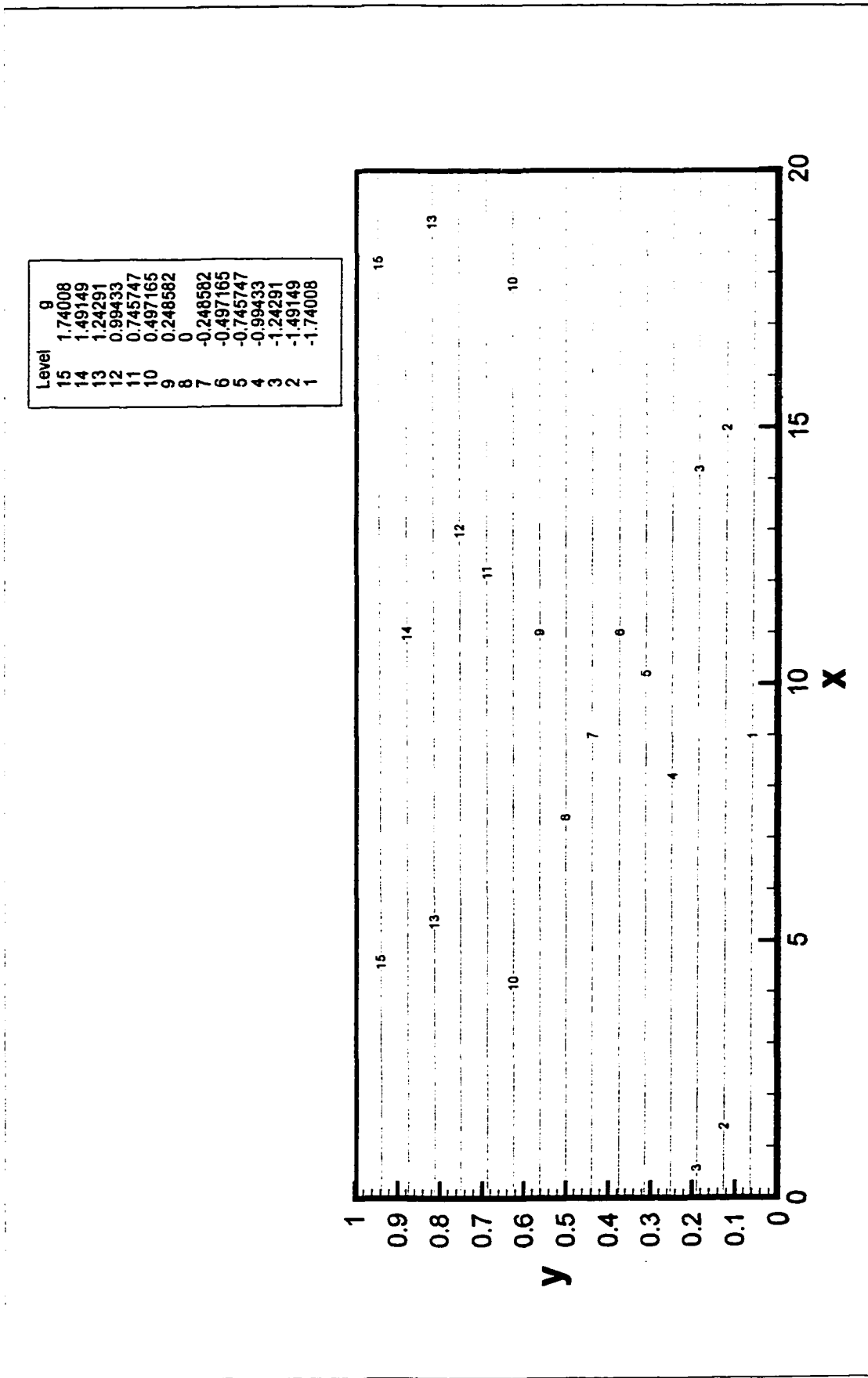


Figure 5.21. Micro-gyration contour ($Re=100, k=0.1$)

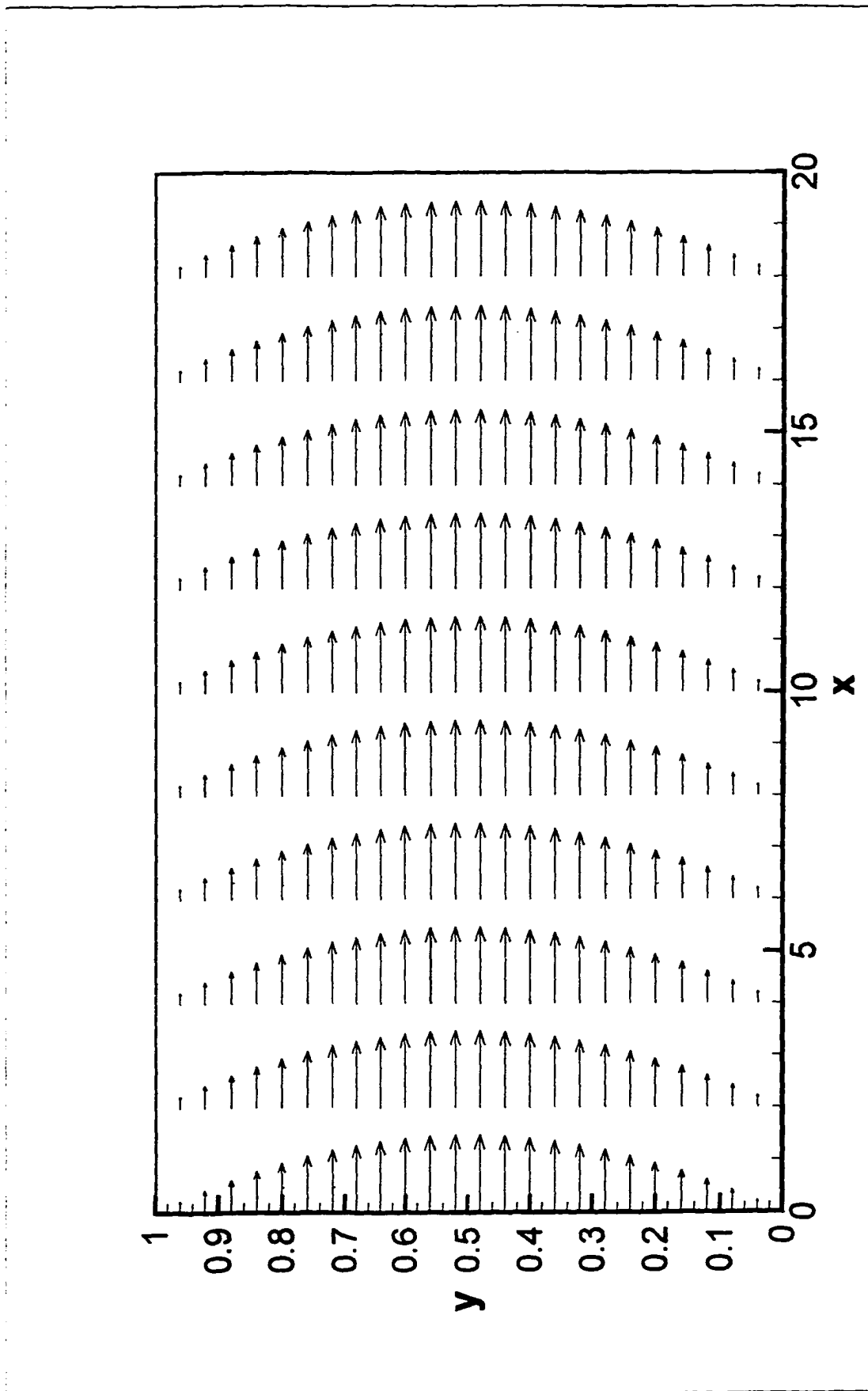


Figure 5.22. Velocity field for $Re=100$, $k=1$

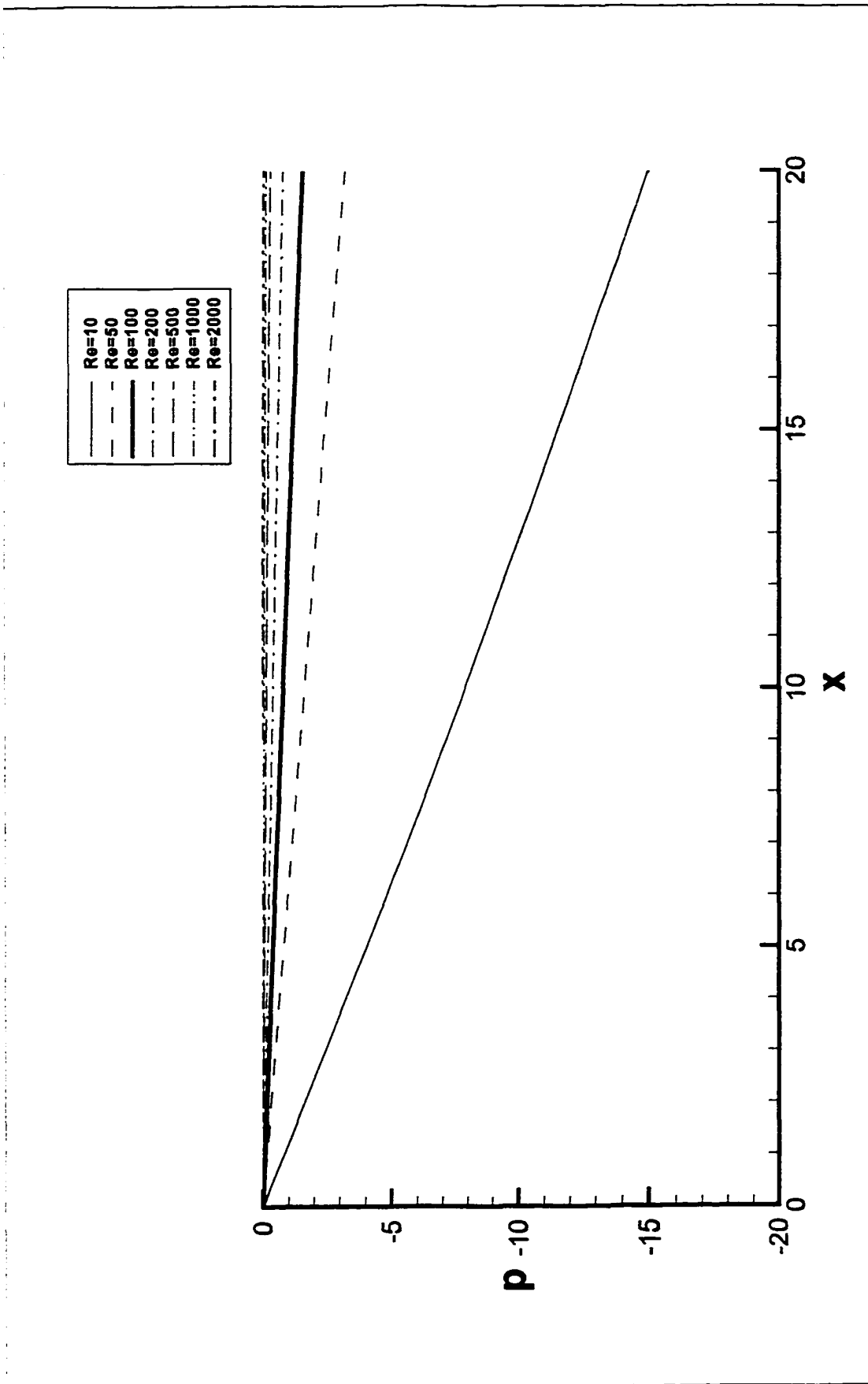


Figure 5.23. Variation of pressure with channel distance for $k=0.1$

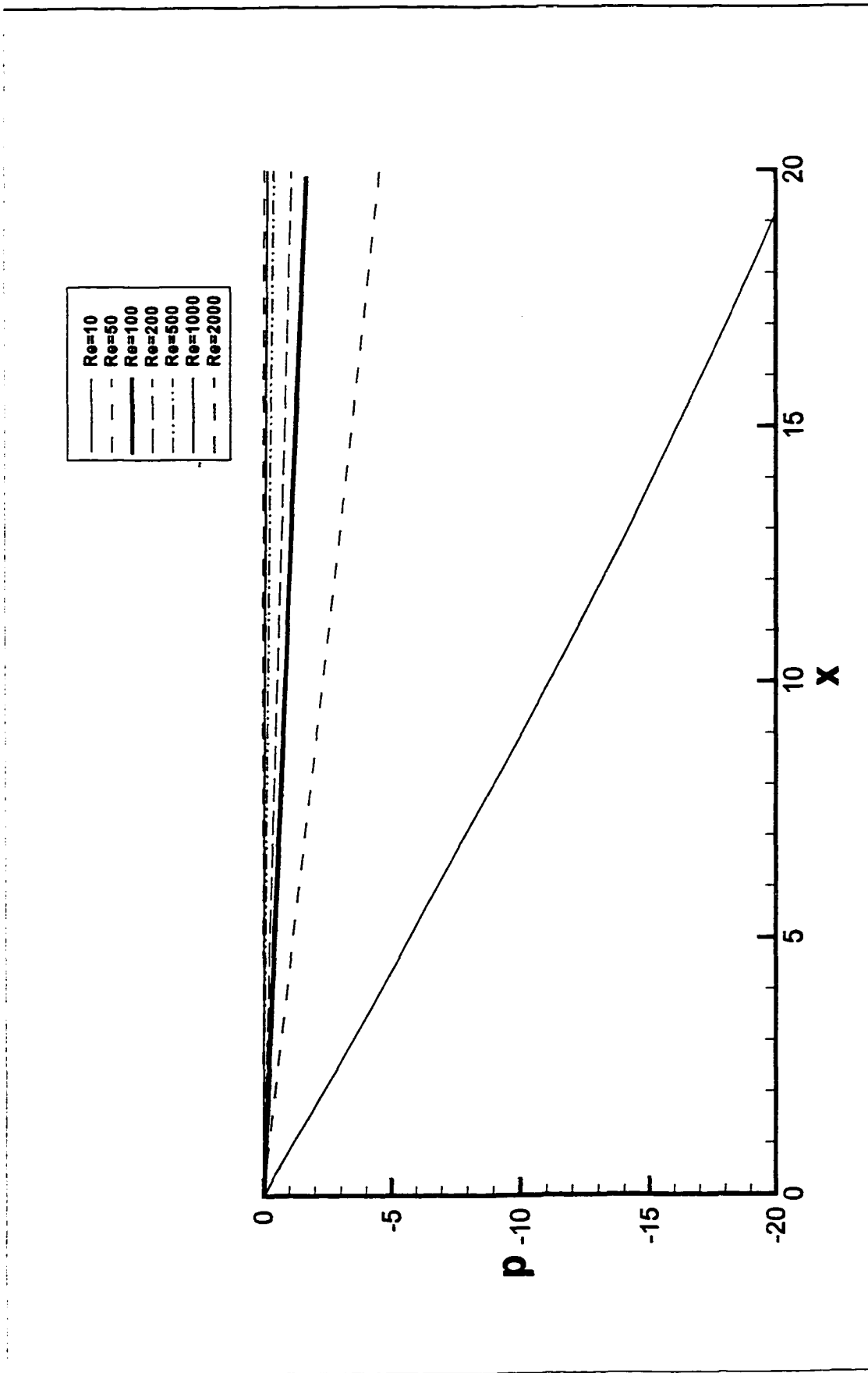


Figure 5.24. Variation of pressure with channel distance for $k=1$

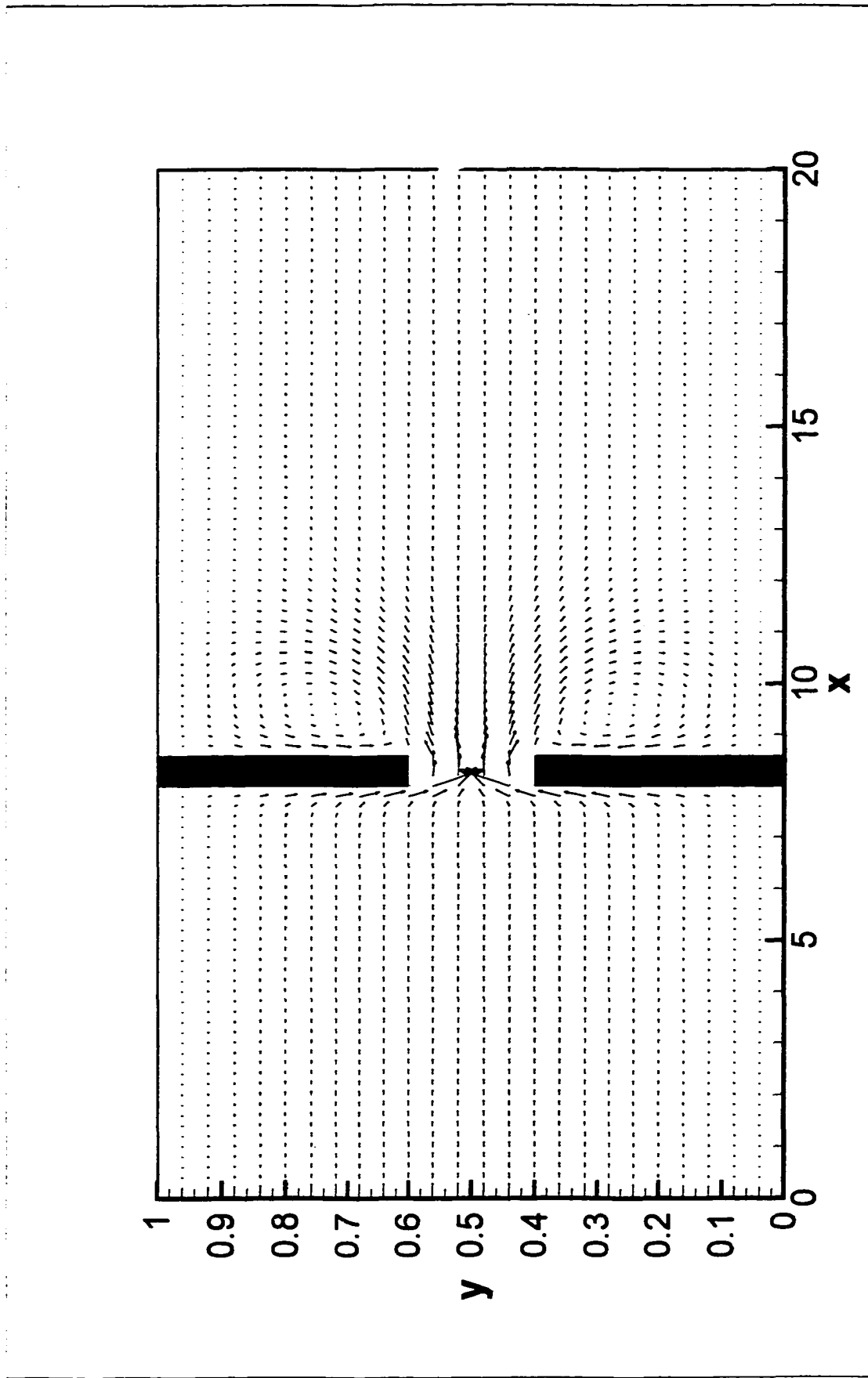


Figure 5.25 Velocity field for flow through a straight channel with restriction 0.2, $k=0$

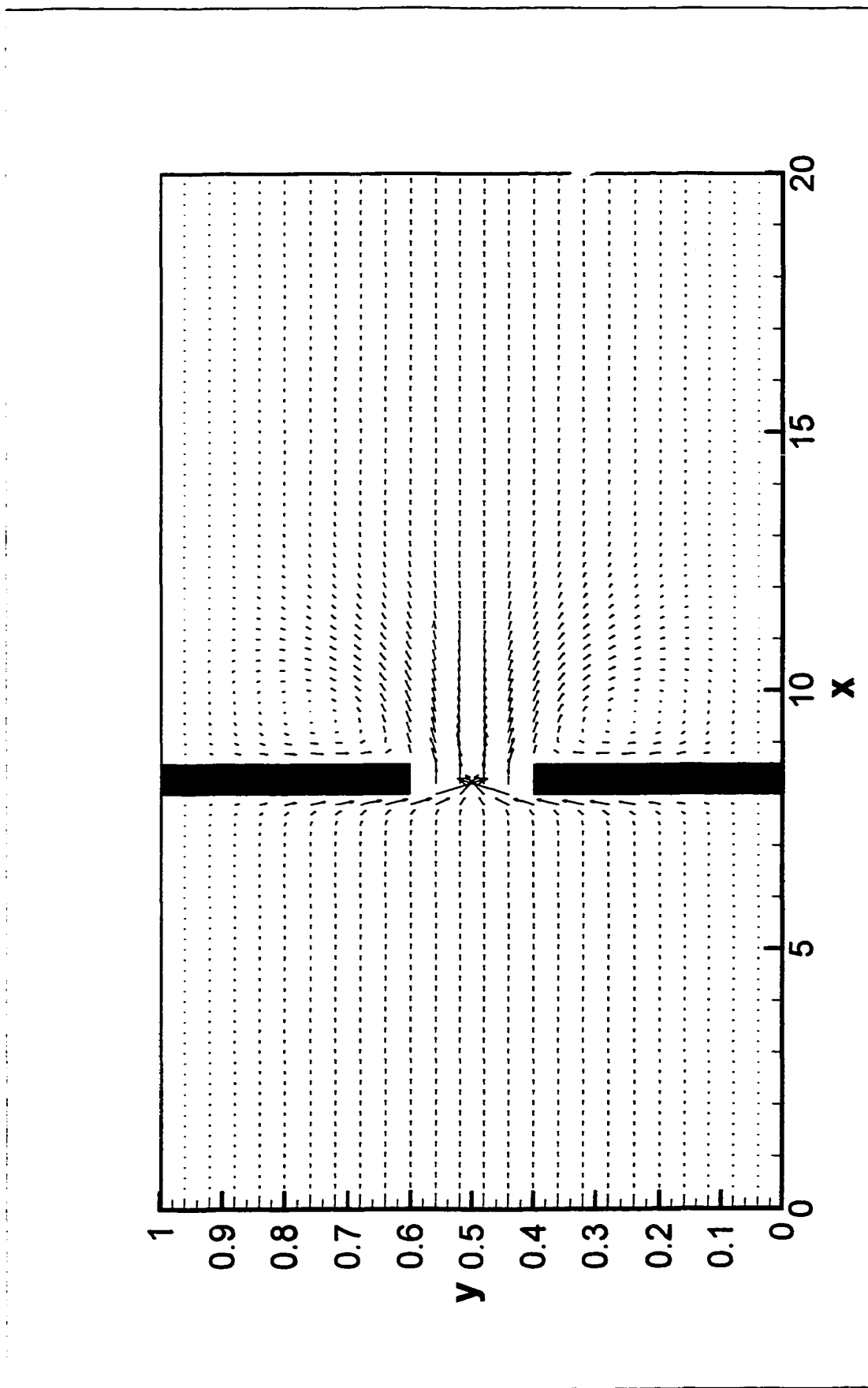


Figure 5.26 Velocity field for flow through a straight channel with restriction 0.2, $k=0.1$

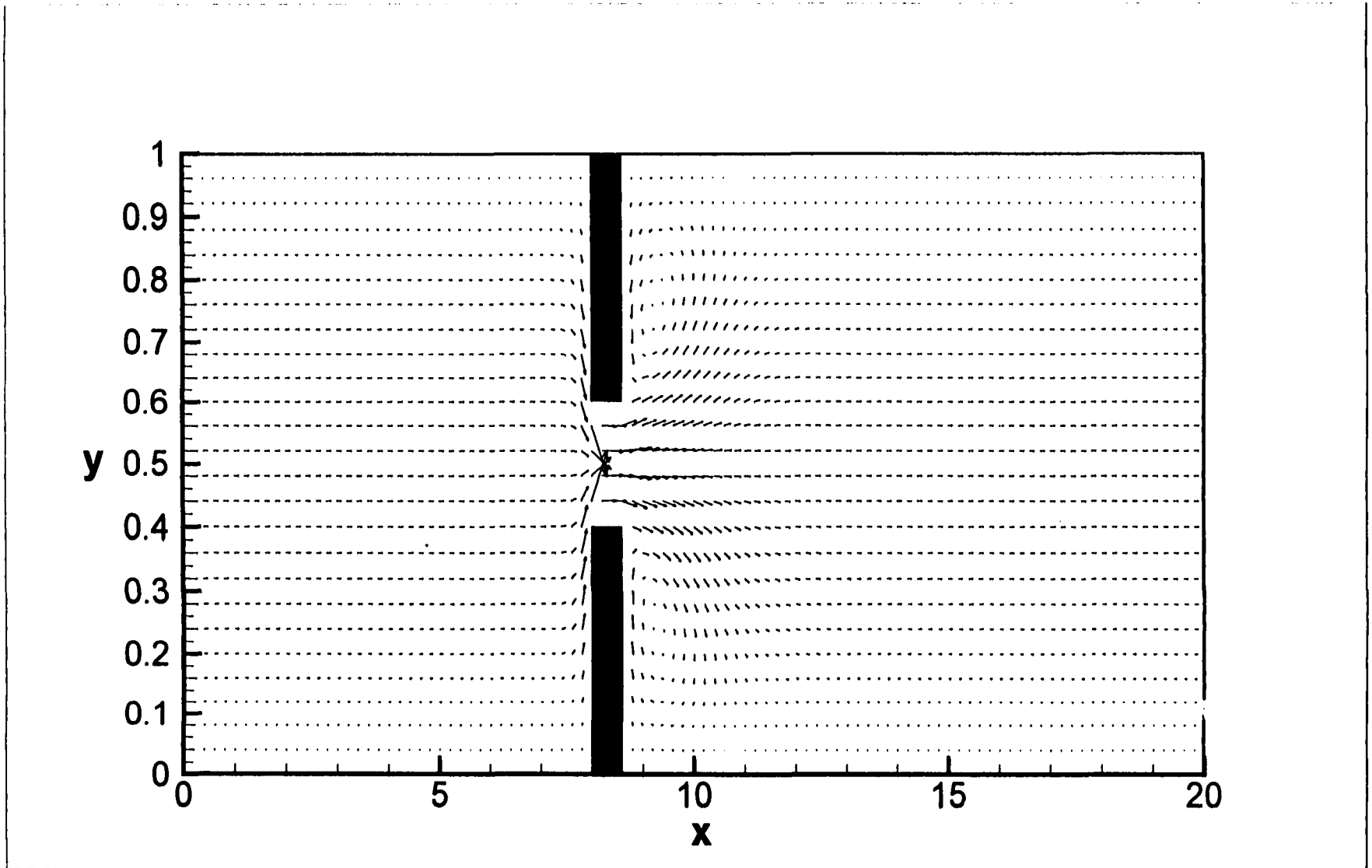


Figure 5.27 Velocity field for flow through a straight channel with restriction 0.2, $k=1$

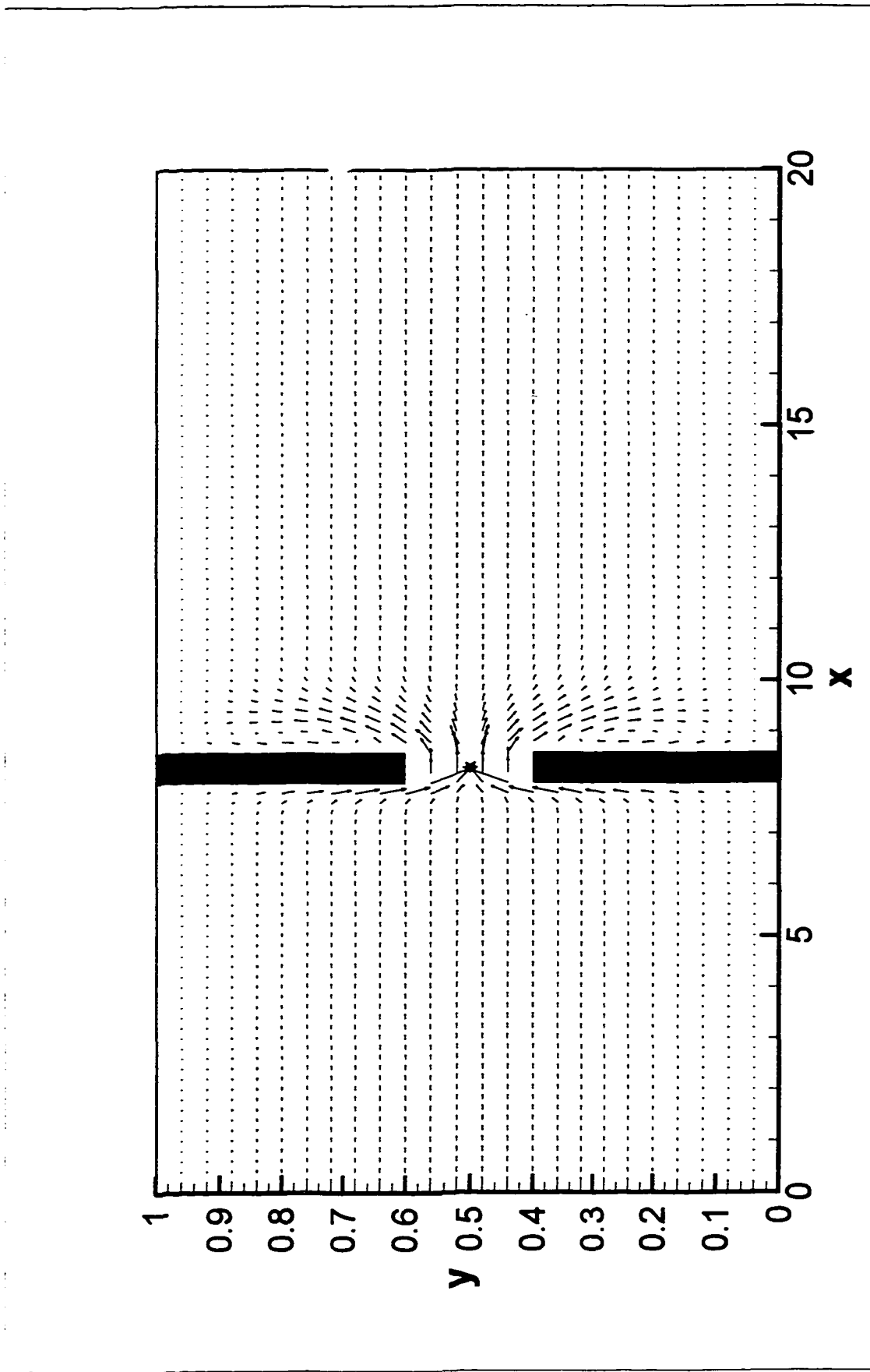


Figure 5.28 Velocity field for flow through a straight channel with restriction 0.2, $k=5$

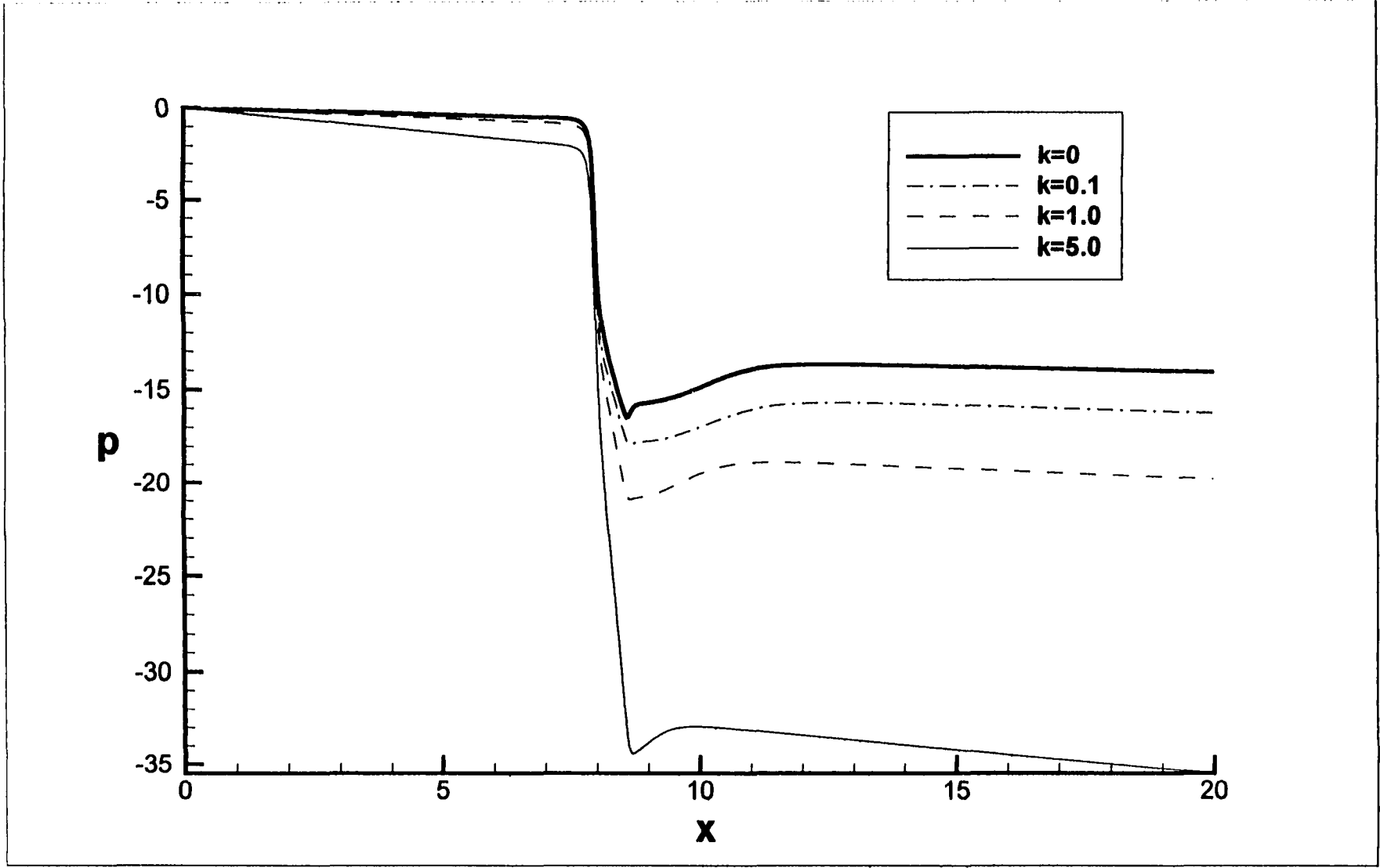


Figure 5.29 Variation of pressure with the downstream distance for flows through a straight channel with restriction 0.2

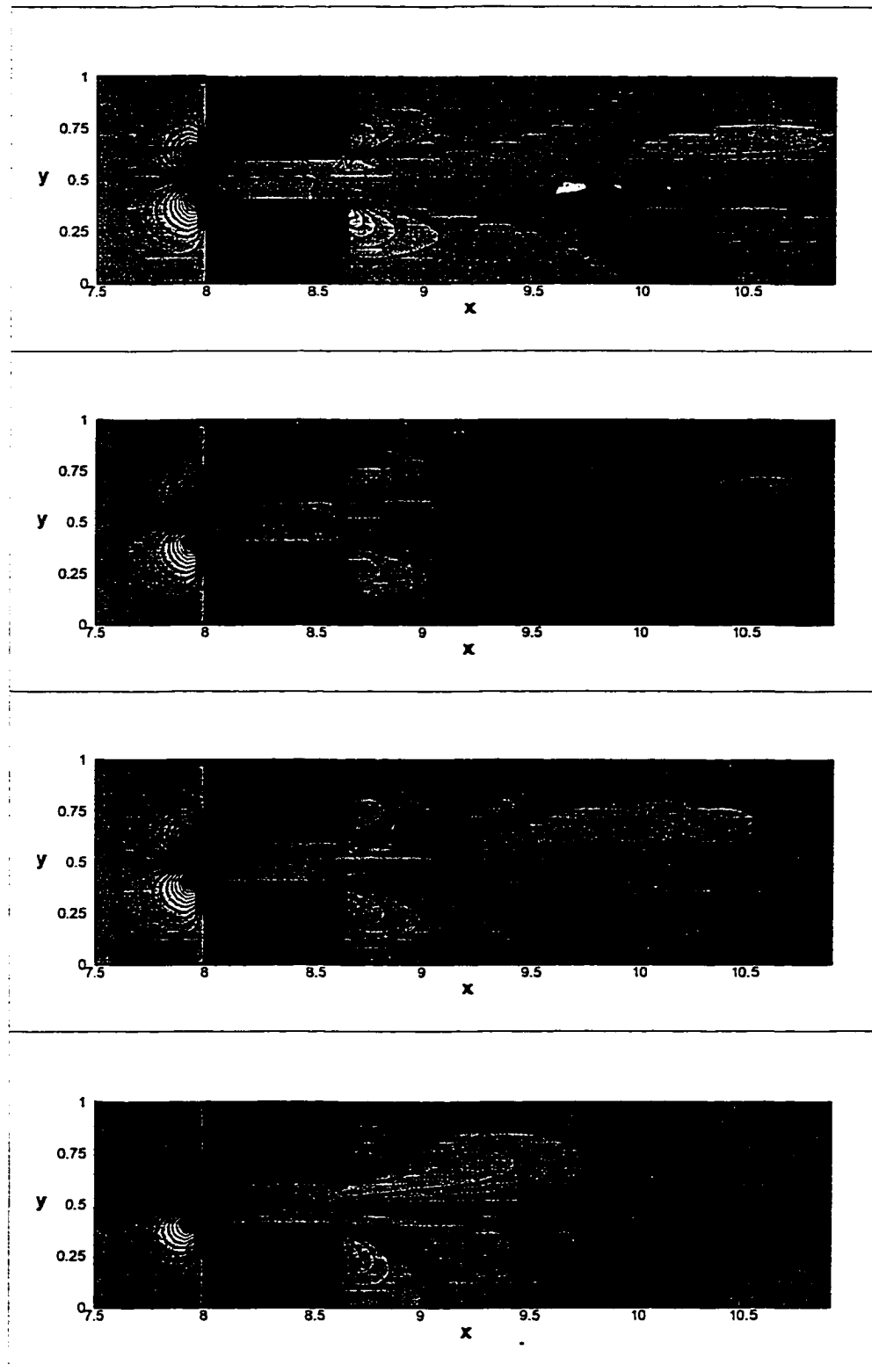


Figure 5.30. Plots of v - component contour for flows through a straight channel with restriction 0.2. From top to bottom, $k=0, 0.1, 1$ and 5 , respectively.

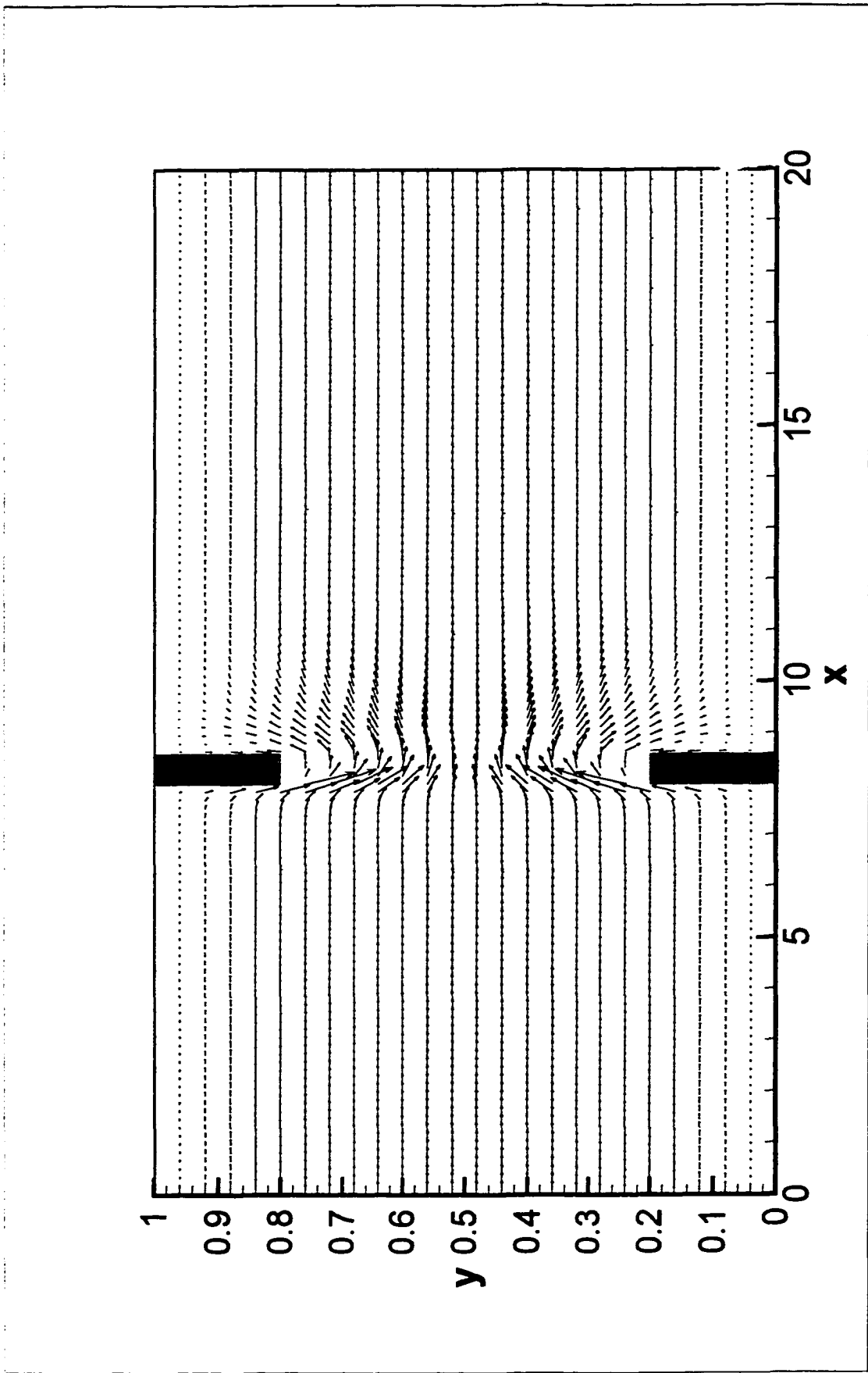


Figure 5.31 Velocity field for flow through a straight channel with restriction 0.6, $k=0$

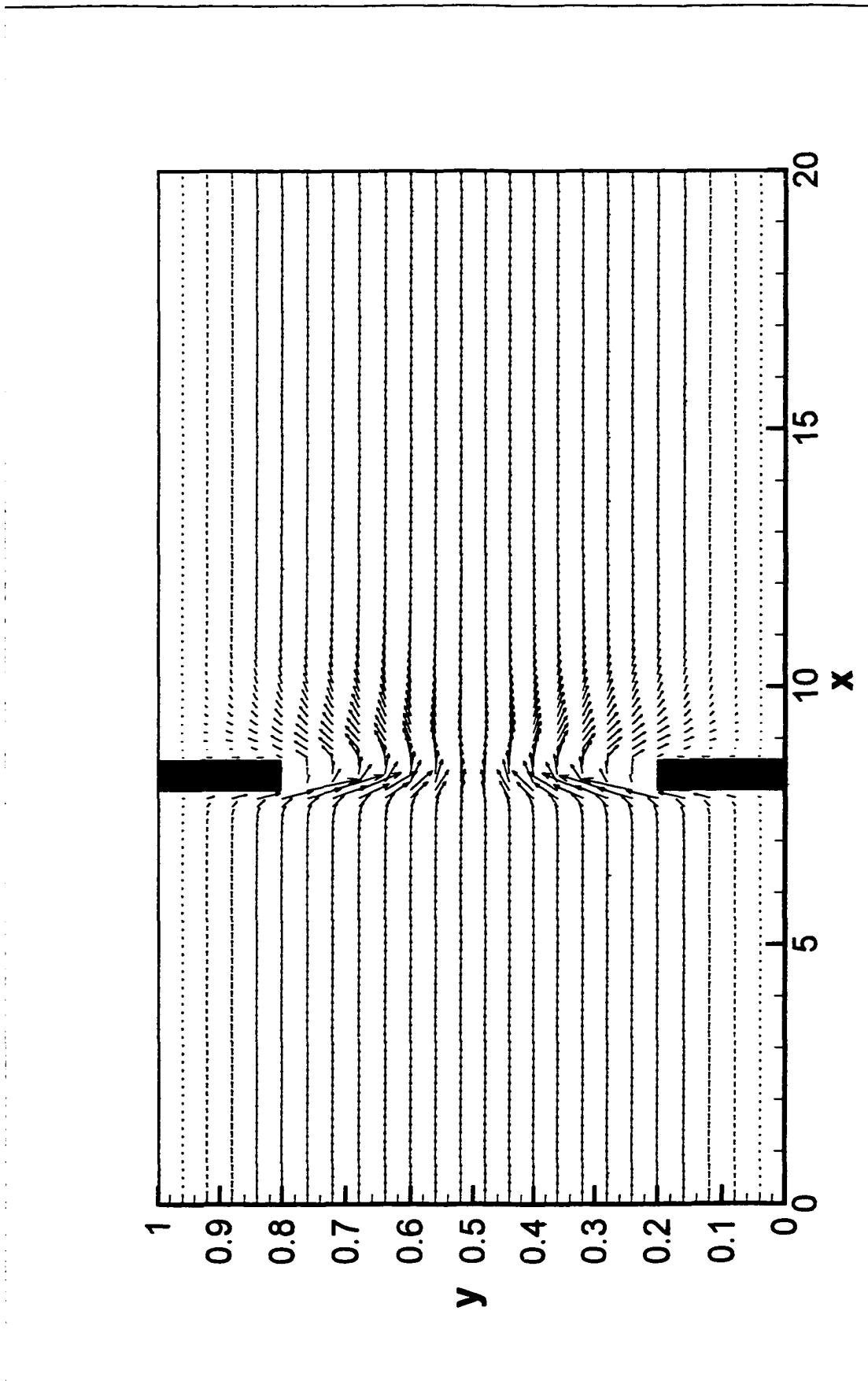


Figure 5.32 Velocity field for flow through a straight channel with restriction 0.6, $k=0.1$

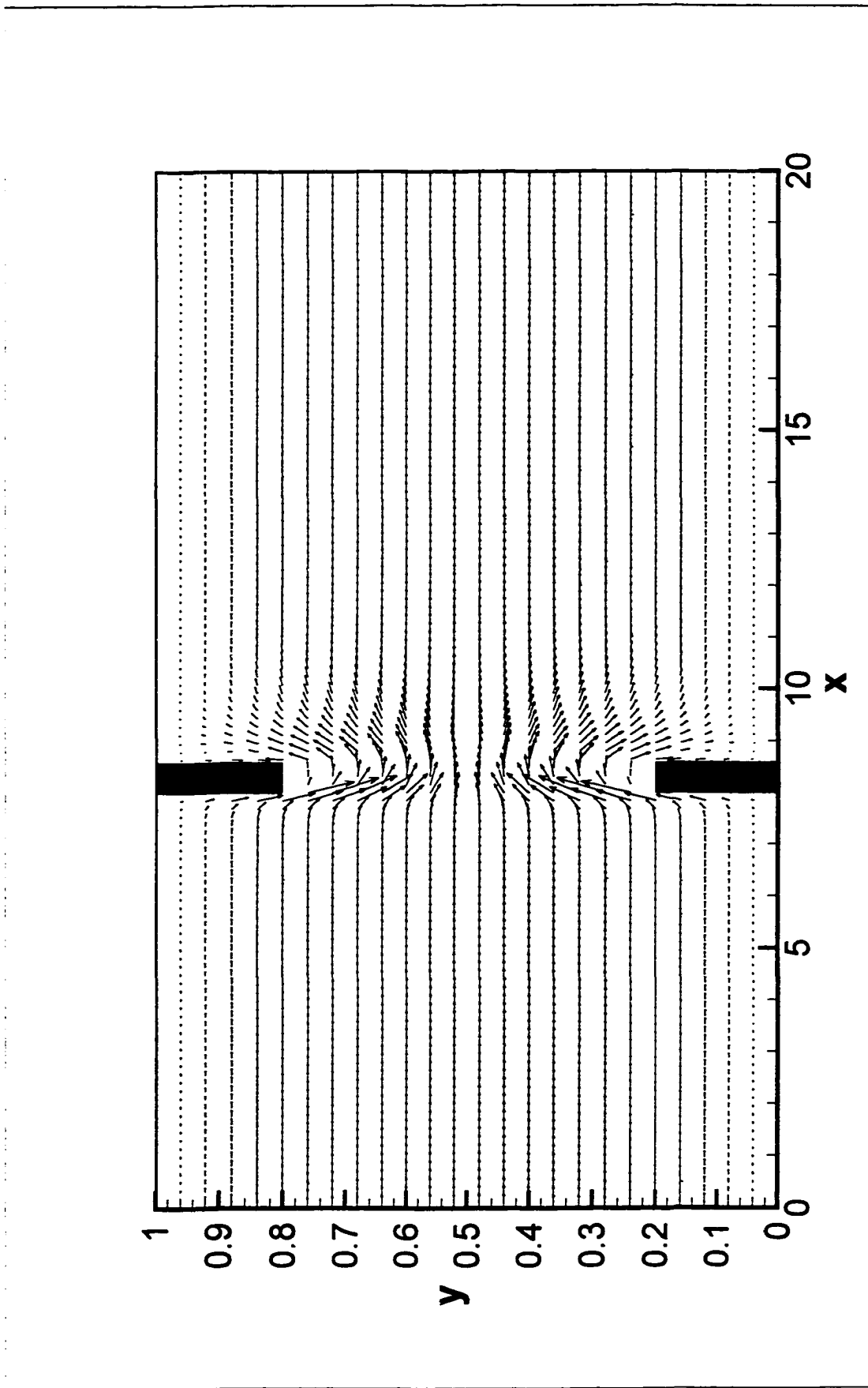


Figure 5.33 Velocity field for flow through a straight channel with restriction 0.6, $k=1$

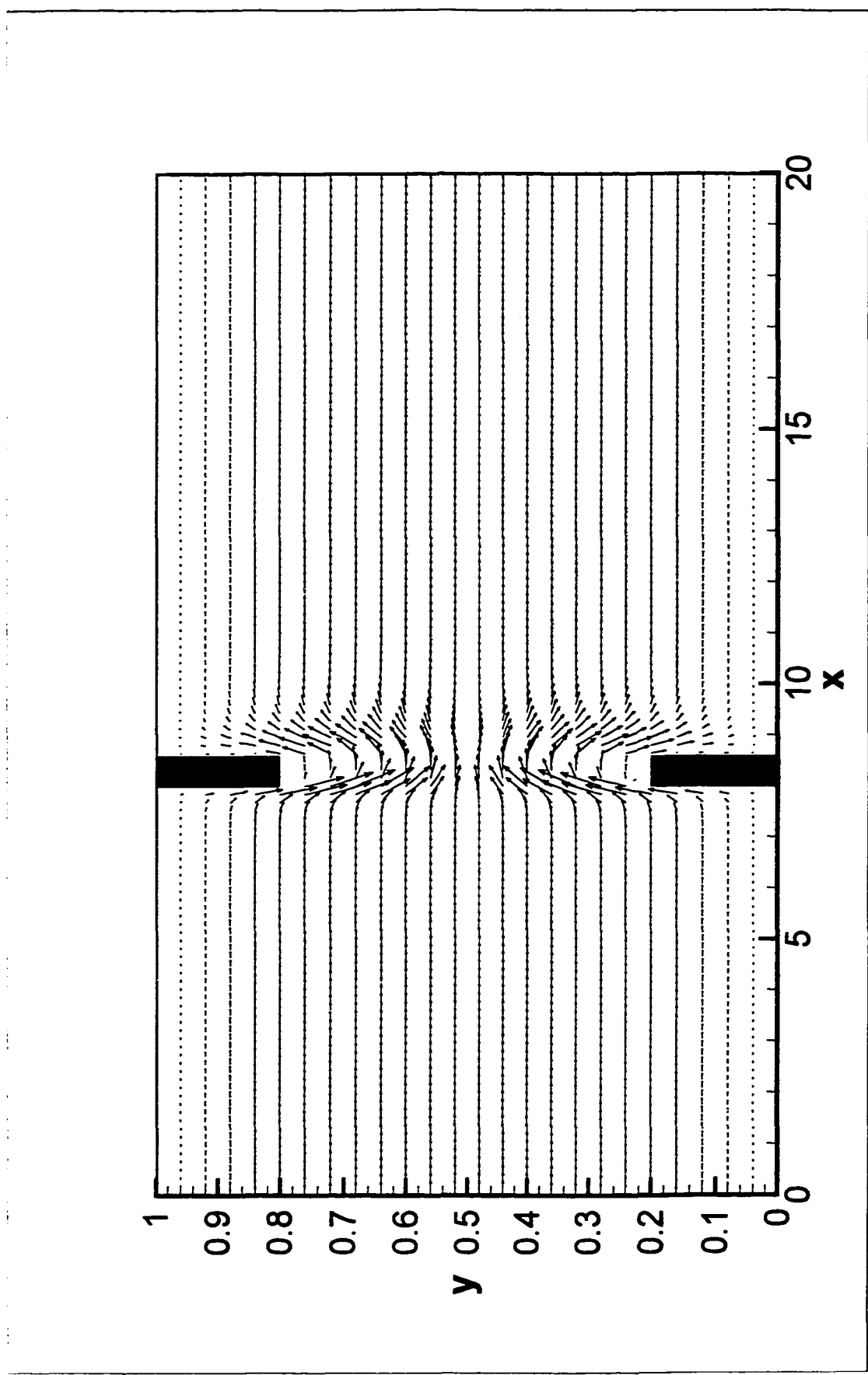


Figure 5.34 Velocity field for flow through a straight channel with restriction 0.6, $k=5$

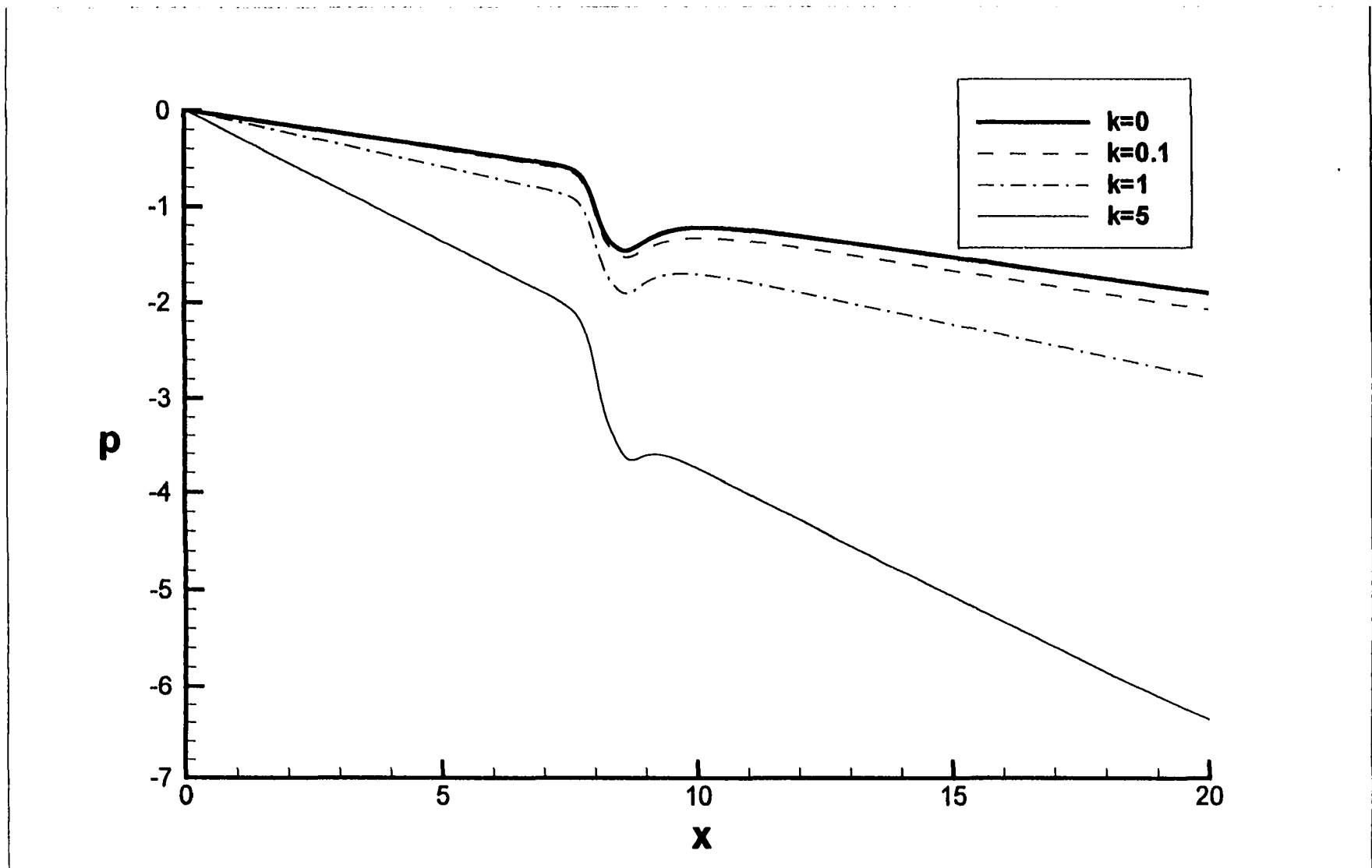


Figure 5.35 Variation of pressures with the downstream distance for flows through a straight channel with restriction 0.6

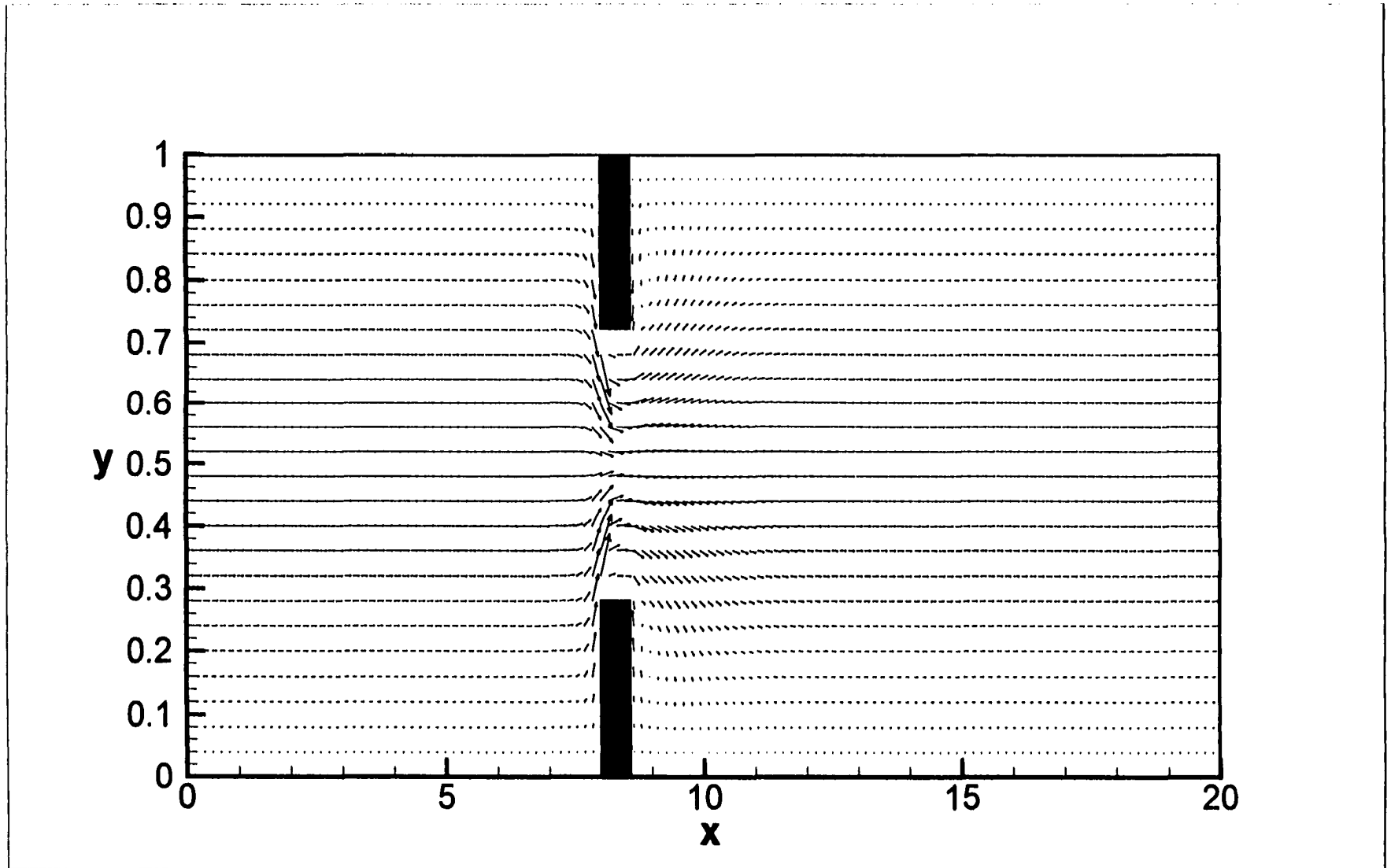


Figure 5.36 Velocity field for flow through a straight channel with restriction 0.44, $k=0$

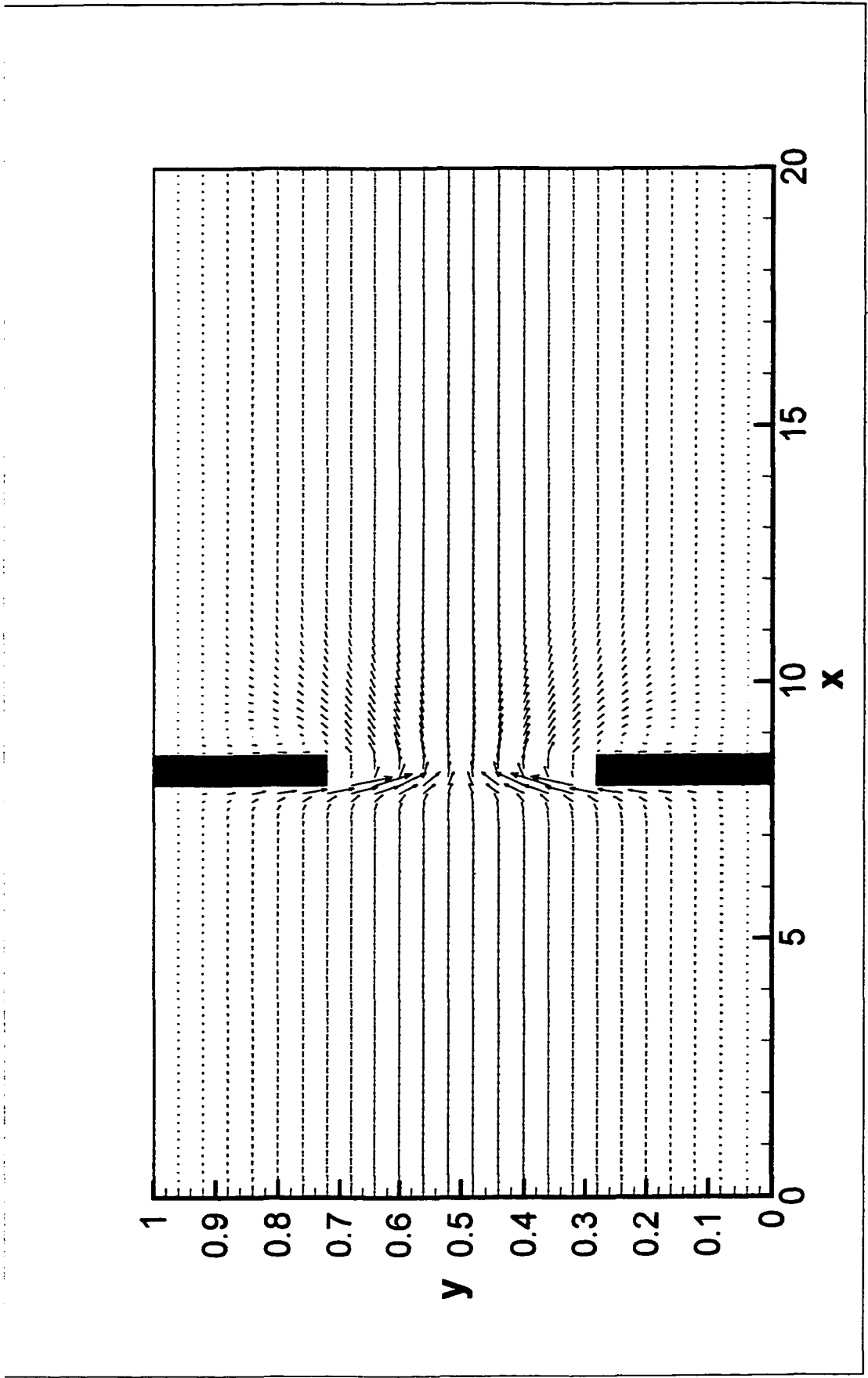


Figure 5.37 Velocity field for flow through a straight channel with restriction 0.44, $k=0.1$

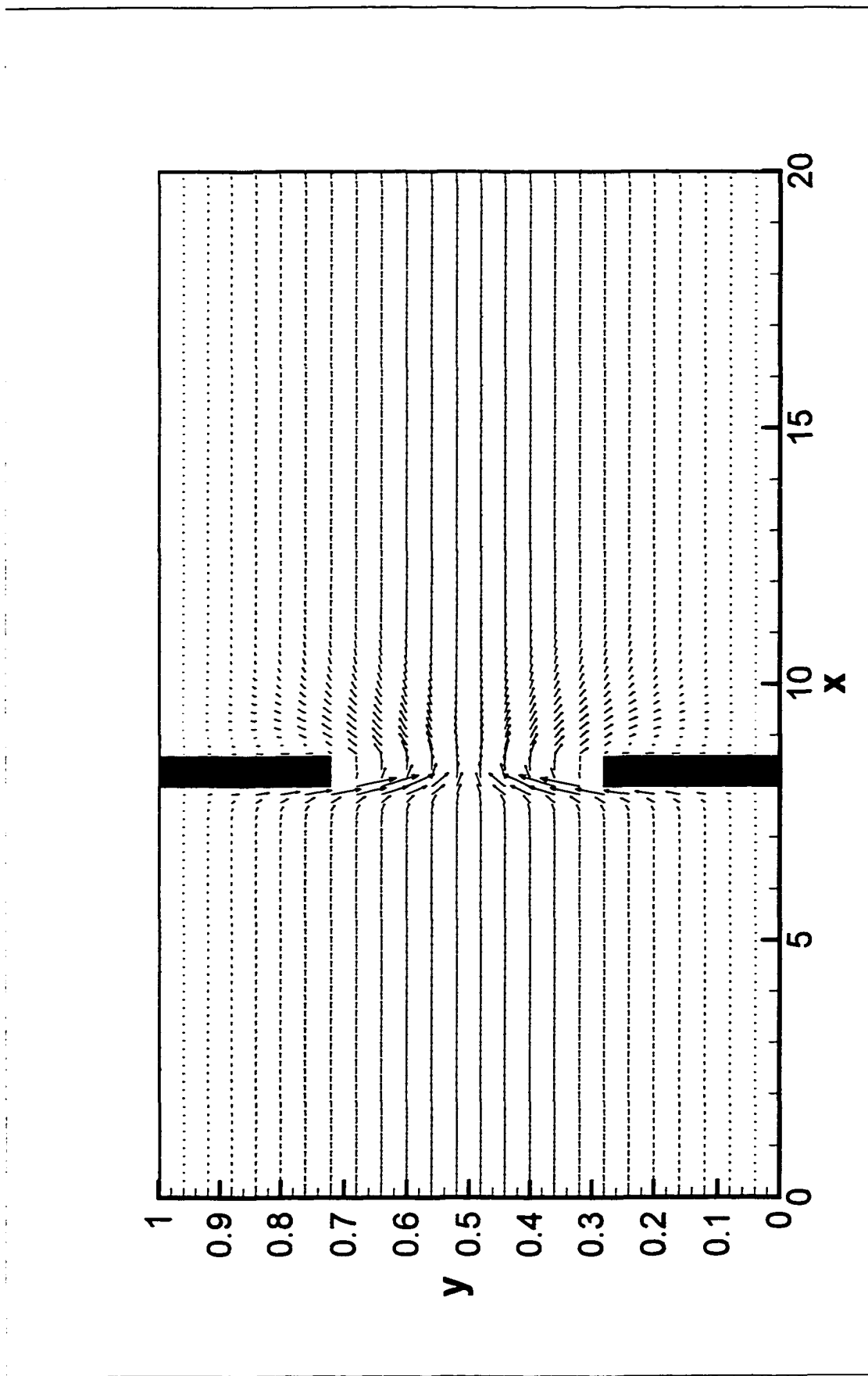


Figure 5.38 Velocity field for flow through a straight channel with restriction 0.44, $k=1$

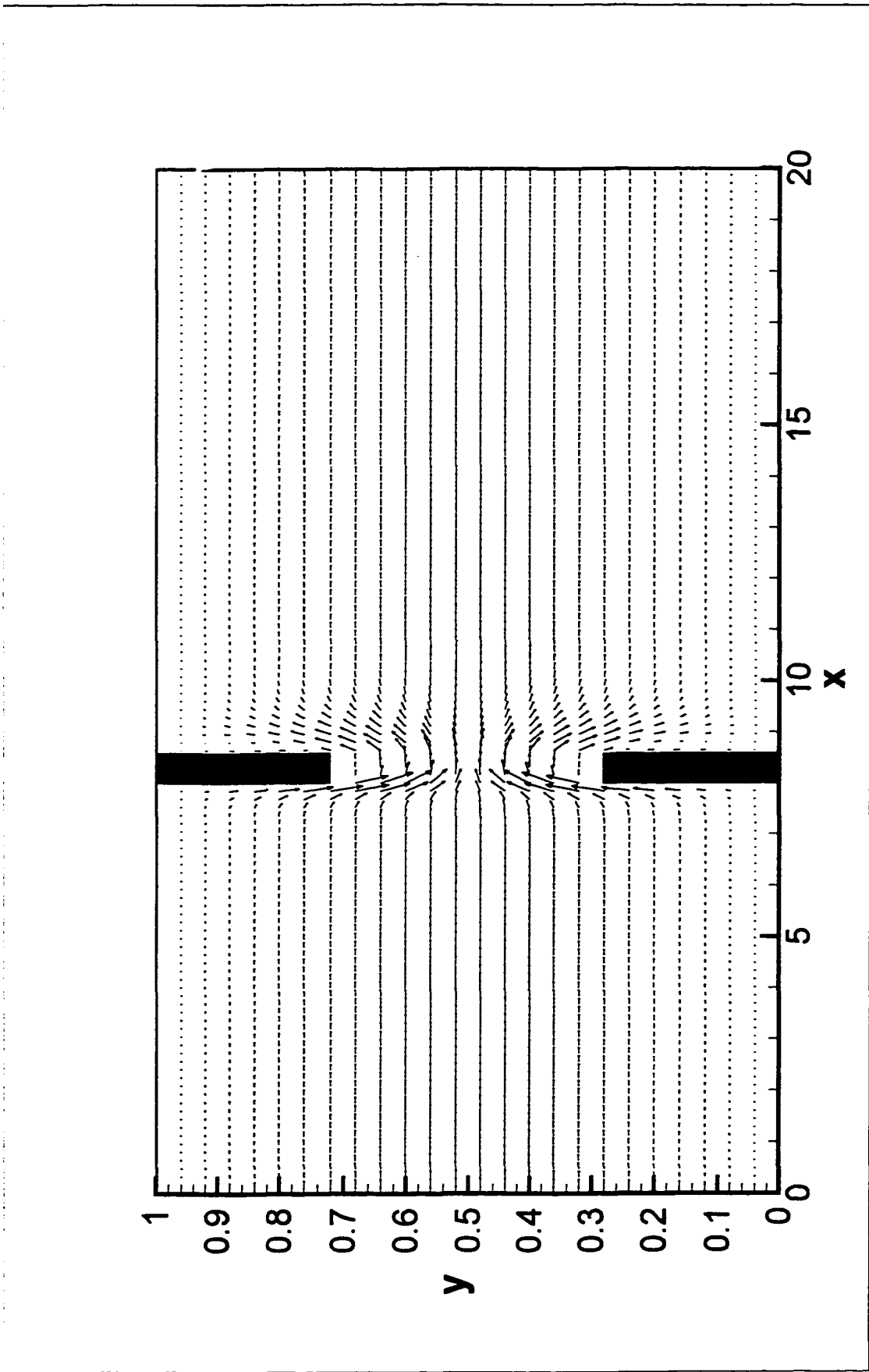


Figure 5.39 Velocity field for flow through a straight channel with restriction 0.44, $k=5$

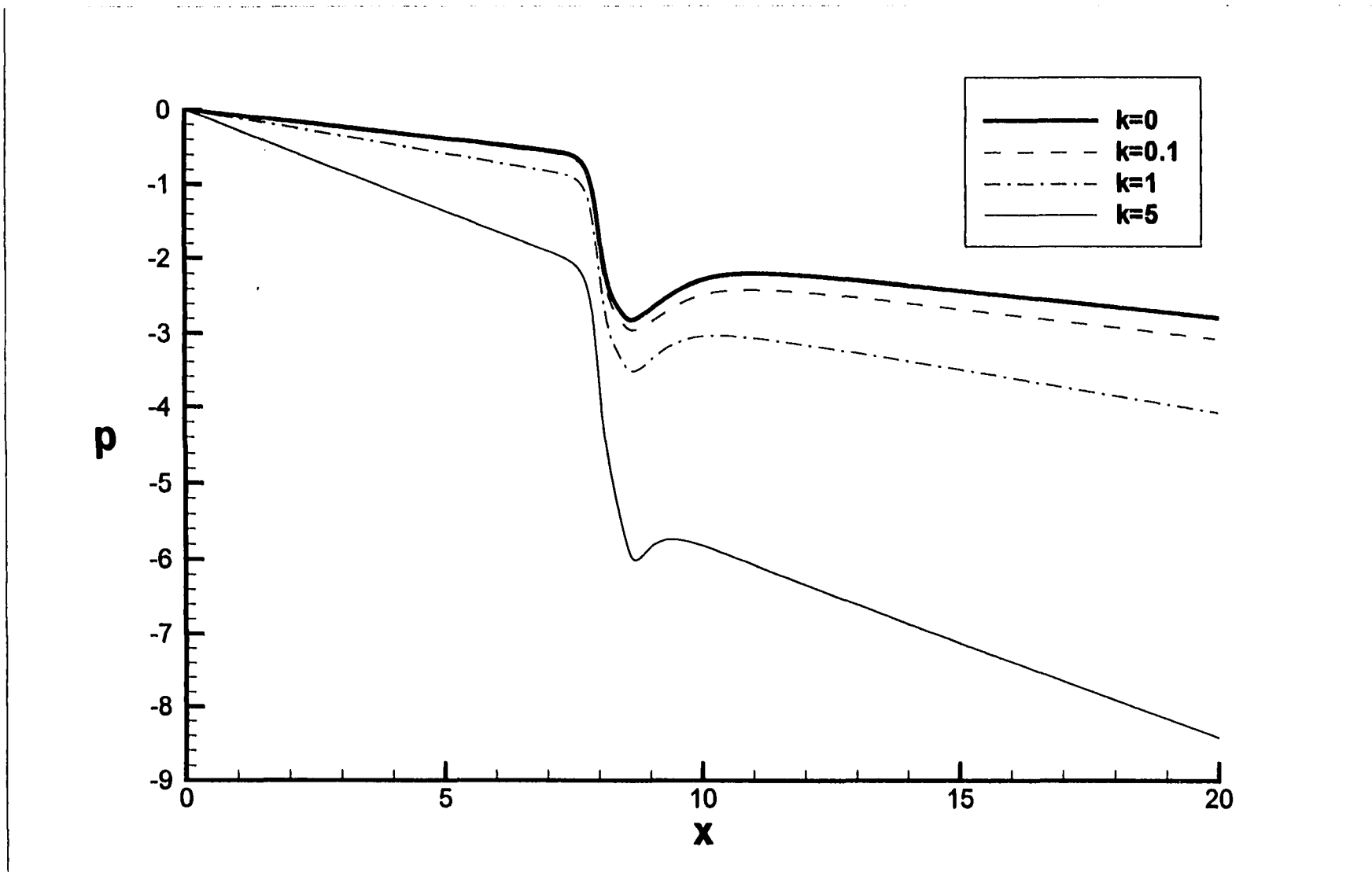


Figure 5.40 Variation of pressure with the downstream distance for flows through a straight channel with restriction 0.44

CHAPTER 6

CONCLUSION AND DISCUSSION

Micro-channel flows have been computed to investigate the influence of the Navier-Stokes formulation for the slip-flow boundary condition, and the micro-polar fluid model, respectively.

Results of the slip boundary condition show that the current methodology is valid for slip-flow regime (i.e., for values of Knudsen number less than approximately 0.1). Drag reduction phenomena apparent in some micro-channels can be explained by the slip-flow theory. These results are in agreement with some computations and experiments in the literature.

We also developed an *ad hoc* micro-polar fluid model to investigate the influence of the micro-gyration in micro-scale flows. Our model contains a new flow variable, micro-gyration g , as well as other conventional fluid dynamic variables. There are also two material constants, μ and κ , one scale parameter, $m \times Kn$, and one boundary condition parameter n in this model. Compared with the general micro-polar fluid model, the parameter number is significantly reduced, making the model practical.

The scale parameter $m \times Kn$ introduced the Knudsen number into the micro-polar fluid dynamics by a statistical argument. By introducing this parameter, the effect of rarefaction can be accounted for in the model.

The parameter μ is the classical bulk viscosity and needs little explanation. The vortex viscosity κ is related to micro-gyration, and needs modeling at current time. It affects the flow field in two aspects, by modifying the apparent viscosity and by introducing the effect of micro-gyration. In the simplest case of fully-developed channel flow, the overall effect is equivalent to lessening the Reynolds number by $(1+k/2)$.

The relationship between the material constants may need to be further examined in the micro-scale range, as well as the parameter n in the boundary condition.

The current micro-polar fluid model explains the drag increase phenomena in some micro-channel flows from both experimental and computational data. This result is exactly opposite to that predicted by slip-flow theory. The existence of micro effect needs to be taken into account for the micro-scale flow.

In the numerical analysis, a projection method solves the difficulty of an implicit pressure equation and also has the advantage of being extended to three dimensional and unsteady flow. A four variable (u, v, p, g) staggered grid is specifically developed here to suit the micro-polar fluid model. An explicit Euler scheme is used for solving the pseudo-time-dependent flow, which is equivalent somehow to an iteration method. It is recommended that one use the implicit scheme to improve the computation efficiency.

Computations for a straight channel with a restriction block are extended in this thesis. The flow restriction ratio, defined as the narrowest passage height to the standard channel height, varied from 0.2 to 0.6. In the case where the restriction ratio was smallest, the largest pressure drop was observed around the restriction block, which agrees with the Navier-Stokes solution. For the same restriction, pressure drop varied with the micro-gyration: the larger the micro-gyration, the larger the pressure drop. The velocity field is

also affected by the micro-gyration parameter. When the micro-gyration increases, the length of the back vortex in the down stream from the restriction decreases. The pair of back vortices attained maximum length down stream when no micro-gyration existed.

Table 6.1 ΔP across orifice vs. k and r/d

	$r/d = 0.2$	$r/d = 0.44$	$r/d = 0.6$
$k = 0$	-15.5	-2.0	-0.76
$k = 0.1$	-16.9	-2.1	-0.80
$k = 1.0$	-19.7	-2.5	-0.90
$k = 5.0$	-31.9	-3.7	-1.44

Micro-scale effects on orifice pressure drop may be significant and play an important role in developing micro flow meter as shown in Table 6.1. This data can be useful for the placement of pressure sensing ports before and after the orifice in a flow measuring device.

Flow of impinging jet into straight channel is also computed via micro-polar fluid model. The effect of micro-gyration is similar to that down stream after the restriction block in the straight channel flow with restrictions.

The effect of micro-gyration differs depends on the flow geometries. The micro-polar flow in a complex geometrical configuration may deviate significantly from its corresponding Navier-Stokes solution. There is no explicit expression of the effect of micro-gyration on the friction factor in general geometries, but the overall effect is that the micro-gyration increases the friction factor.

By inheriting the general concepts of classical fluid dynamics, such as field analysis and volume element, the micro-polar fluid model may share the same methodology used in Navier-Stokes dynamics. In a very specific circumstance, it even can employ a similar scheme in numerical simulation. For instance, we use the projection method to treat the implicit pressure difficulty in both models. On the other hand, since the micro-polar fluid model relaxes the restriction of infinitesimal fluid point with more general microstructure concept, it may make a breakthrough in a much finer world, e.g., a micron scale flow. With this promising perspective of benefits, commensurate difficulties do exist not only in the dramatically increased size of the variable and the equation, but also in understanding the physical meaning of the flow variables and the material parameters.

In terms of future work, applications of the current model for flows in complex geometrical configurations are the next natural step. For example, grooved-channel flows with periodic boundary condition, which may simulate the flow in a micro-bearing device, may be extended from the current numerical package with a little change of the boundary condition treatment.

Experimental work is also strongly suggested to verify the principle of the current model and improve the model parameters. In fact Dr. Hegab has been performing some related flow measurements which will definitely help to achieve this goal.

Another interesting extension from this work is combining a micro-polar fluid model and slip-flow boundary condition. The micro-polar fluid model extends the continuity assumption in the flow field, and slip-flow boundary treatment focuses on the

micro effect of the flow scale on the solid-fluid interface. Their combination may better encompass the general micro-scale flow.

APPENDIX

THE COMPLETE GOVERNING EQUATIONS

FOR THE MICRO-POLAR FLUID MODEL

Continuity:

$$\frac{\partial \rho}{\partial t} + \frac{\partial(\rho u)}{\partial x} + \frac{\partial(\rho v)}{\partial y} + \frac{\partial(\rho w)}{\partial z} = 0 \quad (\text{A.1})$$

Conservation of micro-inertia:

$$\frac{\partial j_{11}}{\partial t} + u \frac{\partial j_{11}}{\partial x} + v \frac{\partial j_{11}}{\partial y} + w \frac{\partial j_{11}}{\partial z} - (j_{31} + j_{21})g_2 + (j_{21} + j_{31})g_3 = 0 \quad (\text{A.2})$$

$$\frac{\partial j_{12}}{\partial t} + u \frac{\partial j_{12}}{\partial x} + v \frac{\partial j_{12}}{\partial y} + w \frac{\partial j_{12}}{\partial z} + j_{11}g_1 - j_{32}g_2 + (j_{22} - j_{31})g_3 = 0 \quad (\text{A.3})$$

$$\frac{\partial j_{13}}{\partial t} + u \frac{\partial j_{13}}{\partial x} + v \frac{\partial j_{13}}{\partial y} + w \frac{\partial j_{13}}{\partial z} - j_{11}g_1 + (j_{21} - j_{33})g_2 + j_{23}g_3 = 0 \quad (\text{A.4})$$

$$\frac{\partial j_{21}}{\partial t} + u \frac{\partial j_{21}}{\partial x} + v \frac{\partial j_{21}}{\partial y} + w \frac{\partial j_{21}}{\partial z} + j_{31}g_1 - j_{22}g_2 + (j_{32} - j_{11})g_3 = 0 \quad (\text{A.5})$$

$$\frac{\partial j_{22}}{\partial t} + u \frac{\partial j_{22}}{\partial x} + v \frac{\partial j_{22}}{\partial y} + w \frac{\partial j_{22}}{\partial z} + (j_{32} + j_{12})g_1 - (j_{12} + j_{32})g_3 = 0 \quad (\text{A.6})$$

$$\frac{\partial j_{23}}{\partial t} + u \frac{\partial j_{23}}{\partial x} + v \frac{\partial j_{23}}{\partial y} + w \frac{\partial j_{23}}{\partial z} + (j_{33} - j_{12})g_1 + j_{22}g_2 + j_{13}g_3 = 0 \quad (\text{A.7})$$

$$\frac{\partial j_{31}}{\partial t} + u \frac{\partial j_{31}}{\partial x} + v \frac{\partial j_{31}}{\partial y} + w \frac{\partial j_{31}}{\partial z} - j_{21}g_1 + (j_{11} - j_{23})g_2 + j_{33}g_3 = 0 \quad (\text{A.8})$$

$$\frac{\partial j_{32}}{\partial t} + u \frac{\partial j_{32}}{\partial x} + v \frac{\partial j_{32}}{\partial y} + w \frac{\partial j_{32}}{\partial z} + (j_{13} - j_{22})g_1 + j_{12}g_2 - j_{33}g_3 = 0 \quad (\text{A.9})$$

$$\frac{\partial j_{33}}{\partial t} + u \frac{\partial j_{33}}{\partial x} + v \frac{\partial j_{33}}{\partial y} + w \frac{\partial j_{33}}{\partial z} - (j_{13} + j_{23})g_1 + (j_{13} + j_{23})g_2 = 0 \quad (\text{A.10})$$

Balance of momentum:

$$\begin{aligned} & \rho \frac{\partial u}{\partial t} + \rho u \frac{\partial u}{\partial x} + \rho v \frac{\partial u}{\partial y} + \rho w \frac{\partial u}{\partial z} - \frac{\partial p}{\partial x} + \\ & + (\lambda + \mu) \left(\frac{\partial^2 u}{\partial x^2} + \frac{\partial^2 v}{\partial x \partial y} + \frac{\partial^2 w}{\partial x \partial z} \right) + (\mu + \kappa) \left(\frac{\partial^2 u}{\partial x^2} + \frac{\partial^2 u}{\partial y^2} + \frac{\partial^2 u}{\partial z^2} \right) + \kappa \left(\frac{\partial g_3}{\partial y} - \frac{\partial g_2}{\partial z} \right) = 0 \end{aligned} \quad (\text{A.11})$$

$$\begin{aligned} & \rho \frac{\partial v}{\partial t} + \rho u \frac{\partial v}{\partial x} + \rho v \frac{\partial v}{\partial y} + \rho w \frac{\partial v}{\partial z} - \frac{\partial p}{\partial y} + \\ & + (\lambda + \mu) \left(\frac{\partial^2 u}{\partial x \partial y} + \frac{\partial^2 v}{\partial y^2} + \frac{\partial^2 w}{\partial y \partial z} \right) + (\mu + \kappa) \left(\frac{\partial^2 v}{\partial x^2} + \frac{\partial^2 v}{\partial y^2} + \frac{\partial^2 v}{\partial z^2} \right) + \kappa \left(\frac{\partial g_1}{\partial z} - \frac{\partial g_3}{\partial x} \right) = 0 \end{aligned} \quad (\text{A.12})$$

$$\begin{aligned} & \rho \frac{\partial w}{\partial t} + \rho u \frac{\partial w}{\partial x} + \rho v \frac{\partial w}{\partial y} + \rho w \frac{\partial w}{\partial z} - \frac{\partial p}{\partial z} + \\ & + (\lambda + \mu) \left(\frac{\partial^2 u}{\partial x \partial z} + \frac{\partial^2 v}{\partial y \partial z} + \frac{\partial^2 w}{\partial z^2} \right) + (\mu + \kappa) \left(\frac{\partial^2 w}{\partial x^2} + \frac{\partial^2 w}{\partial y^2} + \frac{\partial^2 w}{\partial z^2} \right) + \kappa \left(\frac{\partial g_2}{\partial x} - \frac{\partial g_1}{\partial y} \right) = 0 \end{aligned} \quad (\text{A.13})$$

Balance of momentum moments:

$$\begin{aligned} & \frac{\partial}{\partial t} (\rho j_{11} g_1 + \rho j_{12} g_2 + \rho j_{13} g_3) + u \frac{\partial}{\partial x} (\rho j_{11} g_1 + \rho j_{12} g_2 + \rho j_{13} g_3) + \\ & + v \frac{\partial}{\partial y} (\rho j_{11} g_1 + \rho j_{12} g_2 + \rho j_{13} g_3) + w \frac{\partial}{\partial z} (\rho j_{11} g_1 + \rho j_{12} g_2 + \rho j_{13} g_3) + \\ & + (\alpha + \beta) \left(\frac{\partial^2 g_1}{\partial x^2} + \frac{\partial^2 g_2}{\partial x \partial y} + \frac{\partial^2 g_3}{\partial x \partial z} \right) + \gamma \left(\frac{\partial^2 g_1}{\partial x^2} + \frac{\partial^2 g_1}{\partial y^2} + \frac{\partial^2 g_1}{\partial z^2} \right) + \kappa \left(\frac{\partial w}{\partial y} - \frac{\partial v}{\partial z} \right) - 2\kappa g_1 = 0 \end{aligned} \quad (\text{A.14})$$

$$\begin{aligned}
& \frac{\partial}{\partial t}(\rho j_{21} g_1 + \rho j_{22} g_2 + \rho j_{23} g_3) + u \frac{\partial}{\partial x}(\rho j_{21} g_1 + \rho j_{22} g_2 + \rho j_{23} g_3) + \\
& + v \frac{\partial}{\partial y}(\rho j_{21} g_1 + \rho j_{22} g_2 + \rho j_{23} g_3) + w \frac{\partial}{\partial z}(\rho j_{21} g_1 + \rho j_{22} g_2 + \rho j_{23} g_3) + \\
& + (\alpha + \beta) \left(\frac{\partial^2 g_1}{\partial x \partial y} + \frac{\partial^2 g_2}{\partial y^2} + \frac{\partial^2 g_3}{\partial y \partial z} \right) + \gamma \left(\frac{\partial^2 g_2}{\partial x^2} + \frac{\partial^2 g_2}{\partial y^2} + \frac{\partial^2 g_2}{\partial z^2} \right) + \kappa \left(\frac{\partial u}{\partial z} - \frac{\partial w}{\partial x} \right) - 2\kappa g_2 = 0
\end{aligned}
\tag{A.15}$$

$$\begin{aligned}
& \frac{\partial}{\partial t}(\rho j_{31} g_1 + \rho j_{32} g_2 + \rho j_{33} g_3) + u \frac{\partial}{\partial x}(\rho j_{31} g_1 + \rho j_{32} g_2 + \rho j_{33} g_3) + \\
& + v \frac{\partial}{\partial y}(\rho j_{31} g_1 + \rho j_{32} g_2 + \rho j_{33} g_3) + w \frac{\partial}{\partial z}(\rho j_{31} g_1 + \rho j_{32} g_2 + \rho j_{33} g_3) + \\
& + (\alpha + \beta) \left(\frac{\partial^2 g_1}{\partial x \partial z} + \frac{\partial^2 g_2}{\partial y \partial z} + \frac{\partial^2 g_3}{\partial z^2} \right) + \gamma \left(\frac{\partial^2 g_3}{\partial x^2} + \frac{\partial^2 g_3}{\partial y^2} + \frac{\partial^2 g_3}{\partial z^2} \right) + \kappa \left(\frac{\partial v}{\partial x} - \frac{\partial u}{\partial y} \right) - 2\kappa g_3 = 0
\end{aligned}
\tag{A.16}$$

REFERENCES

- Ahmad, G. (1976). "Self-Similar Solution of Incompressible Micropolar Boundary Layer Flow over a Semi-Infinite Plate." *Int. J. Engng. Sci.*, Vol. 14, 639-646.
- Allen, S. J., DeSilva, C. N., and Kline, K. A. (1967). "Theory of Simple Deformable Directed Fluids." *Phys. Fluids*, Vol. 10, 2551-2555.
- Ariman, T., and Cakmak, A. S. (1967). "Couple Stresses in Fluids." *Phys. Fluids*, Vol. 10, 2497-2499.
- Ariman, T., Cakmak, A. S., and Hill, L. R. (1967). "Flow of Micropolar Fluids between Two Concentric Cylinders." *Phys. Fluids*, Vol. 10, 2545-2550.
- Ariman, T., Turk, M. A., and Sylvester, N. D. (1973). "Microcontinuum Fluid Mechanics – A Review." *Int. J. Engng. Sci.*, Vol. 11, 905-930.
- Ariman, T., Turk, M. A., and Sylvester, N. D. (1974). "Applications of Microcontinuum Fluid Mechanics." *Int. J. Engng. Sci.*, Vol. 12, 273-293.
- Arkilic, E. B., Breuer, K. S., and Schmidt, M. A. (1994). "Gaseous Flow in Microchannels." *Int. Mechanical Engineering Congress and Exposition*, Chicago, ASME, FED-Vol. 197, 57-66.
- Bailey, D. K., Ameel, T. A., Warrington, R. O. Jr., and Savoie, T. I. (1995) "Single Phase Forced Convection Heat Transfer in Microgeometries – A Review." *30th Intersociety Energy Conversion Engineering Conference*, Orlando, Florida.
- Bassous, E., Taub, H. H., and Kuhn, L. (1977). "Ink Jet Printing Nozzle Arrays Etched in Silicon." *Appl. Phys. Lett.*, Vol. 31, 135-137.
- Batchelor, G. K. (1967). "An Introduction to Fluid Dynamics." Cambridge University Press.
- Beskok, A., and Karniadakis, G. E. (1992). "Simulation of Slip-Flows in Complex Micro-Geometries." ASME, DSC, Vol. 40, 355-370. Book No. G00743.
- Beskok, A., and Karniadakis, G. E. (1993). "Simulation of Heat and Momentum Transfer in Complex Micro-Geometries." *AIAA 93-3269*, Orlando, FL.

- Beskok, A., and Karniadakis, G. E. (1994). "Simulation of Heat and Momentum Transfer in Complex Microgeometries." *J. Thermophysics & Heat Transfer*, Vol. 8, 647-655.
- Beskok, A., and Karniadakis, G. E. (1995). "Rarefaction, Compressibility and Thermal Creep Effects in Micro-Flows." *ASME-95*.
- Beskok, A. (1996). "Simulations and Models for Gas Flows in Microgeometries." Ph.D. Dissertation, Princeton.
- Beskok, A., Karniadakis, G. E., and Trimmer, W. (1996). "Rarefaction and Compressibility Effects in Gas Microflows." *J. Fluids Engng.*, Vol. 118, 448-456.
- Beskok, A., and Karniadakis, G. E. (1997). "Modeling Separation in Rarefied Gas Flows." *ALAA 97-1883*, Snowmass Village, CO.
- Bird, G. (1994). "Molecular Gas Dynamics and the Direct Simulation of Gas Flows." Oxford Engineering Science, Oxford University Press, New York.
- Can, N. H., Huy, N. X., and Cau, T. N. (1989). "On the Convective Motion in a Micropolar Viscous Fluid." *Int. J. Engng. Sci.*, Vol. 27, 1183-1202.
- Caruana, C. M. (1996). "ChEs Seek Big Gains From Process Miniaturization." *Chemical Engineering Progress*, Vol. 92, April, 12-19.
- Cercignani, C. (1975). "Theory and Application of the Boltzmann Equation." Scottish Academic.
- Chen, C. S., Lee, S. M., and Sheu, J. D. (1998). "Numerical Analysis of Gas Flow in Microchannels." *Numerical Heat Transfer, Part A*, Vol. 33, 749-762.
- Choi, S. B., Barron, R. F., and Warrington, R. O. (1991). "Fluid Flow and Heat Transfer in Micro Tubes." *Micromechanical Sensors, Actuators, and Systems, DSC*, ASME, New York. Vol. 32, 123-134.
- Ciarletta, M. (1995). "On the Theory of Heat-Conducting Micropolar Fluids." *Int. J. Engng. Sci.*, Vol. 33, 1403-1417.
- Das, M. L., and Sanyal, D. C. (1990). "Unsteady Flow of a Micropolar Fluid Through a Rectangular Channel." *Int. J. Engng. Sci.*, Vol. 28, 863-870.
- Easwaran, C. V., and Majumdar, S. R. (1990). "Causal Fundamental Solutions for the Slow Flow of a MicroPolar Fluid." *Int. J. Engng. Sci.*, Vol. 28, 843-850.

- Ebert, W. A., and Sparrow, E. M. (1965). "Slip Flow in Rectangular and Annular Ducts." *Trans. ASME J Basic Eng.*, Vol. 87, 1018-1024.
- Epstein, A. H., *et al.* (1997). "Power MEMS and Microengines." *1997 International Conference on Solid-State Sensors and Actuators*, Chicago, June, 753-756.
- Eringen, A. C. (1964). "Simple Microfluids." *Int. J. Engng. Sci.*, Vol. 2, 205-217.
- Eringen, A. C. (1969). "Micropolar Fluids with Stretch." *Int. J. Engng. Sci.*, Vol. 7, 115-127.
- Eringen, A. C. (1972). "Theory of Thermomicrofluids." *J. Mathematical Analysis & Applications.*, Vol. 38, 480-496.
- Eringen, A. C. (1980). "Theory of Anisotropic Micropolar Fluids." *Int. J. Engng. Sci.*, Vol. 18, 5-17.
- Eringen, A. C., and Okada, K. (1995). "A Lubrication Theory for Fluids with Microstructure." *Int. J. Engng. Sci.*, Vol. 33, 2297-2308.
- Gass, V., van der Schoot, B. H., and de Rooij, N. F. (1993). "Nanofluid Handling by Micro-Flow-Sensor Based on Drag Force Measurements." *Proc 93 IEEE MicroElectroMechSys (MEMS)*. 167-172.
- Grad, H. (1949). "On the Kinetic Theory of Rarefied Gas Dynamics." *Commun. Pure Appl. Math.* Vol. 2, 331-407.
- Gravesen, P., Branebjerg, J., and Jensen, O. S. (1993). "Microfluidics – A Review." *J. Micromech. Microeng.* Vol. 3, 168-182.
- Harley, J. C., Huang, Y., Bau, H. H., and Zemel, J. N. (1995). "Gas Flow in Micro-Channels." *J. Fluid Mech.*, Vol. 284, 257-274.
- Ho, C., and Tai, Y. (1996). "Review: MEMS and Its Applications for Flow Control." *J. Fluids Engng.*, Vol. 118, 437-447.
- Huang, P. G., and Leschziner, M. A. (1984). "An Introduction and Guide to the Computer Code: TEAM." Mechanical Engineering Department, University of Manchester Institute of Science and Technology.
- Hung, C., Tsai, J., and Chen, C. (1996). "Nonlinear Stability of the Thin Micropolar Liquid Film Flowing Down on a Vertical Plate." *J. Fluids Engng.*, Vol. 118, 498-505.

- Kavehpour, H. P., Faghri, M., and Asako, Y. (1997). "Effects of Compressibility and Rarefaction on Gaseous Flows in Microchannels." *Numerical Heat Transfer, Part A*, Vol. 32, 677-696.
- Kline, K. A., and Allen, S. J. (1970). "Nonsteady Flows of Fluids with Microstructure." *Phys. Fluids*, Vol. 13, 263-270.
- Kogan, M. N. (1972). "Molecular Gas Dynamics." *Annual Review of Fluid Mechanics*, Vol. 5, 383-404.
- Kolpashchikov, V. L., Migun, N. P., and Prokhorenko, P. P. (1983). "Experimental Determination of Material Micropolar Fluid Constants." *Int. J. Engng. Sci.*, Vol. 21, 405-411.
- Ma, S. W., and Gerner, F. M. (1993). "Forced Convection Heat Transfer From Microstructures." *J. Heat Transfer*. Vol. 115, 872-880.
- Olmstead, W. E., and Majumdar, S. R. (1983). "Fundamental Oseen Solution for the 2-Dimensional Flow of a Micropolar Fluid." *Int. J. Engng. Sci.*, Vol. 21, 423-430.
- Papautsky, I., Brazzle, J., Ameel, T. A., and Frazier, A. B. (1998). "Microchannel Fluid Behavior Using Micropolar Fluid Theory." *Proceedings of the IEEE Micro Electro Mechanical Systems (MEMS)*, Heidelberg, Germany, 544-549.
- Patankar, S. V. (1980). "Numerical Heat Transfer and Fluid Flow." Hemisphere Publishing Corporation, McGraw Hill.
- Peng, X. F., and Wang, B. X. (1994). "Experimental Investigation on Liquid Forced-Convection Heat Transfer Through Microchannels." *Int. J. Heat Mass Transfer*, Vol. 37, Suppl. 1, 73-82.
- Peng, X. F., Peterson, G. P., and Wang, B. X. (1994a). "Heat Transfer Characteristics of Water Flowing Through Microchannels." *Exp. Heat Transfer*, Vol. 7, 249-264.
- Peng, X. F., Peterson, G. P., and Wang, B. X. (1994b). "Frictional Flow Characteristics of Water Flowing Through Microchannels." *Exp. Heat Transfer*, Vol. 7, 265-283.
- Peyret, R., and Taylor, T. (1990). "Computational Methods for Fluid Flow." Springer-Verlag.
- Pfahler, J. N. (1992). "Liquid Transport in Micron and Submicron Size Channels." Ph.D. Dissertation. University of Pennsylvania.

- Pfahler, J., Harley, J., Bau, H., and Zemel, J. N. (1991). "Gas and Liquid Flow in Small Channels." *Micromechanical Sensors, Actuators, and Systems, DSC*, ASME, New York. Vol. 32, 49-60.
- Piekos, E. S., and Breuer, K. S. (1996). "Numerical Modeling of Micromechanical Devices Using the Direct Simulation Monte Carlo Method." *J. Fluids Engng.*, Vol. 118, 464-469.
- Pong, K. C., and Ho., C. M. (1994). "Non-Linear Pressure Distribution in Microchannels." *Int. Mechanical Engineering Congress and Exposition*, Chicago, ASME, FED-Vol. 197, 51-56.
- Rees, D. A. S., and Bassom, A. P. (1996). "The Blasius Boundary-Layer Flow of a Micropolar Fluid." *Int. J. Engng. Sci.*, Vol. 34, 113-124.
- Stokes, V. K. (1966). "Couple Stresses in Fluids." *Phys. Fluids*, Vol. 9, 1709-1715.
- Stokes, V. K. (1984). "Theories of Fluids with Microstructure." Springer-Verlag .
- Wegeng, R. S., and Drost, M. K. (1994). "Developing New Miniature Energy Systems." *Mechanical Engineering*, September, 82-85.
- Wegeng, R. S., Call, C. J., and Drost, M. K. (1996). "Chemical System Miniaturization." *PNNL-SA-27317*. Pacific Northwest National Laboratory.
- Wu, P., and Little, W. A. (1983). "Measurement of Friction Factors for the Flow of Gasses in Very Fine Channels Used for Microminiature Joule-Thompson Refrigerators." *Cryogenics*. May, 273-277.
- Wu, P., and Little, W. A. (1984). "Measurement of Heat Transfer Characteristics for Gas Flow in Fine Channel Heat Exchangers Used for Microminiature Refrigerators." *Cryogenics*. August, 415-420.
- Yu, D., Warrington, R., Barron, R., and Ameel, T. (1994). "An Experimental and Theoretical Investigation of Fluid Flow and Heat Transfer in Microtubes." ASME/JSME International Thermal Engineering Conference, Maui, Hawaii.